INVESTIGATING ACQUIRED TEMOZOLOMIDE RESISTANCE IN ADULT GLIOBLASTOMA

Submission for the degree of Master of Science (by Research),

MSc (Res) in Oncology

NAME : ZHI YI WONG

STUDENT NO. : 1189501

SUPERVISOR : DR VALENTINE MACAULAY

MICHAELMAS 2020

ST. EDMUND HALL

UNIVERSITY OF OXFORD

Table of Contents

Table of Contents 2

List of illustrations 6

List of tables 10

List of abbreviations 11

Acknowledgement 16

Abstract 17

Chapter 1: Introduction 19

1.1 Glioblastoma multiforme 21

1.1.1 Survival 22

1.1.2 Pathophysiology 23

1.1.3 Clinical presentation 26

1.1.4 Macroscopic and Histological Features 28

1.1.5 Classification of GBM 29

1.1.6 Current standards of care 36

1.2 Temozolomide (TMZ) 39

1.2.1 Mechanism of action 40

1.3 TMZ resistance 42

1.3.1 O-6-methylguanine-DNA methyltransferase (MGMT) 42

1.3.2 Mismatch Repair (MMR) 43

1.3.3 Base Excision Repair 44

1.3.4 Other DNA Repair Pathways 45

1.3.5 Drug Efflux 46

1.3.6 Metabolic pathways 46

1.3.7 Other mechanisms 48

Hypothesis 50

Objectives 50

Disclaimer 50

Chapter 2: Materials and Methods 51

2.1 Cell Lines and Reagents 51

2.2 Cell Culture 52

2.3 Viability Assays 53

2.4 Clonogenic Assays 54

2.5 Protein Extraction 55

2.5.1 Snap freezing 55

2.5.2 Cell Lysis 55

2.6 Sodium Dodecyl Sulfate–Polyacrylamide Gel Electrophoresis (SDS-PAGE) 56

2.7 Western Blotting 57

2.8 RNA Extraction 58

2.9 Reverse Transcription 60

2.10 Real-time quantitative Polymerase Chain Reaction (qRT-PCR) 61
2.10.1 Primer Sequences 61
2.10.2 qRT-PCR Cycles 65
2.11 siRNA Knockdown 66
2.11.1 siRNA sequence 66
2.11.2 Forward Transfection 69
2.12 Statistical Analyses 70
Chapter 3: Characterisation of temozolomide-resistant sublines 71
3.1 Results 71
3.1.1 Response of GaMG and TMZ-resistant GaMG sublines to TMZ and other drugs 71
3.1.2 Response of GaMG and TMZ-resistant GaMG sublines to IR 81
3.1.3 Characterisation of mismatch repair proteins and MGMT in GaMG, T-20 and T-100 cells 84
3.1.4 The effect of O6BG on the sensitivity of GaMG sublines to TMZ 88
3.2 Discussion 94
Chapter 4: Investigation of genetic alterations underlying acquired temozolomide resistance in GBM 98

4.1 Results 98

4.1.1 Differential expression analysis across GaMG sublines 98

4.1.2 Heterogeneity of GaMG and TMZ-resistant GaMG sublines 105

4.1.3 Validation of Differentially Expressed Genes 119

4.2 Discussion 133

Chapter 5: Investigation of differentially expressed genes as potential novel drivers of acquired temozolomide resistance in GBM 136

5.1 Results 136

5.1.1 The effects of individual gene knockdown on TMZ resistance 136

5.1.2 The effects of dual depletion of candidate genes on TMZ resistance in GaMG sublines 149

5.1.3 The effect of *BCAT1*:*CT83* co-depletion with MGMT inhibition 161

5.2 Discussion 164

Chapter 6: Conclusion 167

Chapter 7: References 171

List of illustrations

Figure 1.1: IDH wildtype and IDH mutant in cellular metabolism ... 30

Figure 1.2: WHO classification of GBM 31

Figure 1.3: TMZ mechanism of action. 41

Figure 3.1: TMZ dose response curves of GaMG and TMZ-resistant GaMG sublines. 73

Figure 3.2: Dose response of GaMG and TMZ-resistant GaMG sublines towards MNU, MMS and MMC..... 77

Figure 3.3: Radiation dose response of GaMG, T-20 and T-100 cells. 82

Figure 3.4: Characterisation of the MMR proteins in GaMG and TMZ-resistant GaMG sublines..... 85

Figure 3.5: Characterisation of MGMT protein and mRNA expression in GaMG and GaMG sublines. 87

Figure 3.6: Investigation of the effect of O6BG on GaMG parental, T-20 and T-100 cell viability after TMZ treatment. 91

Figure 3.7: Level of MGMT protein after TMZ exposure. 93

Figure 4.1: Differential expression analyses between GaMG, T-20 and T-100 (by Dr Voukantsis).....100

Figure 4.2: The enriched GO terms for the DE genes between GaMG and T-20 cells (by Dr Voukantsis). 102

Figure 4.3: The enriched GO terms for the DE genes between GaMG and T-100 cells (by Dr Voukantsis).....103

Figure 4.4: The enriched KEGG pathways for the DE genes between GaMG and T-20 cells (by Dr Voukantsis). 104
Figure 4.5: t-SNE plots showing the heterogeneity analysis of GaMG, T-20 and T-100 cells (by Dr Voukantsis). 105
Figure 4.6: UMAP projections showing different clusters of GaMG sublines (by Dr Voukantsis).....107
Figure 4.7: Pseudotime trajectories of the four different clusters (by Dr Voukantsis).....108
Figure 4.8: Comparison of number of DE genes between the four clusters (by Dr Voukantsis). 109
Figure 4.9: The enriched GO terms for the DE genes between cluster 2 and 0 (by Dr Voukantsis). 110
Figure 4.10: The enriched GO terms for the DE genes between cluster 1 and 2 (by Dr Voukantsis). 111
Figure 4.11: The enriched GO terms for the DE genes between cluster 1 and 0 (by Dr Voukantsis). 112
Figure 4.12: The enriched GO terms for the DE genes between cluster 3 and 0 (by Dr Voukantsis). 113
Figure 4.13: The enriched GO terms for the DE genes between cluster 2 and 3 (by Dr Voukantsis). 114
Figure 4.14: The enriched GO terms for the DE genes between cluster 1 and 3 (by Dr Voukantsis). 115
Figure 4.15: The enriched KEGG pathways for the DE genes between cluster 2 and 3 (by Dr Voukantsis). 116

Figure 4.16: The enriched KEGG pathways for the DE genes between cluster 1 and 3 (by Dr Voukantsis). 117
Figure 4.17: The enriched KEGG pathways for the DE genes between cluster 2 and 0 (by Dr Voukantsis). 118
Figure 4.18: Validation of *MGMT* expression in GaMG, T-20 and T-100 cells. 120
Figure 4.19: Validation of the upregulated genes from the 20 genes that were differentially expressed between all three sublines.....123
Figure 4.20: Validation of the downregulated genes from the 20 genes that were differentially expressed between all three sublines.....125
Figure 4.21: Validation of the DE genes that had been reported to drive TMZ resistance. 126
Figure 4.22: Validation of the genes encoding ribonucleotide reductase subunits. 128
Figure 4.23: Validation of other selected genes. 132
Figure 5.1: Effect of *BCAT1* knockdown on dose response of GaMG parental, T-20 and T-100 to TMZ. 138
Figure 5.2: Effect of *CT83* knockdown on dose response of GaMG parental, T-20 and T-100 to TMZ. 140
Figure 5.3: Effect of *CPNE8* knockdown on dose response of GaMG parental, T-20 and T-100 to TMZ. 142
Figure 5.4: Effect of *EBF1* knockdown on dose response of GaMG parental, T-20 and T-100 to TMZ. 145

Figure 5.5: Effect of *E2F1* knockdown on dose response of GaMG parental, T-20 and T-100 to TMZ. 148
Figure 5.6: Effect of *BCAT1* and *CT83* co-depletion on dose response of GaMG parental, T-20 and T-100 to TMZ.....151
Figure 5.7: Effect of co-depleting two genes on TMZ resistance in GaMG.....154
Figure 5.8: Effect of co-depleting two genes on TMZ resistance in T-20. 156
Figure 5.9: Effect of co-depleting two genes on TMZ resistance in T-100.....158
Figure 5.10: Effect of *EBF1* and *E2F1* co-depletion on dose response of GaMG parental, T-20 and T-100 to TMZ. 160
Figure 5.11: Effect of BCAT1 and CT83 co-depletion, with or without O6BG, on dose response of GaMG parental, T-20 and T-100 to TMZ. 163

List of tables

Table 1.1: WHO classification of CNS tumours. 21

Table 1.2: Summary of gene alterations in different GBM subtypes. 35

Table 2.1: Culture medium formula 52

Table 2.2: RIPA buffer formula. 56

Table 2.3: List of Primary Antibodies in Western Blotting. 58

Table 2.4: List of Secondary Antibodies in Western Blotting. 58

Table 3.1: Statistical testing of the TMZ dose response of GaMG, T-20 and T-100 cells. 74

Table 3.2: Statistical testing of the MNU dose response of GaMG, T-20 and T-100 cells. 78

Table 3.3: Statistical testing of the MMS dose response of GaMG, T-20 and T-100 cells. 79

Table 3.4: Statistical testing of the MMC dose response of GaMG, T-20 and T-100 cells. 80

Table 3.5: Statistical testing of the radiation dose response of GaMG, T-20 and T-100. 83

List of abbreviations

53BP1	p53-binding protein 1
5'dRP	5'deoxyribose phosphate
ABC	ATP-binding cassette
AIC	5-aminoimidazole-4-carboxamide
ALDH1A1	Aldehyde dehydrogenase 1 family member A1
APE1	Apurinic/apyrimidinic endonuclease 1
ATM	Ataxia telangiectasia mutated
BER	Base excision repair
BRCA1	Breast cancer 1
CDK1	Cyclin dependent kinase 1
CDKN2A	Cyclin dependent kinase inhibitor 2A
CDKN2b	Cyclin dependent kinase inhibitor 2B
CNS	Central nervous system
CSF	Cerebrospinal fluid
DE	Differentially expressed
DGM1	Denovo genomic marker 1
DSB	Double-strand break
DTT	Dithiothreitol
DYNC2H1	Dynein, cytoplasmic 2, heavy chain 1
EGFR	Epidermal growth factor receptor
eGFP	Enhanced green fluorescent protein
ERBB2	Erb-B2 Receptor Tyrosine Kinase 2
FA	Fanconi anaemia

FACS	Fluorescence-activated cell sorting
FDA	U.S. Food and Drug Administration
FoxM1	Forkhead box M1
GBM	Glioblastoma multiforme
GFAP	Glial fibrillary acidic protein
GO	Gene Ontology
GSC	Glioma stem cells
H3F3A	Histone 3 variant H3.3
HGF	Hepatocyte growth factor
HK2	Hexokinase 2
HR	Homologous recombination
IDH	Isocitrate dehydrogenase
IGF	Insulin-like growth factor
IGF-1R	Type 1 IGF receptor
IMRT	Intensity modulated radiotherapy
IR	Irradiation
IUPAC	International Union of Pure and Applied Chemistry
KEGG	Kyoto Encyclopedia of Genes and Genomes
KIT	KIT proto-oncogene receptor tyrosine kinase
KPS	Karnofsky performance status
LOH 10q	Loss of heterozygosity on chromosome 10q
MCM7	Minichromosome maintenance complex component 7
MDR1	Multiple drug resistance-1
MGMT	O-6-methylguanine-DNA methyltransferase

MLH1	MutL homolog 1
MMC	Mitomycin C
MMR	Mismatch repair
MMS	Methyl methanesulfonate
MNU	N-methyl-N-nitrosourea
MPG	N-methylpurine DNA glycosylase
MRI	Magnetic resonance imaging
MSH2	MutS homolog 2
MSH6	MutS homolog 6
MTIC	3-methyl-(triazen-1-yl) imidazole-4-carboximide
NADPH	Nicotinamide dinucleotide phosphate (reduced)
NEFL	Neurofilament light
NF1	Neurofibromatosis type 1
NFIA	Nuclear factor I A
NF-κB	Nuclear factor kappa-light-chain-enhancer of activated B cells
NG2	Neuron-glial antigen 2
NHEJ	Non-homologous end-joining (NHEJ)
NICE	National Institute for Health and Care Excellence
NKX2–2	NK2 Homeobox 2
NOS	Not otherwise specified (GBM classification)
O6BG	O6-Benzylguanine
OLIG2	Oligodendrocyte transcription factor 2
OPCs	Oligodendrocyte progenitor cells

PARP	Poly (ADP-ribose) polymerase
PBS	Phosphate buffered saline
PCNA	Proliferating cell nuclear antigen
PCV	Procarbazine, lomustine and vincristine
PDGFRα	Platelet derived growth factor receptor alpha
P-gp	P-glycoprotein
PI3K	Phosphatidylinositol-3-kinase
PLK4	Polo like kinase 4
PMS2	PMS1 homolog 2
Polβ	DNA polymerase β
RB	Retinoblastoma tumour suppressor
RIZ1	Retinoblastoma protein-interacting zinc-finger gene 1
RNR	Ribonucleotide reductase
ROS	Reactive oxygen species
RRAD	Ras-Related Associated with Diabetes
RT	Radiation therapy
RTK	Receptor tyrosine kinase
scRNA-seq	Single-cell RNA sequencing
SGO1	Shugoshin 1
SLC8A2	Solute carrier family 8 member 2
SOX	SRY-related HMG-box
SSB	Single-strand break
SYK	Spleen tyrosine kinase
TCA	Tricarboxylic acid

TCGA	The Cancer Genome Atlas
TENM3	Teneurin transmembrane protein 3
TERT	Telomerase reverse transcriptase
TP53	Tumour protein p53
TSC	Tuberous sclerosis complex
TMZ	Temozolomide
t-SNE	T-distributed stochastic neighbour embedding
UMAP	Uniform manifold approximation and projection
WHO	World Health Organisation

Acknowledgement

Since the beginning of my research, I have received a great deal of support and assistance. First of all, I would like to thank my supervisor Dr Valentine Macaulay for giving me this precious opportunity to complete this research degree under her supervision. Her knowledge and expertise have been invaluable in formulating the research topic as well as providing support throughout the duration of this project. She is always kind, supportive, patient and considerate towards her students. Having a supervisor who is always encouraging and enthusiastic to discuss ideas, results, experiments or even problems faced has helped in my personal development.

I would like to extend my sincere gratitude towards Yayasan Khazanah and Oxford Centre for Islamic Studies for their generous support in funding my MRes study under the Merdeka Scholarship.

Also, I would like to thank my dear colleague Matthew Ellis for his continual support, guidance and help in my development as a scientist. I am equally grateful for all the other members of the Macaulay group: Dr Guillaume Rieunier, Dr Eliot Osher, Dr Monica Mantri, Dr Avigail Taylor, Jack Mills, Xiaoning Wu, Ashwin Nandakumar and Jinseon Kim. They have been warm and welcoming since my arrival into the laboratory and shared much of their wisdom with me throughout the course.

Abstract

Glioblastoma is the most aggressive primary malignant brain tumour in adults with very poor prognosis. Current management includes surgery, radiotherapy and temozolomide (TMZ), which causes three types of DNA methylation: O^6-methylguanine (O^6-meG), N^7-methylguanine and N^3-methyladenine. N-methylated lesions are mostly recognised and repaired by base excision repair (BER), while the most toxic DNA adduct is O6-meG. This is directly repaired by O6-methylguanine-DNA methyltransferase (MGMT), and subsequently degraded. If not removed, O^6-meG leads to mispairing, futile cycles of mismatch repair (MMR) and eventually double strand breaks. The acquisition of TMZ resistance presents a major clinical challenge; mechanisms reported to be involved include MGMT upregulation, MMR deficiency and drug efflux. We hypothesise that more genes contributing to acquired TMZ resistance are yet to be identified. To better understand this resistance, TMZ-resistant sublines T-20 and T-100 were generated from TMZ-sensitive, MGMT-negative GaMG parental cells by previous students, by exposure to TMZ concentrations equivalent to cerebrospinal fluid and plasma levels. Herein, the TMZ-resistant phenotype was confirmed, and T-20 and T-100 cells were found to be cross-resistant to other methylating agents MNU and MMS but not intercalating agent MMC. MGMT was markedly overexpressed in TMZ-resistant cells and was reduced after TMZ exposure, suggesting that TMZ was entering the cells and causing MGMT consumption, hence

making an efflux pump resistance mechanism unlikely. TMZ resistance was partially reversed in T-20 but not at all in T-100 by MGMT inhibitor O^6-benzylguanine. Neither was there change in expression of MMR proteins, suggesting MGMT/MMR-independent resistance. To investigate potentially novel resistance mechanisms, scRNA-seq data generated by a previous student were examined. These revealed significant transcriptional differences, with upregulation of genes including *MGMT*, *BCAT1*, *CT83*, *CPNE8* in resistant sublines and *EBF1, E2F1, RRM2* in GaMG parental cells, which were then validated using RT-qPCR. There were no significant changes in viability after siRNA depletion of *EBF1* and *E2F1* in GaMG cells, or *CPNE8*, *BCAT1* and *CT83* both alone or together in T-20 and T-100 cells. The effect of co-targeting multiple genes was tested, based on the hypothesis that TMZ resistance has multiple drivers. MGMT inhibition alongside *BCAT1*:*CT83* co-depletion might have partially reversed TMZ resistance but results were inconsistent. Nevertheless, cell viability in the absence of TMZ was reduced upon *BCAT1*:*CT83* co-depletion and the percentage change in T20 and T100 was greater than in parental cells. This suggested that even if *BCAT1* and *CT83* were not individually driving TMZ resistance, the cells might be more dependent on these genes for viability. Further investigation of the differentially expressed proteins and their signalling pathways could complement the scRNA-seq data to improve accuracy of identifying potential novel mediators, which may help to suggest new approaches to GBM therapy.

Chapter 1: Introduction

The brain is the central organ of the central nervous system (CNS) and is involved in various functions including processing sensory information, secreting hormones, and regulating blood pressure and respiration (Frackowiak, 2007). In the human CNS, glial cells surround the neurons with very different glia to neuron ratios throughout human brain structures (Herculano-Houzel, 2014).

There are four major groups of glial cells: microglia, oligodendrocytes, neuron-glial antigen 2 (NG2)-glia and astrocytes. Microglia are tissue-resident macrophages, which originate from primitive macrophages in the yolk sac during early embryonal period (Cronk et al., 2013). They actively sense the environment for insults, with each cell guarding separate and regular sized domains, and then destroy pathogens and remove apoptotic neurons and nonessential neuronal synapses by phagocytosis, maintaining the homeostasis of the CNS (Cronk et al., 2013). The main role of oligodendrocytes, akin to Schwann cells in the peripheral nervous system (PNS), is to insulate neuronal axons by creating a myelin sheath. (Bradl et al., 2010). However, perineuronal or satellite oligodendrocytes are non-myelinating (Szuchet et al., 2011, Takasaki et al., 2010). They provide metabolic support for cortical neurons (Takasaki et al., 2010) and safeguard neurons against apoptosis (Taniike et al., 2002). NG2-glia are also known as oligodendrocyte progenitor cells (OPCs), which undergo continuous proliferation and differentiation to produce myelin-

forming oligodendrocytes from the early postnatal period to adulthood (Young et al., 2013). Last but not least, human astrocytes are distinguished into four distinct classes based on morphological and anatomical properties: interlaminar astrocytes, protoplasmic astrocytes, varicose projection astrocytes and fibrous astrocytes, which are located within different layers of the cortex (Vasile et al., 2017). They are involved in many different functions including providing lactates as substrates to oxidative metabolism of adjacent neurons (Ames, 2000), regulating brain blood flow (Attwell et al., 2010), neuronal communication (Dallerac et al., 2016), elimination of neurotransmitters, maintaining ionic homeostasis, formation, maturation and elimination of synapses (Vasile et al., 2017).

According to the Cancer Research UK statistics, brain, other CNS and intracranial tumours were the 9th most common cancers in the UK in 2017 and 12.2% of these patients survived their disease for five or more years (2013 to 2017) (CRUK). There are many different types of CNS tumours. The World Health Organisation (WHO) classification of the CNS tumours is based on phenotypic and genotypic parameters and their gradings are determined by four histologic criteria using the St. Anne–Mayo grading system: cytological atypia, mitosis, endothelial proliferation, and necrosis, where Grade I implies non-infiltrating, slow-growing tumours that do not meet any of the criteria and Grade IV the most aggressive and fastest growing type of tumours that meet three or four of the criteria (Gupta et al., 2017). According to the

classification, CNS tumours are divided into different categories (Table 1.1).

Diffuse astrocytic and oligodendroglial tumours	Neuronal and mixed neuronal-glial tumours
Tumours of the pineal region	Embryonal tumours
Other astrocytic tumours	Ependymal tumours
other gliomas	Choroid plexus tumours
Tumours of the cranial and paraspinal nerves	Melanocytic tumours
Meningiomas	Lymphomas
Histiocytic tumours	Mesenchymal non-meningothelial tumours
Germ cell tumours	Tumours of the sellar region
Metastatic tumours	

Table 1.1: WHO classification of CNS tumours. Adapted from reference (Louis et al., 2016).

1.1 Glioblastoma multiforme

Glioblastoma multiforme (GBM) is the most common and aggressive primary malignant brain tumour in adults, representing 45.2% of primary malignant brain and CNS tumours (Ostrom et al., 2013). It is classified under the category of 'diffuse astrocytic and oligodendroglial tumours' as a Grade IV tumour in the 2016 WHO

Classification of CNS Tumours, i.e. displaying anaplasia, extensive mitotic activity with endothelial proliferation, and/or necrosis (Louis et al., 2016). GBM usually happens in the cerebral hemispheres, with 95% arising in the supratentorial region (Nakada et al., 2011). Glioma is an umbrella term, which refers to the collective tumours arisen from the glial cells.

It should be emphasised that significant and important differences exist between the biology of adult and paediatric GBMs. A whole-exome gene sequencing study reveals that somatic mutations in the histone H3.3–ATRX–DAXX chromatin remodelling pathway occur in almost half of paediatric GBM tumours, particularly mutations in histone 3 variant H3.3 (*H3F3A*) which is involved in post-translational activation or repression (Schwartzentruber et al., 2012). Moreover, paediatric GBMs display frequent chromosome 1q gain as well as platelet derived growth factor receptor alpha (*PDGFRa*) amplification compared to in adult GBMs. However, they also exhibit a lower frequency of chromosome 7 gain and chromosome 10q loss, which are the defining features of adult GBM (Bax et al., 2010, Paugh et al., 2010, Jones et al., 2012). This project focuses only on the adult GBM.

1.1.1 Survival

Between 2007 and 2011, the median overall survival of adult GBM patients in England was 6.1 months and the proportion of patients who survived GBM for 1, 2 and 5 years or more after diagnosis were

28.4%, 11.5% and 3.4% respectively (Brodbelt et al., 2015). In the subgroup treated with maximal combination treatment of surgery, chemotherapy and radiotherapy (RT), patient aged 20-69 years old had a median survival of 14.9 months (Brodbelt et al., 2015).

1.1.2 Pathophysiology

The aetiology of GBM has yet to be elucidated. Hitherto, exposure to high dose ionising radiation (IR) is the only established risk factor (Bondy et al., 2008, Ohgaki, 2009). It is suggested that genetic predisposition may contribute to GBM, as patients with certain syndromes such as neurofibromatosis type 1 (NF1), tuberous sclerosis complex (TSC) and Li-Fraumeni due to mutations in *NF1*, *TSC1*, *TSC2* and *TP53*, have increased risk of developing GBM (Bondy et al., 2008, Walker et al., 2006). Research has shown that certain genes are overexpressed in GBM compared to healthy brain and lower grade astrocytoma, for instance *LAPTM5, GPR65* and *MYO1F*, and the overexpression of these genes are linked to decreased survival in every GBM subtype (Dunwoodie et al., 2018). A tumour profiling study on initial and recurrent GBM samples also reveals frequent mutations in epidermal growth factor receptor (*EGFR*), phosphatase and tensin homolog (*PTEN*), breast cancer 1/2 (*BRCA1/2*), and ataxia telangiectasia mutated (*ATM*) (Ellis et al., 2019).

GBM, being the high-grade astrocytoma, gives the notion that the tumour develops from the star-shaped astrocytes. Nonetheless,

there has been study that shows that GBM arises from neural stem cells in the subventricular zone of the adult human brain containing the driver mutations. In fact, GBM can also arise from oligodendrocyte progenitor cells (Zong et al., 2012).

In GBM pathogenesis, studies have shown frequent genetic aberrations in three main signalling pathways, namely the receptor tyrosine kinase/Ras/phosphatidylinositol-3-kinase (RTK/Ras/PI3K) signalling that mediates proliferation and survival, tumour protein p53 (p53) signalling which responds to cellular stresses that disrupt DNA replication and cell division, and retinoblastoma tumour suppressor (RB) signalling pathways which regulates cell cycle progression (McLendon et al., 2008, Parsons et al., 2008).

Being a member of the receptor tyrosine kinase family, *EGFR* gene amplification is the most common mutation in GBM, occurring in 40–60% of primary GBMs (Brennan et al., 2013).

Loss of tumour suppressor genes such as *p53*, *NF1*, solute carrier family 8 member 2 (*SLC8A2*) and retinoblastoma protein-interacting zinc-finger gene 1 (*RIZ1*) along with tumour suppressor miRNA play an important role in promoting GBM tumorigenicity (Liang et al., 2016, Qu et al., 2017, Zhang et al., 2015, Zhu et al., 2005). On the other hand, upregulation of oncogenes augments GBM progression (Zhang et al., 2018). These cell-intrinsic mechanisms have also helped in shaping the tumour immune landscape of GBM (Wellenstein et al., 2018). For instance, loss of *NF1* drives the recruitment of tumour-

associated macrophages/microglia to the tumour site (Wang et al., 2017) and upregulation of the proto-oncogene *Fyn* downregulates the anti-GBM immune response (Comba et al., 2019).

Apart from cell-intrinsic mechanisms, GBM malignancy also depends on its tumour microenvironment, which is classified into perivascular, perinecrotic and invasive niches (Schiffer et al., 2018a). These niches are important for GBM proliferation, growth, invasion and angiogenesis (Calabrese et al., 2007, Diksin et al., 2017, Schiffer et al., 2018a, Schiffer et al., 2018b). Furthermore, a novel border niche has been described where there is an accumulation of OPCs and microglia at the tumour border areas. GBM cells utilise this border niche for survival and acquisition of stem cell-like and chemo-radioresistant properties (Hide et al., 2019). The tumour-associated microglia within the microenvironment also promotes GBM invasiveness (Hu et al., 2014).

Neurons are key components in the GBM microenvironment. The tumour integrates into and thus hijacks the neural circuits by forming synaptic and electrical connections to promote its own progression (Venkatesh et al., 2019). Astrocytes are important members within the GBM microenvironment. In response to CNS injuries, astrocytes undergo astrogliosis and are transformed into reactive astrocytes, characterised by hypertrophy, increased proliferation, and upregulated glial fibrillary acidic protein (GFAP), nestin and vimentin (Guan et al., 2018). Tumour-associated reactive astrocytes promote proliferation,

invasion and chemo-radioresistance in GBM (Brandao et al., 2019, Guan et al., 2018). A recent study also suggests that crosstalk between tumour-associated reactive astrocytes and microglial cells contributes to the immunosuppressive environment in GBM (Henrik Heiland et al., 2019).

Heterogeneity is an important hallmark of GBM and plays a key role in patient survival (Inda et al., 2014). Tumour heterogeneity consists of inter-tumour and intra-tumour heterogeneity. Inter-tumour heterogeneity of GBM is characterised by the tumours of different molecular subtypes with distinct transcriptional profiles (see section 1.1.5) in different patients (Verhaak et al., 2010). However, multiple molecular subtypes of GBM also exists within the same tumour, giving rise to intra-tumour heterogeneity (Phillips et al., 2006). It has been suggested that glioma stem cells (GSCs) receiving signalling cues from cells of different microenvironmental niches such as endothelial cells, macrophages and astrocytes provide an adaptive response towards therapeutic interventions and contribute to this heterogeneous nature of GBM (Ho et al., 2017).

1.1.3 Clinical presentation

Under magnetic resonance imaging (MRI) scans, GBM appears as a large irregular lesion with a dark and hypodense central necrotic core, within a peripheral ring of contrast enhancement (Smith et al., 2007). Butterfly GBM, where the tumour invades from one hemisphere

to another through septum pellucidum and corpus callosum, is also well identified. This tumour has a poorly supported vascular network with many structural and functional abnormalities, often resulting in haemorrhage (Finneran et al., 2020, Smith et al., 2007).

Approximately half of GBM patients frequently present with non-specific and indistinguishable headaches at diagnosis (Forsyth et al., 1993). The progressive increase in tumour mass and the surrounding oedema results in a shift in intracranial contents and increased intracranial pressure. This explains the unilateral localised pain with increasing intensity or frequency experienced by the patients, usually accompanied by papilloedema, nausea and vomiting (Omuro et al., 2013).

As GBM advances, the healthy brain tissues are gradually damaged due to necrosis, which then leads to focal neural deficit. The signs and symptoms of the malignancy are related to the affected brain region, for example, hearing problems suggest that the tumour is located in the auditory cortex (Hanif et al., 2017). Cognitive impairments and personality changes may develop as a result of a tumour in the frontal lobe (Hanif et al., 2017). Further, when the tumour reaches a significant mass effect, the patient may present with gait imbalance and urinary incontinence (Omuro et al., 2013).

GBM patients may exhibit seizures, which occur in 40% to 60% of patients, either as focal, complex focal or generalised seizures depending on the tumour location (Vecht et al., 2014). This may be

due to raised glutamate concentration in tumour and peritumour tissues, altered expression of glutamate transporter resulting in reduced reuptake of glutamate in synaptic cleft and low glutamine synthetase expression (Rosati et al., 2013, Yuen et al., 2012).

1.1.4 Macroscopic and Histological Features

Macroscopically, GBM is a heterogeneous tumour with cystic and gelatinous areas, featuring multifocal haemorrhage and necrosis (Smith et al., 2007). Some areas of the tumour appear as soft and yellow as a result of the necrosis whereas other regions are firm and white, representing cystic degeneration and haemorrhage (Hanif et al., 2017). Vascular endothelial proliferation and formation of glomeruloid structures are distinguished characteristics of GBM.

Histologically, GBM pleomorphic cell population consists of small poorly differentiated cells and large multinucleated cells undergoing extensive mitotic activity (Smith et al., 2007). Nuclear pseudopalisades surrounding regions of necrosis are also typical of GBM (Wippold et al., 2006). When examined using immunohistochemistry, many GBM cells will be labelled with GFAP and show high percentage of Ki-67, indicating their glial origin and high proliferation respectively (Smith et al., 2007).

1.1.5 Classification of GBM

In humans, there are three isocitrate dehydrogenase (IDH) isoforms (Zou et al., 2016), which play a key role in cellular metabolism. During aerobic respiration, acetyl-coenzyme A is generated through pyruvate oxidation. Then, the tricarboxylic acid (TCA) cycle begins with condensation of oxaloacetate and acetyl-coA to produce citrate, which is subsequently converted to its isomer, isocitrate. IDH1 and IDH2 enzymes catalyse the reversible oxidative decarboxylation of isocitrate to form α-ketoglutarate in the cytoplasm and mitochondria respectively, producing reduced nicotinamide dinucleotide phosphate (NADPH) during the process (Figure 1.1). IDH3 performs the same process of isocitrate-to-α-ketoglutarate conversion but reducing NAD^+ to NADH (Molenaar et al., 2018). IDH is the main source of NADPH which protects the brain against reactive oxygen species (ROS). Mutated IDH catalyse the reductive carboxylation of α-ketoglutarate to D-2-hydroxyglutarate, consuming NADPH and as a result the cells are vulnerable to oxidative stress (Molenaar et al., 2018) (Figure 1.1). D-2-hydroxyglutarate is an onco-metabolite, and its accumulation not only induces oxidative stress but also contributes to GBM progression (Dang et al., 2009, Gilbert et al., 2014). IDH1 and IDH2 are also involved in epigenetic regulation of gene expression and DNA repair (Molenaar et al., 2018).

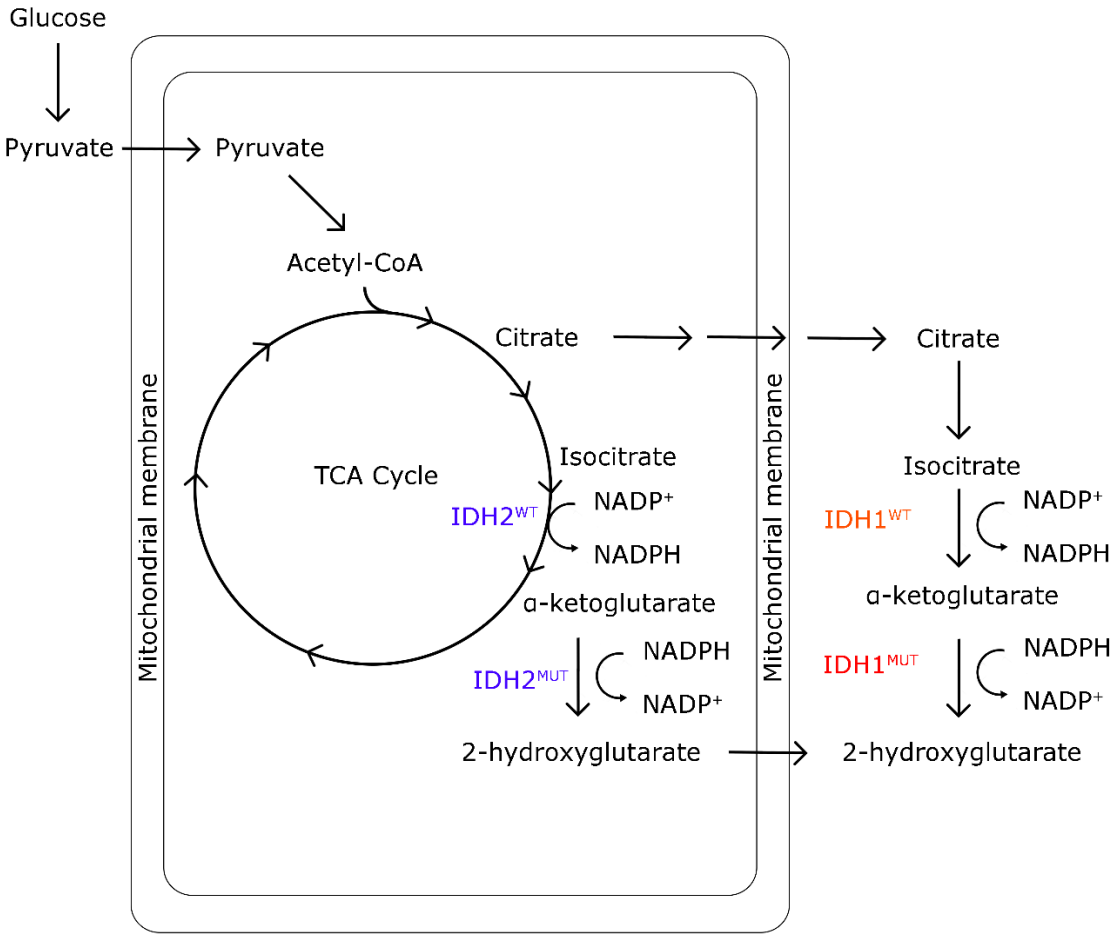


Figure 1.1: IDH wildtype and IDH mutant in cellular metabolism. TCA, Tricarboxylic acid cycle; IDH^{WT}, isocitrate dehydrogenase wildtype; IDH^{MUT}, isocitrate dehydrogenase mutant; $NADP^{+}$, nicotinamide dinucleotide phosphate; NADPH, nicotinamide dinucleotide phosphate (reduced). Schematic adapted from reference (Molenaar et al., 2018).

According to 2016 CNS WHO, GBMs are classified based on their IDH status into 1) GBM, IDH-wildtype, 2) GBM, IDH-mutant and 3) GBM, not otherwise specified (NOS) (Louis et al., 2016) (Figure 1.2).

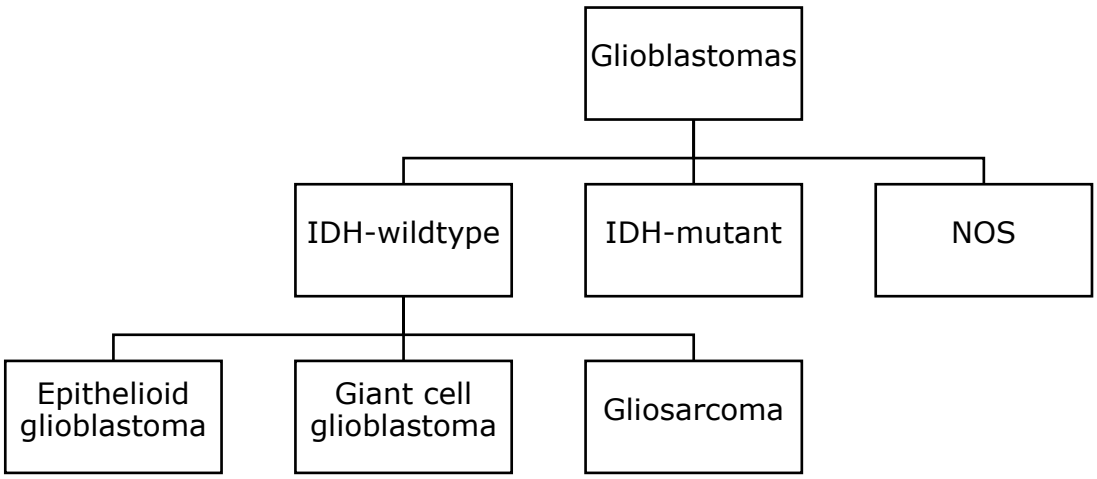


Figure 1.2: WHO classification of GBM (Louis et al., 2016)

The majority of GBM cases (approximately 90%) are IDH-wildtype, which corresponds closely to the clinically defined primary or *de novo* GBM and predominates in patients over 55 years old. On the contrary, IDH-mutant GBM is commonly associated with secondary GBM, mainly occurring in younger patients and contributes approximately 10% of total cases. Secondary GBM tends to progress from a pre-existing lower grade tumour such as diffuse astrocytoma and anaplastic astrocytoma (Vigneswaran et al., 2015). When the IDH status is not identified, it is classified as NOS (Louis et al., 2016, Ohgaki et al., 2013). IDH mutation status is an important prognostic

marker in GBM patients. As such, IDH mutations are associated with better overall survival and progression-free survival in GBM patients (Chen et al., 2016).

Several subcategories have been identified and classified under the umbrella of IDH wildtype GBM, namely epithelioid glioblastoma, giant cell glioblastoma and gliosarcoma (Louis et al., 2016, Smith et al., 2007). Epithelioid glioblastoma usually develops in children and younger adults and is characterised by the huge epithelioid cells with abundant eosinophilic cytoplasm, vesicular chromatin, large nuclei and prominent nucleoli (Louis et al., 2016). Genetic analyses reveal a high percentage of *BRAF* V600E mutation, telomerase reverse transcriptase (*TERT*) promoter mutations, homozygous deletions of cyclin dependent kinase inhibitor 2A or 2B (*CDKN2A/2B*) and hemizygous deletions of teneurin transmembrane protein 3 (*TENM3*, also known as *ODZ3*). Unlike in typical adult IDH wildtype GBM, epithelioid GBM lacks *EGFR* amplification and chromosome 10 losses (Kanemaru et al., 2019, Louis et al., 2016). Giant cell glioblastoma is an extremely rare histopathologic diagnosis (~1% of all GBM cases), featuring abnormal multinucleated giant cells with abundant eosinophilic cytoplasm (Kozak et al., 2009). The rarity of this malignancy has resulted in the limited knowledge about giant cell glioblastoma. There is frequently microsatellite instability and *TP53* mutation while *EGFR* amplification is less common (Martinez et al., 2007). Gliosarcoma is another rare primary malignant brain tumour, accounting for 2–8% of all GBM

(Lutterbach et al., 2001). The bimorphic tumour comprises a gliomatous component that fits into the typical histologic criteria of GBM and an additional sarcomatous component with evidence of mesenchymal differentiation (Zhang et al., 2016). Loss of heterozygosity on chromosome 10q (LOH 10q) and *TERT* promoter mutations often occur in gliosarcoma. Like epithelioid glioblastoma and giant cell glioblastoma, gliosarcoma also lacks *EGFR* amplification (Oh et al., 2016).

Gene expression-based classification of GBM based on the integrated genomic analysis of The Cancer Genome Atlas (TCGA) data divides GBM into four molecular subtypes: classical, mesenchymal, proneural, and neural, which are characterised by the abnormalities in *EGFR*, *NF1*, *PDGFRa /IDH1* and *ERBB2* respectively (Agnihotri et al., 2013). The classical subtype is characterised by high rates of *EGFR* amplification (*EGFRvIII*, which is deficient in ligand-binding domain but is constitutively active, is the most common mutant), loss of *PTEN* and a distinct lack of *TP53* mutation (Agnihotri et al., 2013, An et al., 2018, Verhaak et al., 2010). The main signatures of mesenchymal subtype are low *NF1* expression due to focal hemizygous deletions of a region at 17q11.2 and activation of the nuclear factor kappa-light-chain-enhancer of activated B cells (NF-κB) pathway. GBM patients with the mesenchymal subtype tend to have poor overall survival (Behnan et al., 2019, Verhaak et al., 2010). The proneural subtype is closely associated with secondary GBM and affects mainly younger patients.

The key features of this subtype are amplification of *PDGFRα* and point mutations in *IDH1* (Agnihotri et al., 2013, Verhaak et al., 2010). The neural subtype has overexpressed neuron markers such as neurofilament light (*NEFL*) and frequent mutations in Erb-B2 receptor tyrosine kinase 2 (*ERBB2*). Nonetheless, the gene signature of neural subtype is similar to that of normal brain tissue (Agnihotri et al., 2013, Verhaak et al., 2010) (Table 1.2).

GBM subtype	Gene alteration
Classical	• *EGFR* amplification • Loss of *PTEN* • Lack of *TP53, NF1, PDGFRA* and *IDH1* mutations • Overexpression of neural precursor and stem cell marker (*NES*) • Loss of *INK4A*/*ARF* • Frequent chr7 amplification paired with chr10 loss • Activation of Notch and SHH signalling pathways
Mesenchymal	• Loss of *NF1* • *PTEN* mutation • Loss of *TP53* and *CDKN2A* • Overexpression of mesenchymal markers (*CHI3L1*, *MET*) and astrocytic markers (*CD44*, *MERTK*) • Activation of TNF family and NF-κB pathways

Proneural	• *PDGFRa* amplification • *IDH1* mutation • *TP53* mutation • High expression of oligodendrocytic development markers (*PDGFRa*, *NKX2–2*, and *OLIG2*) • *PIK3CA*/*PIK3R1* mutations • Expression of proneural development genes (*SORPM*enes) • Less prevalent chr7 amplification paired with chr10 loss
Neural	• Elevated levels of neuron markers (*NEFL*) • Frequent *ERBB2* mutation

Table 1.2: Summary of gene alterations in different GBM subtypes. *CHI3L1*, Chitinase 3 Like 1; *DCX,* Doublecortin*; MERTK*, MER Proto-Oncogene, Tyrosine Kinase; *MET*, MET Proto-Oncogene, Receptor Tyrosine Kinase; *NES*, Nestin; *NKX2–2*, NK2 Homeobox 2; *OLIG2*, Oligodendrocyte Transcription Factor 2; *SHH*, Sonic hedgehog; *SOX*, SRY-related HMG-box; *TNF*, Tumour Necrosis Factor. Table adapted from reference (Agnihotri et al., 2013, Verhaak et al., 2010).

1.1.6 Current standards of care

Brain tumours are difficult to treat because of their localisation in the confined space of the skull, surrounded by healthy brain tissue and the limited capacity of the brain to replenish damaged or dead neurones (Aldape et al., 2019). A small increase in tumour size may result in detrimental effects on cognitive function and patient survival.

According to the National Institute for Health and Care Excellence (NICE) guideline NG99, current management involves surgery, radiation, carmustine implants and temozolomide (TMZ) (NICE, 2018). There have not been many promising data on the prognostic benefit of tumour resection (Almenawer et al., 2015, Hatiboglu et al., 2013, Ringel et al., 2016). Besides, surgical removal of the entire GBM tumour is almost impossible due to the finger-like tentacles that extend from the main tumour mass into the neighbouring healthy brain tissue (Cenciarini et al., 2019). Nonetheless, patients sometimes undergo partial resection, considering patient-associated factors such as age, existing medical comorbidities, polypharmacy, and physiological reserve (Almenawer et al., 2015). However, these patients do poorer compared with total resection in terms of overall survival and progression-free survival (Haj et al., 2017).

Post-surgical RT is the main pillar of GBM management, but radioresistance resulting from preferential activation of DNA damage response in GSC, hyperactivation of certain signalling pathways such

as Akt and Notch pathways, presence of specific microRNAs, and hypoxia poses a major clinical challenge for GBM treatment (Bao et al., 2006, Han et al., 2017). Chemoresistance results partly from the overexpression of O-6-methylguanine-DNA methyltransferase (MGMT), imbalance in base excision repair (BER) pathway, the upregulation of multidrug resistance genes, and the dysregulation of apoptosis-regulating genes (Kitange et al., 2009, Sarkaria et al., 2008, Shervington et al., 2008). The presence of the blood brain barrier and transporter proteins also present challenges for drug delivery, severely limiting the accumulation of drugs at the tumour site and thus reducing their therapeutic efficacy (Agarwal et al., 2013, Bhowmik et al., 2015).

GBM recurrence inevitably occurs in almost all patients (Seystahl et al., 2016), and in these cases, no clear standard of care is established and there is no expert consensus on the treatment (Weller et al., 2014). The general options are repeated tumour resection, re-radiation and changes in chemotherapy drug choice, for instance considering PCV (procarbazine, lomustine and vincristine) chemotherapy or single agent lomustine as an alternative to TMZ, but each has to be considered on a case-by-case basis, taking into consideration patients' preferences, Karnofsky performance status (KPS), previous treatment, time from last treatment, tumour molecular markers, and quality of life (NICE, 2018, Weller et al., 2014). Repeated resections are commonly offered and survival is prolonged by 4-8 months after each additional resection but at the cost

of increased complication risk and reduction in the KPS (Chaichana et al., 2013, Hoover et al., 2013). Furthermore, there is a limited arsenal of chemotherapy drugs approved for use in GBM (NCI, 2019).

There are ongoing clinical trials in GBM patients that investigate different drug targets. Some of them involve various poly (ADP-ribose) polymerase (PARP) inhibitors such as the phase I/IIa study investigating olaparib as radiosensitising agent, in combination with TMZ and intensity modulated radiotherapy (IMRT) in first line treatment for unresectable or partially resectable GBM (Lesueur et al., 2019), and the phase II/III trial study (NCT02152982) comparing veliparib and TMZ to TMZ alone in treating patients with newly diagnosed GBM (ClinicalTrials.gov, 2020a). A preclinical study involving the novel third-generation EGFR inhibitor AZD9291 (osimertinib) suggests that the drug demonstrates excellent blood brain barrier penetration and continuous inhibition of EGFR/ERK signalling in GBM cells, which might overcome the adaptive activation of the ERK pathway that drives primary resistance to the first-generation EGFR inhibitor erlotinib (Liu et al., 2019). Further, a phase IIb clinical trial (NCT03776071) studying the effect of Enzastaurin, which is a protein kinase Cβ inhibitor, plus TMZ during and following RT as compared to RT and TMZ only in patients with newly diagnosed GBM with or without the novel genomic biomarker, Denovo genomic marker 1 (DGM1) (ClinicalTrials.gov, 2020b).

1.2 Temozolomide (TMZ)

TMZ, sold under the brand name of Temodal® and Temodar®, belongs to the imidazotetrazine class of compounds which is chemically related to dacarbazine (Moody et al., 2014). The International Union of Pure and Applied Chemistry (IUPAC) nomenclature of TMZ is 3-methyl-4-oxoimidazo[5,1-d][1,2,3,5]tetrazine-8-carboxamide. It was initially approved by the U.S. Food and Drug Administration (FDA) to treat adult anaplastic astrocytoma in 1999 (Cohen et al., 2005). The results from a randomised open-label, multicentre trial in 2005 demonstrated the clinical benefit of TMZ by showing that concomitant use of TMZ and RT prolong the median survival of GBM patients from 12.1 months (RT alone) to 14.6 months (Cohen et al., 2005). Thus, the FDA approved TMZ for treatment of adult patients with newly diagnosed GBM concomitantly with RT and subsequently as a monotherapy treatment. According to the summary of product characteristics of TMZ, newly diagnosed GBM adult patients are given 75 mg/m^2/day of TMZ concomitantly with focal RT of 60 Gy administered in 30 fractions for 6 weeks. Then, 4 weeks after finishing the combination treatment, TMZ is given as monotherapy for 6 cycles where cycle 1 consists of 150 mg/m^2 once daily for 5 days, followed by 23 days without treatment prior to the next cycle. From cycle 2 onwards, TMZ dose is increased to 200 mg/m^2 once daily for 5 days, then 23 days without treatment.

1.2.1 Mechanism of action

Clinical effectiveness of TMZ requires proficient and active DNA mismatch repair (MMR) proteins for activity (Moody et al., 2014). TMZ is stable in acidic conditions (pH < 5) but under physiological conditions, it is spontaneously converted to the short-lived metabolite 3-methyl-(triazen-1-yl) imidazole-4-carboximide (MTIC) via chemical hydrolysis (Reid et al., 1997). It is further hydrolysed into 5-aminoimidazole-4-carboxamide (AIC) and the electrophilic methyldiazonium cation which subsequently methylates DNA (Agarwala et al., 2000). The DNA methylation primarily occurs at guanine residues, forming O^6- (5%) and N^7- (60-80%) methylguanine, and the N^3 position of adenine (10-20%), forming N^3-methyladenine (Friedman et al., 2000, Hombach-Klonisch et al., 2018). Although still contributing to the cytotoxicity of TMZ, the N-methylated DNA lesions (N^7-methylguanine and N^3-methyladenine) are mostly recognised and effectively repaired by the BER pathway without damaging the DNA, rendering them less cytotoxic (Strobel et al., 2019). Despite being the least frequently alkylated DNA adduct, O^6-methylguanine is the most lethal alkyl adduct that is responsible for the cytotoxic effect of TMZ. It mispairs to thymine rather than cytosine (Warren et al., 2006). The MMR machinery recognises and excises the mispairing thymine but the O^6-methylguanine, left intact by MMR, again mispairs to thymine, resulting in a futile cycling of DNA repair (Li et al., 2016). The persisting O^6-methylguanine and endonuclease activity of the MMR

machinery introduces single strand breaks (SSBs), extended by exonuclease I to form elongating regions of single-stranded gap (Li, 2008). After at least 2 cycles of replication, this results replication fork arrest which generates double-strand breaks (DSBs), resulting in activation of the apoptotic pathway (Agarwala et al., 2000, Strobel et al., 2019, Quiros et al., 2010).

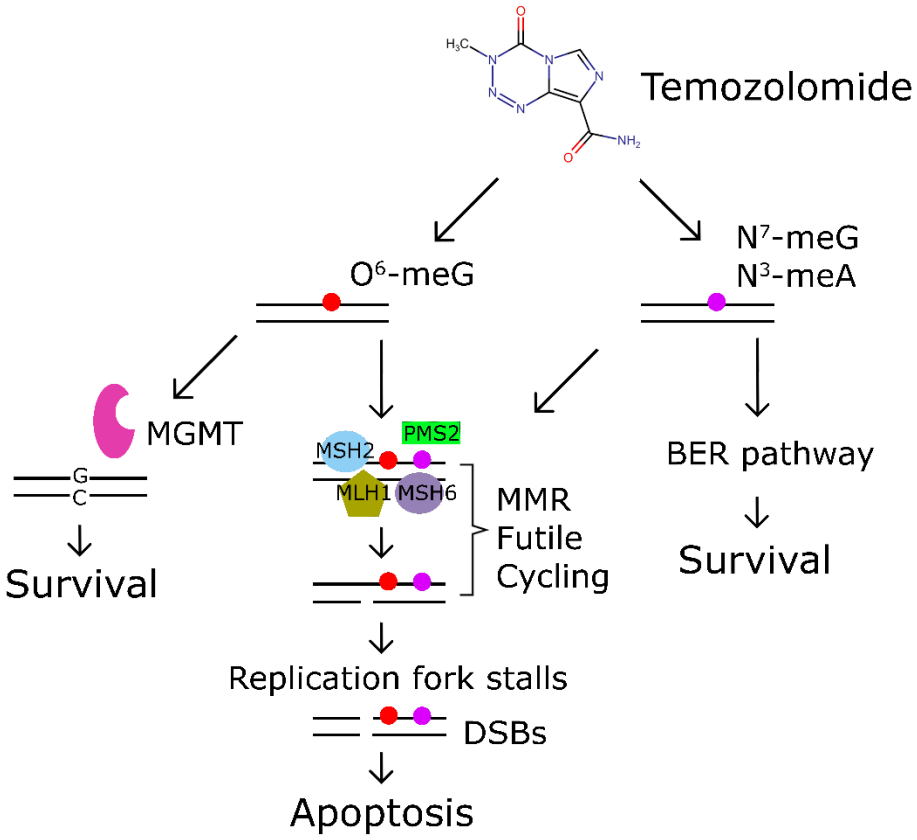


Figure 1.3: TMZ mechanism of action.

DSBs, double-strand breaks; O^6-meG, O^6-methylguanine; N^7-meG, N^7-methylguanine; N^3-meA, N^3-methyladenine. Drawn based on information in reference (Agarwala et al., 2000, Strobel et al., 2019).

1.3 TMZ resistance

TMZ resistance presents a major clinical challenge in GBM management. At least half of the patients treated with TMZ do not respond to the drug (Lee, 2016). The lack of response is usually due to intrinsic or acquired resistance of tumours towards TMZ and acquired TMZ resistance occurs in more than 90% of recurrent gliomas (González-Gómez et al., 2011). It has been suggested that resistance is due to a number of factors, including MGMT status and activity of certain DNA repair pathways.

1.3.1 O-6-methylguanine-DNA methyltransferase (MGMT)

MGMT is a demethylating protein, which removes the methyl group directly from the O^6 position of guanine and transfers it to a cysteine residue at the active site of the molecule (Pegg, 2000, Kaina et al., 2010). After that, MGMT is inactivated and degraded via ubiquitin-mediated pathway (Fan et al., 2013, Tolcher et al., 2003). The *MGMT* gene is silenced by the process of methylation, which reduces its expression and repair activity and improves TMZ sensitivity. Therefore, it is recommended to test all high-grade glioma specimens including GBM for *MGMT* promoter methylation status to determine prognosis and guide treatment (NICE, 2018). Nonetheless, *MGMT* promoter methylation analysis shows that *MGMT* is only expressed in approximately half of GBM tumours (Brennan et al., 2013, Hegi et al., 2005).

Although MGMT inhibition has worked effectively in preclinical models (Kaina et al., 2010), the addition of inhibitors has not shown additional benefits than TMZ alone in clinical trials in melanoma and GBM, owing to increased toxic side effects hence resulting in significant dose reduction of TMZ (Jiang et al., 2014, Ranson et al., 2007, Yu et al., 2020). The combination treatment of O^6-benzylguanine (O6BG) and TMZ has been reported to cause myelosuppression without any significant clinical benefit in patients with recurrent TMZ-resistant malignant glioma (Quinn et al., 2009).

1.3.2 Mismatch Repair (MMR)

In MMR, there are several components that regulate the repair process. Firstly, heterodimer of MutS homolog 2 (MSH2) and MutS homolog 6 (MSH6) binds to the DNA base mismatches, which then recruit another heterodimeric complex of MutL homolog 1 (MLH1) and PMS1 homolog 2 (PMS2) (Stojic et al., 2004).

As mentioned above, a functioning MMR machinery is the prerequisite for TMZ-induced cytotoxicity. Defects in MMR have been implicated in TMZ resistance, even in the absence of MGMT (Liu et al., 1996). Using an *in vitro* model, it is demonstrated that a modest decrease in *MSH2* and *MSH6* expression is sufficient to increase TMZ resistance (McFaline-Figueroa et al., 2015). However, microsatellite instability analysis of patients' tumour reveals that MMR deficiency does not drive TMZ resistance in GBM (Maxwell et al., 2008). In fact,

GBM patients with *MGMT* promoter methylated and EGFRvIII positive tumours have improved TMZ sensitivity due to upregulation of MSH2 and MSH6 proteins (Struve et al., 2020). These contradicting data may be due to the heterogeneity of GBM tumours.

1.3.3 Base Excision Repair

During BER, N-methylpurine DNA glycosylase (MPG, also known as APNG and AAG) recognises and excises the TMZ-induced N-methylated DNA lesions (Jacobs et al., 2012). The resulting abasic site is cleaved by apurinic/apyrimidinic endonuclease 1 (APE1), generating 3'-hydroxyl and 5'deoxyribose phosphate (5'dRP) ends. The repair process is followed by gap filling and ligation by DNA polymerase β (Polβ) and DNA ligase (Krokan et al., 2013). In both *in vitro* and *in vivo* GBM models, it is demonstrated that forced expression of *MPG* improves the repair of TMZ-induced N-methylation and contribute to TMZ resistance. Meanwhile, GBMs with higher nuclear *MPG* expression are associated with poorer prognosis (Agnihotri et al., 2012). It has also been shown that imbalance within the BER pathway (*MPG* overexpression, DNA polymerase β deficiency and BER inhibition using methoxyamine or PARP inhibitors) enhances TMZ-induced cytotoxicity due to saturation of the rate-limiting enzyme Polβ along with the accumulation of the cytotoxic 5'dRP (Tang et al., 2010, Tang et al., 2011).

1.3.4 Other DNA Repair Pathways

PARP is a sensor protein that recognises SSBs and then initiates the downstream repair process (Caldecott, 2008). It is demonstrated that PARP inhibition reverses TMZ resistance in MMR-deficient GBM cells and xenografts (Cheng et al., 2005, Curtin et al., 2004). As PARP is also actively involved in BER pathway, it is possible that PARP inhibition shifts the cytotoxic locus of TMZ from O^6-meG to N^7-meG and N^3-meA (Curtin et al., 2004).

DSBs are repaired by non-homologous end-joining (NHEJ) and homologous recombination (HR) but it is shown that O^6-meG-induced DSBs are repaired by HR rather than NHEJ (Roos et al., 2009) and enhanced HR has been reported to mediate TMZ resistance in GBM (Gil Del Alcazar et al., 2016, Roos et al., 2018). In addition, BRCA1, a key player in HR-mediated repair, has been shown to modulate TMZ resistance in p53 wild-type GBM based on bioinformatical analysis from a high-throughput shRNA-based synthetic lethality screening (Ding et al., 2019). However, NHEJ has also been described to play a role in acquired TMZ resistance in GBM due to upregulation of key canonical NHEJ factors (Zhang et al., 2019a).

In addition, upregulation of dynein, cytoplasmic 2, heavy chain 1 (DYNC2H1), which is a key protein required for cargo trafficking in cilia, has also been reported to be involved in acquired temozolomide resistance in MGMT-deficient GBM cells, where it regulates the nuclear transportation of DNA repair proteins (Yi et al., 2019).

The Fanconi anaemia (FA) pathway is important in repairing interstrand crosslinks, stabilising stalled replication forks, and facilitating fork restart and replication after repair completion (Ceccaldi et al., 2016). The FA repair pathway is activated by TMZ and confer cellular resistance to TMZ in GBM (Chen et al., 2007).

1.3.5 Drug Efflux

There are 48 human ATP-binding cassette (ABC) transporter genes which are subclassified into seven families and the expression of these ABC transporters especially multiple drug resistance-1 (*MDR1*, also known as P-glycoprotein [P-gp]) results in chemoresistance (Robey et al., 2018). ABC transporters are overexpressed in GBM cells (Rama et al., 2014). They are also widely expressed at the blood brain barrier, localised at the endothelial luminal membrane (Wijaya et al., 2017). TMZ is a substrate of MDR1 and increased MDR1 confers TMZ resistance (Munoz et al., 2015b). In GBM, TMZ resistance occurs via two mechanisms: firstly, TMZ induces P-gp into its active conformation, and secondly TMZ stimulates production of EGF which in turn increases *MDR1* expression (Munoz et al., 2014).

1.3.6 Metabolic pathways

There are abnormalities in GBM metabolism, where there are shifts in glycolysis, TCA cycle, glutamine metabolism, lipid metabolism and nucleotide metabolism (Zhou et al., 2019). For instance, there is

evidence that GBMs exhibit increased glycolysis for energy production and accumulation of glutamine (Marin-Valencia et al., 2012). Furthermore, only less than half of GBM acetyl-coenzyme A pool is derived from glucose (Maher et al., 2012), the tumours utilise acetate as the bioenergetic source to the TCA cycle (Mashimo et al., 2014). In acquired TMZ-resistant GBM models, there is an increase in indoleacetaldehyde and lipid metabolites, which suggest tryptophan metabolism disruption and dysregulation in mitochondrial metabolism respectively (Tiek et al., 2018). Nonetheless, metabolic heterogeneity has been detected in GBMs and it has been shown that TMZ-resistant cells adapt to TMZ treatment by utilising alternative metabolic pathways to drive their progression as well as resistance (Petővári et al., 2020).

Hexokinase 2 (HK2) is an important glycolytic enzyme for aerobic glycolysis and is upregulated in the perinecrotic region of human GBMs and HK2 depletion improves the sensitivity of GBM cells towards TMZ-induced apoptosis (Wolf et al., 2011). Furthermore, non-glycolytic enzymes may also be involved in TMZ resistance. High expression of aldehyde dehydrogenase 1 family member A1 (*ALDH1A1*) is correlated with poor prognosis in GBM patients and overexpression of *ALDH1A1* confers TMZ resistance in GBM cells (Schäfer et al., 2012). This protein family is usually involved in the detoxification of endogenous and exogenous aldehyde substrates (Tomita et al., 2016). Preliminary results from an ongoing clinical trial

investigating the combination of disulfiram (ALDH inhibitor), TMZ and RT demonstrate significant improvement in GBMs with *IDH1*, *BRAF* or *NF1* mutations (Huang et al., 2019).

1.3.7 Other mechanisms

Other mechanisms of TMZ resistance include microRNAs, histone modification, hypoxia and GSCs (Banelli et al., 2015, Li et al., 2018, Munoz et al., 2015a, Woo et al., 2019). Hitherto, no mechanism of resistance has led to the introduction of a clinically effective treatment for TMZ-resistant GBM, suggesting that there are more resistance mechanisms that remain to be identified.

The research focus of the Macaulay group has traditionally been the role of insulin-like growth factor (IGF) signalling in tumour biology, especially prostate cancer. Previous results from the group have shown that type 1 IGF receptor (IGF-1R) inhibition leads to sensitisation towards IR in paediatric GBM and TMZ in melanoma (Ramcharan et al., 2015, Simpson et al., 2020). However, IGF-1R inhibition did not sensitise adult or paediatric GBM cells to TMZ *in vitro* (Simpson, 2016).

To better understand the acquisition of TMZ resistance, TMZ-resistant sublines T-20 and T-100 were generated from TMZ-sensitive GaMG parental cells by previous students from the Macaulay group by exposure to TMZ concentrations equivalent to cerebrospinal fluid (CSF; 20 μM) and circulating (100 μM) levels (Simpson, 2016, Ma, 2019).

Furthermore, single-cell RNA sequencing (scRNA-seq) had been performed to identify differentially expressed genes but only limited validation had been performed, which confirmed that Ras-Related associated with diabetes (*RRAD*) was upregulated in TMZ-resistant cells (Ma, 2019). This gene has already been implicated in TMZ resistance, with findings that *RRAD* expression associates with TMZ resistance and poor survival in patients with GBM, and depletion of *RRAD* enhances sensitivity of TMZ-resistant GBM cells (Yeom et al., 2014). This finding supports the clinical relevance of the TMZ-resistance model investigated in this thesis.

It was hypothesised that multiple dysregulated genes contributed to growth and chemoresistance of GBM. Therefore, this project was designed to explore the acquired TMZ resistance in GBM.

Hypothesis

There are more genes contributing to the acquired TMZ resistance in GBM that are yet to be identified.

Objectives

I. To confirm the TMZ-resistant phenotype in induced-TMZ-resistant cell lines

II. To validate selected differentially expressed genes from scRNA-seq data analysis

III. To test the functional contribution of the differentially expressed genes in acquired TMZ resistance

Disclaimer

All the data in my MRes are my own work except the following:

- Generation of TMZ-resistant cell lines by Aaron Simpson and Victoria Ma (Macaulay Group)
- Irradiation by Matthew Ellis and Xiaoning Wu (Macaulay Group)
- scRNA-seq by Neil Ashley (WIMM)
- Bioinformatics analysis by Dr Dimitrios Voukantsis (Buffa Group)

Chapter 2: Materials and Methods

2.1 Cell Lines and Reagents

Adult human GBM cell line GaMG was purchased from The Leibniz Institute DSMZ - German Collection of Microorganisms and Cell Cultures GmbH (DSMZ no. ACC 242). The cell line was established from the biopsy specimens of a 42-year-old female GBM patient with unknown subtype. GaMG cells with acquired resistance to 20 μM of TMZ (T-20) and 100 μM of TMZ (T-100) were generated previously by Aaron Simpson and Victoria Ma (both Macaulay group) by passaging GaMG cells in the culture medium containing gradually increasing TMZ concentration up to 20 μM for T-20 and 100 μM for T-100 respectively. All cells in culture were tested regularly for mycoplasma contamination using MycoAlert™ Mycoplasma Detection Kit (#LT07-318, Lonza). The identity of both GaMG parental and TMZ-resistant sublines had not been independently authenticated.

TMZ was purchased from Sigma Aldrich (#T2577) and reconstituted from powder in DMSO into 50 mM stock solution. They were aliquoted into 50 μL and 100 μL vials and stored in -20°C freezer. N-methyl-N-nitrosourea (MNU) was kindly provided by Prof. Geoffrey Margison from University of Manchester and reconstituted in DMSO into 50 mM stock solution. The aliquots were stored in -20°C freezer. Methyl methanesulfonate (MMS, #129925) was obtained from Sigma Aldrich. The liquid was diluted with ultrapure water to 50 mM stock

solutions and divided into 500 µL and 100 µL aliquots. They were stored in -20°C freezer. Mitomycin C powder from *Streptomyces caespitosus* (MMC, #M4287) was bought from Sigma Aldrich and reconstituted in ultrapure water into 5 mM stock solution. They were aliquoted into 500 µL and 100 µL vials and stored in -20°C freezer. O6BG (#ab142739) was acquired from Abcam and the powder was reconstituted in DMSO to 80 mM stock solutions and then aliquoted before storing in -20°C freezer.

2.2 Cell Culture

Component	Company	Catalogue no.	Vol. (mL)
Dulbecco's Modified Eagle Medium (DMEM) containing pyruvate	Gibco	#41966-029	500
100 units/mL penicillin and 100 µg/mL streptomycin	Gibco	#15140-122	5
Fetal bovine serum (FBS)	Gibco	#10500-064	50
100X MEM non-essential amino acids solution	Gibco	#11140-035	20

Table 2.1: Culture medium formula

GaMG cells were cultured in medium prepared as Table 2.1 at 37°C in 5% CO_2. T-20 and T-100 were also cultured as above but with

added TMZ so that the culture media contained 20 μM and 100 μM of TMZ respectively. The TMZ was replaced at each subculture.

During routine subculture, the media were aspirated. The cells, after achieving 60–80% confluency, were rinsed with sterile phosphate buffered saline (PBS, Sigma Aldrich #P4417) before being removed from the culture vessel surface into suspension using 1:1 trypsin/PBS (Trypsin/EDTA solution, Lonza #BE02-007E). For storage, the cells were banked in a solution consisting of 10% DMSO, 50% FBS, and 40% full medium, and then cooled at a rate of 1°C/min to -80°C.

2.3 Viability Assays

Using TMZ-free medium, cells were seeded at 1000 cells per well into clear flat-bottomed and clear-walled 96-well microplate (#3595, Corning®) and incubated at 37°C in 5% CO_2 overnight, and experimental treatments were applied the next day. The cells were seeded in 80 μL of medium, and treatments were added in 20 μL at 5x concentration. The plates were incubated at 37°C in 5% CO_2 for 5 - 7 days. Then, cell viability was estimated using CellTiter-Blue® from Promega (#G8080). This assay relies on the metabolic capacity of viable cells to reduce resazurin (dark blue) into resorufin, which is pink and highly fluorescent ($579_{Ex}/584_{Em}$). CellTiter-Blue® Reagent (20 μL) was added into each well and the plates were incubated at 37°C in 5% CO_2 for at least 3 hours. The fluorescent signal was then measured using POLARstar Omega plate reader spectrophotometer (BMG

Labtech). The IC_{50} values were calculated using GraphPad Prism 8 software. All conditions were done as triplicate or quadruplicate wells and tested for one to three independent repeats.

2.4 Clonogenic Assays

GaMG, T-20 and T-100 cells were seeded at 5000 single cells per plate into 10 cm plates and incubated at 37°C in 5% CO_2 overnight. The following day, the plates were irradiated by DPhil students Matthew Ellis and Xiaoning Wu at doses of 0 to 10 Gy in a Gamma-Service Medical GmbH Caesium-137 irradiator (GSR D1; Serial number: A0108; maximum activity: 197.1 TBq) at Old Road Campus Research Building, University of Oxford.

After irradiation, the plates were incubated at 37°C in 5% CO_2 for 10 - 12 days until colonies of more than 50 cells had been observed. The media were removed and the plates were rinsed with non-sterile PBS. The colonies were fixed and stained using Coomassie Brilliant Blue stain (0.1% Brilliant Blue, 7% acetic acid, 50% methanol and dH_2O), incubated at room temperature for 30 minutes. The plates were rinsed with first tap water then Milli-Q® water. The colonies were counted using GelCount automated counter (Oxford Optronix). All conditions were performed in triplicate plates and tested for three independent repeats.

2.5 Protein Extraction

2.5.1 Snap freezing

The cells were lifted from the flask surface using trypsin/EDTA (see section 2.2) and collected into different 15 mL falcon tubes, then centrifuged at 1,500 RPM for 5 minutes at 4°C. The medium was removed and the cell pellet was resuspended in 1 mL of ice-cold PBS, then centrifuged at 15,000 RPM for 30 seconds at 4°C. The PBS was removed and the cell pellets were snap frozen in dry ice and ethanol. All the pellets were stored in -80°C freezer until use.

2.5.2 Cell Lysis

Lysis buffer was made by supplementing RIPA buffer (see Table 2.2) with phosphatase inhibitor cocktails 2 and 3 (#P5726 and #P0044, Sigma Aldrich) as well as cOmplete™ EDTA-free protease inhibitor cocktail (#11873580001, Roche), all at 1:50 of RIPA buffer volume and freshly added each time. The cell pellets were lysed in 70 µL of lysis buffer on ice for 20 minutes, vortexed in between, then centrifuged at 15,000 RPM for 12 to 15 min at 4°C and supernatants collected. Pierce BCA Protein assay (#23225, ThermoFisher Scientific) was carried out to quantify the soluble protein levels of each lysate. The volume needed for 30 to 50 µg of protein was calculated. The protein lysates were stored at -20°C until use.

Stock	Volume (mL)	Final Concentration
Tris HCl pH 7.5	5	50 mM
5 M NaCl	3	150 mM
0.5 M EDTA	0.2	1 mM
10% Sodium deoxycholate	2.5	0.25%
NP-40 (IGEPAL CA-630)	1	1%
10% SDS	1	0.1%
dH_2O	87.3	

Table 2.2: RIPA buffer formula. Table shows volumes to prepare 100 mL (prepared by Xiaoning Wu and stored at 4°C until use).

2.6 Sodium Dodecyl Sulfate–Polyacrylamide Gel Electrophoresis (SDS-PAGE)

Each protein lysate (30-50 µg total protein) was added with 6.25 µL of NuPAGE LDS Sample Buffer (4X) (#NP0008, ThermoFisher Scientific) and 2.5 µL of 1 M dithiothreitol (DTT), then Milli-Q® water to achieve final volume of 25 µL. The samples were heated at 95°C for 10 minutes, then briefly centrifuged to ensure the samples were collected at the bottom of the vials.

Lysate mixtures (25 µL) were loaded into each well of the 4–15% Criterion™ TGX™ Precast Midi Protein Gel (#5671084, Bio-Rad) and 5 µL of Spectra™ multicolour broad range protein ladder (#26634, ThermoFisher Scientific) was added as a molecular-weight size marker.

Electrophoresis was performed at 100 – 125 V for approximately 60 to 90 minutes in 1X Tris/Glycine/SDS Electrophoresis Buffer (#1610772, Bio-Rad). The separated proteins on the gel were electrotransferred onto nitrocellulose or polyvinylidene difluoride (PVDF; pre-activated in methanol) membranes using Trans-Blot® Turbo™ Transfer System with Trans-Blot® Turbo™ transfer buffer at 1.3 A (25 V) for 7 min.

2.7 Western Blotting

After the electrotransfer, the membranes were blocked in 5% bovine serum albumin (BSA) in PBS with 0.1% Tween-20 (PBS-T) for 20 - 60 minutes at room temperature and then left overnight at 4°C for incubation with the primary antibodies. Next, the membranes were washed in PBS-T for 5 minutes thrice before incubating with horseradish peroxidase-conjugated secondary antibodies for 1 hour at room temperature. All the primary and secondary antibodies were diluted in 5% BSA in PBS-T. A further 3 x 5 minutes PBS-T washes were carried out. The aforementioned blocking, washing and incubating were all performed on a gyro-rocker. Presence of proteins were detected using ECL Western Blotting Substrate (#W1001, Promega) and the chemiluminescence was measured using The ChemiDoc XRS+ System (Bio-Rad).

Target	Company	Catalogue no.	Source	Dilution
MGMT	CST	#2739S	Rabbit	1:1000
MLH1	CST	#3515S	Mouse	1:1000
MSH2	CST	#2850S	Mouse	1:1000
MSH6	CST	#12988S	Mouse	1:1000
β-Tubulin	Sigma	#T4026	Mouse	1:1000

Table 2.3: List of Primary Antibodies in Western Blotting.

CST: Cell Signaling Technology

Type	Company	Catalogue no.	Dilution
Anti-Rabbit IgG, HRP-linked Antibody	CST	#7074	1:2000
Anti-Mouse IgG, HRP-linked Antibody	CST	#7076	1:2000

Table 2.4: List of Secondary Antibodies in Western Blotting.

CST: Cell Signaling Technology

2.8 RNA Extraction

The cells were snap frozen as described in section 2.5.1. RNA was extracted with ReliaPrep™ RNA Miniprep Systems (#Z6011, Promega). In brief, 100 µL of BL + TG buffer was added to the cell pellet and mixed well by vortexing or pipetting. Then, 35 µL of 100%

isopropanol was added and mixed by vortexing for 5 seconds. The lysate was transferred to a ReliaPrep™ Minicolumn (placed into a Collection Tube) and centrifuged at 13,000 RPM for 30 seconds at room temperature. Liquid in the Collection Tube was discarded. After that, 500 µL of RNA Wash Solution was added to the Minicolumn and centrifuged at 13,000 RPM for 30 seconds. The Collection Tube was emptied. DNase I incubation mix was prepared by mixing 24 µL of Yellow Core Buffer, 3 µL of 0.09 M $MnCl_2$ and 3 µL of DNase I enzyme. The incubation mix was added directly to Minicolumn membrane and incubated at room temperature for 15 minutes. Then, 200 µL of Column Wash Solution was added to the Minicolumn and centrifuged at 13,000 RPM for 15 seconds. A further 500 µL of RNA Wash Solution was added and centrifuged at 13,000 RPM for 30 seconds. The wash solutions were emptied and the Collection Tube discarded. The Minicolumn was transferred to a new Collection Tube. RNA Wash Solution (300 µL) was added to the Minicolumn and centrifuged at 13,000 RPM for 2 minutes. The Minicolumn was transferred from the ReliaPrep™ Minicolumn to an Elution Tube. Next, 15 µL of nuclease-free water was added to the Minicolumn membrane and centrifuged at 13,000 RPM for 1 minute. The Minicolumn was discarded. The Elution Tube containing the purified RNA was stored at -80°C until use. The above-mentioned DNase I, BL + 1-Thioglycerol (TG) Buffer, RNA Wash Solution and Column Wash Solution were reconstituted or prepared as per instructions from Promega.

The concentration and purity (260/280 and 260/230 absorbance ratios) of the RNAs were measured using NanoDrop spectrophotometer. The volume needed for 1000 ng of RNA was calculated.

2.9 Reverse Transcription

Complementary DNA (cDNA) synthesis from the purified RNA was performed using SuperScript™ III First-Strand Synthesis SuperMix for qRT-PCR (#11752050, Invitrogen). The volume needed for 1000 ng of RNA sample was added to PCR tube and nuclease-free water was added to make up the volume to 8 µL. Each RNA sample was added with 10 µL of 2X RT Reaction Mix and 2 µL of RT Enzyme Mix. The PCR tube containing the reaction mixtures was placed into the Applied Biosystems SimpliAmp™ PCR Thermal Cycler (#A24811) and incubated at 25°C for 10 minutes, then 50°C for 30 minutes and finally terminated at 85°C for 5 minutes, before chilling on ice. After that, 1 µL of *Escherichia coli* RNase H was added into each tube and incubated at 37°C for 20 minutes. The cDNA was stored in -20°C freezer until use.

The concentration of the cDNA was determined using NanoDrop spectrophotometer and the volume required for 200 ng of cDNA was calculated.

2.10 Real-time quantitative Polymerase Chain Reaction (qRT-PCR)

2.10.1 Primer Sequences

Target-specific primers were designed and checked for specificity using Primer-BLAST by National Center for Biotechnology Information and ordered from Integrated DNA Technologies (IDT). All the primers had GC content between 45 to 65%. Primers were reconstituted with nuclease-free water to 100 µM stock. Then, primer mixes were prepared by mixing 50 µL of the forward and reverse primers, and 400 µL of nuclease-free water, resulting in 10 µM of each primer. The primer sequences were as below:

β-actin

Forward: 5'-GATGAGATTGGCATGGCTTT-3'

Reverse: 5'-CACCTTCACCGTTCCAGTTT-3'

CATSPER1

Forward: 5'-CTACGTCCAGAGCACTTCCC-3'

Reverse: 5'-GGTGTGCTACGTGATAGGGG-3'

CKS1B

Forward: 5'-AGGAATCTTGGCGTTCAGCA-3'

Reverse: 5'-AGCAAGATGTGAGGTTCTGGTT-3'

CPNE8

Forward: 5’-ATGGACAGCCGCTACAACAG-3’

Reverse: 5’-AGATTTCTGCAGGACACGGA-3’

CT83

Forward: 5’-CGCCGCTTTCAGAGAAACAC-3’

Reverse: 5’-CCCGAGAGAGGTCGTAGACT-3’

CXCL1

Forward: 5’-GCGCCCAAACCGAAGTCATA-3’

Reverse: 5’-ATGGGGGATGCAGGATTGAG-3’

DTYMK

Forward: 5’-TCCGGTTCCCGGAAAGATCA-3’

Reverse: 5’-TCCGCCAGCTGTAAACTTGT-3’

E2F1

Forward: 5’-CCGGGGAATGAAGGTGAACA-3’

Reverse: 5’-GAGCAAAAGGGCCGAAAGTG-3’

EBF1

Forward: 5’-CAGCTTCTCTACAGCAATGGGA-3’

Reverse: 5’-TGAGCAAGACTCGGCACATT-3’

FAM96B

Forward: 5’-TTCGCTCCATCAATGACCCG-3’

Reverse: 5’-TGTACTCTCGGGGTCGCTAA-3’

F2R

Forward: 5’-TGGACCCTGATCTTACCCGT-3’

Reverse: 5’-CTCTCTCCTGACTTCTGCGG-3’

HGF

Forward: 5’-AAGGTGACTCTGAATGAGTC-3’

Reverse: 5’-GGCACATCCACGACCAGGAACAATG-3’

Kif22

Forward: 5’-GATCTCAGGAGCTGGTCGC-3’

Reverse: 5’-GTTCCATCCACAAATGGCCG-3’

KIT

Forward: 5’-CCCACCCTGGTCATTACAGA-3’

Reverse: 5’-TATCGCTGCAGGAAGACTCC-3’

LIN9

Forward: 5’-CTCGTTCAAGATGGCGGAGC-3’

Reverse: 5’-CTGAAAGGCATTTCCACAGCAG-3’

MCM7

Forward: 5’-GGTCAGTTCTCCACTCACGG-3’

Reverse: 5’-CATACATTGATCGACTGGCG-3’

MEST

Forward: 5’-TTTCCAACATCCAGCTACGA-3’

Reverse: 5’-GGCCTGCTCAAATATGGAAT-3’

RRM1

Forward: 5’-CATGTGATCAAGCGAGATGGC-3’

Reverse: 5’-GGTGACCCCACTGTACAAGC-3’

RRM2

Forward: 5’-TTTAAAGGCTGCTGGAGTGAGG-3’

Reverse: 5’-GCAGCTGCTTTAGTTTTCGGCT-3’

SGO1

Forward: 5’-CAAGGTATCGTTCTGGACGC-3’

Reverse: 5’-TCCTTGGCCATCTTTTGCCTTA-3’

SYK

Forward: 5’-TGCCCAAAATGAGGAAGAGCC-3’

Reverse: 5’-CCCCGTAACCTCCTCTCCTTA-3’

β-actin was employed as the housekeeping gene for normalisation of the difference in mRNA expression due to the difference in loading.

2.10.2 qRT-PCR Cycles

The PCR reactions were carried out in MicroAmp™ Optical 96-Well Reaction Plates (#4346907, Applied Biosystems). For each reaction, the volume needed for 200 ng of cDNA sample was made up to the volume of 9 µL with nuclease-free water and mixed with 1 µL of 10 µM reconstituted primer pairs and 10 µL of Luna® Universal qPCR Master Mix (#M3003X, New England Biolabs), resulting in total volume of 20 µL per well. No template control (NTC) for each primer pair containing only nuclease-free water without cDNA template was also used to monitor for contamination and primer-dimer formation. The plates were sealed with optical adhesive film (#AB1170, Thermo Scientific) and centrifuged at 4,000 RPM for 1 minute at room temperature. The PCR cycles were then run on StepOnePlus™ Real-Time PCR System (Applied Biosystems) at standard speed using relative quantitation of Comparative Ct (ΔΔCt). The cycle steps were as follow: initial denaturation at 95°C for 60 seconds, then 45 cycles of denaturation at 95°C for 15 seconds and extension at 60°C for 30 seconds (+plate read). Each reaction condition was conducted in triplicate wells and repeated for three independent times. Quantification of gene expression relative to *β-actin* was calculated

using the $2^{-\Delta\Delta Ct}$ method (Livak et al., 2001), where Ct = threshold cycle, which was the number of cycles of amplification required to cross the fixed fluorescence threshold.

2.11 siRNA Knockdown

2.11.1 siRNA sequence

BCAT1 siRNA was purchased as Dharmacon™ siGENOME SMARTpool from Horizon Discovery (#M-012084-01-0005), resuspended in RNase-free 1x siRNA buffer (#B-002000-UB-100, Horizon Discovery) to 20 μM stock and stored at -20°C in 50 μL aliquots. Details of the siRNAs were as follow:

siGENOME SMARTpool siRNA D-012084-01, *BCAT1*

Target/Sense Sequence: 5'-CAACUCUGCCGGUAUUUGA-3'

siGENOME SMARTpool siRNA D-012084-02, *BCAT1*

Target/Sense Sequence: 5'-GGAGAGGACCAUCAGAUCA-3'

siGENOME SMARTpool siRNA D-012084-03, *BCAT1*

Target/Sense Sequence: 5'-GAAGUGGGAACUAUGAAUC-3'

siGENOME SMARTpool siRNA D-012084-04, *BCAT1*

Target/Sense Sequence: 5'-GCAUUUCGAGGAGUAGAUA-3'

CT83 siRNA was ordered from ThermoFisher Scientific (siRNA ID: #s47508) as Silencer® Select Pre-designed siRNA, resuspended in sterile nuclease-free water to 20 μM stock and stored at -20°C in 50 μL aliquots. The sequences were:

s47508

Sense: 5’-CGAAUAUUGGUAAACCUCAtt-3’

Antisense: 5’-UGAGGUUUACCAAUAUUCGct-3’

EBF1 siRNA was purchased as Dharmacon™ ON-TARGETplus SMARTpool from Horizon Discovery (#L-011848-01-0005), resuspended in RNase-free 1x siRNA buffer (#B-002000-UB-100, Horizon Discovery) to 20 μM stock and stored at -20°C in 50 μL aliquots. Details of the siRNAs were as follow:

ON-TARGETplus SMARTpool siRNA J-011848-09, *EBF1*

Target/Sense Sequence: 5’-GAUCGAGAGGACAGCGUUU-3’

ON-TARGETplus SMARTpool siRNA J-011848-10, *EBF1*

Target/Sense Sequence: 5’-GGAACAGCCUGCAAGCGAU-3’

ON-TARGETplus SMARTpool siRNA J-011848-11, *EBF1*

Target/Sense Sequence: 5’-GCGGGAAACCCACGUGACA-3’

ON-TARGETplus SMARTpool siRNA J-011848-12, *EBF1*

Target/Sense Sequence: 5’-CUGGUGACCCUGAGCGUUU-3’

CPNE8 siRNA was purchased as Dharmacon™ siGENOME SMARTpool from Horizon Discovery (#M-017584-02-0005), resuspended in RNase-free 1x siRNA buffer (#B-002000-UB-100, Horizon Discovery) to 20 μM stock and stored at -20°C in 50 μL aliquots. Details of the siRNAs were as follow:

siGENOME SMARTpool siRNA D-017584-01, *CPNE8*

Target/Sense Sequence: 5’-AAGGAUAUCUCACGAAUUU-3’

siGENOME SMARTpool siRNA D-017584-02, *CPNE8*

Target/Sense Sequence: 5’-GGAUGGAGAUGAUGUAAGA-3’

siGENOME SMARTpool siRNA D-017584-03, *CPNE8*

Target/Sense Sequence: 5’-GAAUUAAACUGUUGCAGGG-3’

siGENOME SMARTpool siRNA D-017584-18, *CPNE8*

Target/Sense Sequence: 5’-AGUCACAAUUCAACGUAUA-3’

E2F1 siRNA aliquot was a kind gift from Dr Guillaume Rieunier (Post-doctoral researcher, Macaulay Group), which was purchased from ThermoFisher Scientific (siRNA ID: #s4405).

2.11.2 Forward Transfection

GaMG, T-20 and T-100 cells were seeded at 3 x 10^5 cells per well into transparent 6-well plate and incubated at 37°C in 5% CO_2 overnight. The next day, thawed 20 µM *BCAT1* siRNA stock was diluted to 5 µM solution with 1x siRNA buffer. For each well, Tube 1 was prepared by adding 10 µL of 5 µM siRNA to 190 µL of serum-free medium and Tube 2 by adding 2 µL of DharmaFECT 1 Transfection Reagent (#T-2001-01) to 198 µL of serum-free medium. The contents of each tube were gently mixed and incubated for 5 minutes at room temperature. Contents of Tube 1 were added to Tube 2 for a total volume of 400 µL per well and incubated for 20 minutes at room temperature. Complete medium (1600 µL) was added to the mixtures, resulting in total transfection volume of 2 mL per well. The culture media were removed from the wells of the 6-well plate and 2 mL of the appropriate transfection medium containing 25 nM of siRNA was added to each well. *EBF1* and *CPNE8* were also transfected as above.
For *CT83* siRNA, Tube 1 was prepared by adding 1.1 µL of 20 µM siRNA stock to 249.2 µL of Opti-MEM® (OM) (#331985-047, Gibco) and Tube 2 by adding 2 µL of Oligofectamine™ (OF) (#12252011, Invitrogen) to 67 µL of OM, incubated separately for 10 minutes at room temperature. The contents of Tube 1 and Tube 2 were mixed and incubated for 25 minutes at room temperature. The culture media were removed and cells of each well were washed twice with 2.5 mL of OM. OM (127.3 µL) was first added to each well, then 319.3 µL of the

transfection medium containing 50 nM of siRNA. The plate was incubated at 37°C in 5% CO_2 for at least 4 hours, then topped up each well with 44.7 µL of FBS and 1.8 mL of complete medium. *E2F1* was also transfected as above.

For combinations of siRNAs transfection, both DharmaFECT 1 and Oligofectamine were used. Post transfection, the cells were incubated at 37°C in 5% CO_2 for 24 hours. Then, they were lifted from the well surface using trypsin/EDTA (see section2.2) and seeded at 1000 cells per well into clear flat-bottomed and clear-walled 96-well microplate (#3595, Corning®) and incubated at 37°C in 5% CO_2 for 6 to 9 hours until seeded to the bottom of wells. After that, the cells were treated with TMZ for 5 - 7 days and cell viability was estimated using CellTiter-Blue® (see section 2.3).

2.12 Statistical Analyses

All the graphs and statistical analyses were created and performed using GraphPad Prism 8 software. All grouped data were presented as mean ± standard deviation. Statistical differences between two groups were analysed using Student's t test. One-way ANOVA was performed to test for statistical differences between more than two groups with one independent variable, and two-way ANOVA was used for more than two groups with more than one independent variables. P values of less than 0.05 were considered statistically significant.

Chapter 3: Characterisation of temozolomide-resistant sublines

3.1 Results

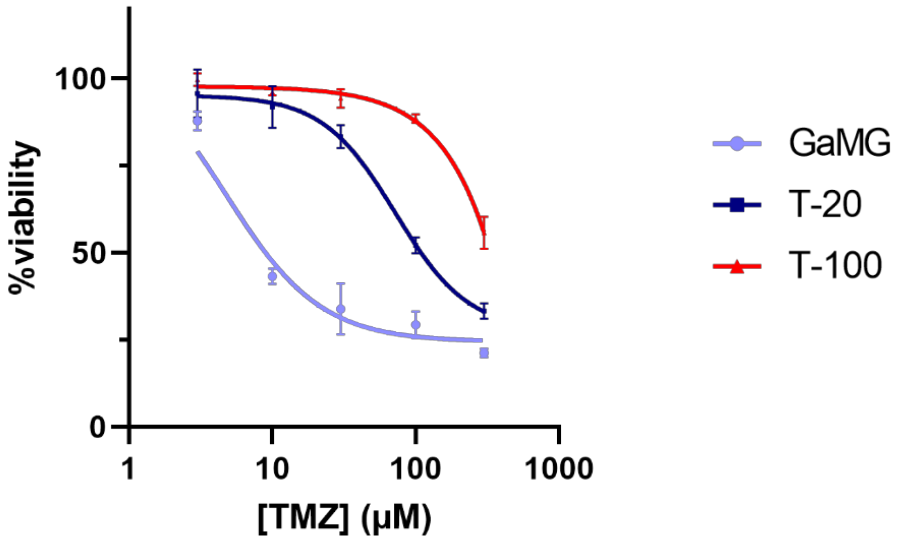
3.1.1 Response of GaMG and TMZ-resistant GaMG sublines to TMZ and other drugs

TMZ, a small molecule with a molecular weight of 194.15 g/mol, has 100% oral bioavailability, which means it is rapidly and completely absorbed after oral administration, achieving peak plasma concentration within 2 hours (Moody et al., 2014). Studies in humans show that the peak plasma concentration of TMZ is approximately 60 μM after the dose of 200 mg/m^2 (Agarwala et al., 2000, Middleton et al., 2000). The lipophilic nature of the drug also gives rise to its excellent blood-brain barrier penetration (Friedman et al., 2000), achieving a CSF concentration that is approximately 30% of the plasma concentration (Agarwala et al., 2000, Cohen et al., 2005). Therefore, TMZ concentration in the CSF is approximately 20 μM.

To better understand the acquisition of TMZ resistance, TMZ-resistant sublines T-20 and T-100 were previously generated in the Macaulay lab from TMZ-sensitive GaMG parental cells by exposure to TMZ concentrations similar to CSF (20 μM) and plasma levels (100 μM).

To confirm the TMZ resistance phenotype, the viability of GaMG, T-20 and T-100 cells were tested after treatment with TMZ. GaMG

parental cells showed significant reduction in viability at increasing concentrations of TMZ with a mean IC_{50} value of 6.88 μM, indicative of its sensitive phenotype. In contrast, T-20 and T-100 cells showed significantly higher viabilities than GaMG parental cells in the presence of 3 - 300 μM of TMZ. The mean IC_{50} values of the T-20 and T-100 cells were 98.85 μM and >300 μM respectively, confirming their resistant phenotype (Figure 3.1, Table 3.1). At 100 μM, there were significant differences in viabilities between T-20 and T-100 with T-100 maintaining higher viability (Figure 3.1, Table 3.1). This suggested that the degree of acquired resistance towards TMZ depends on the TMZ concentration the resistant sublines were repeatedly exposed to. In other words, T-20 was resistant to TMZ up to concentration of 20 μM and T-100 up to 100 μM.



Cell Line	TMZ IC_{50} (µM)
GaMG	6.88 ± 1.85
T-20	98.85 ± 14.88
T-100	>300

Figure 3.1: TMZ dose response curves of GaMG and TMZ-resistant GaMG sublines. Cells were seeded into 96-well plates and incubated overnight. The next day, the wells were treated with TMZ at 0 - 300 µM. Cell viability was tested after 5 days. Points on the graph are means ± SD of triplicate or quadruplicate technical replicates from one experiment. The table displays mean IC_{50} values for each cell line (mean ± SD), calculated based on pooled triplicate values from three independent experiments.

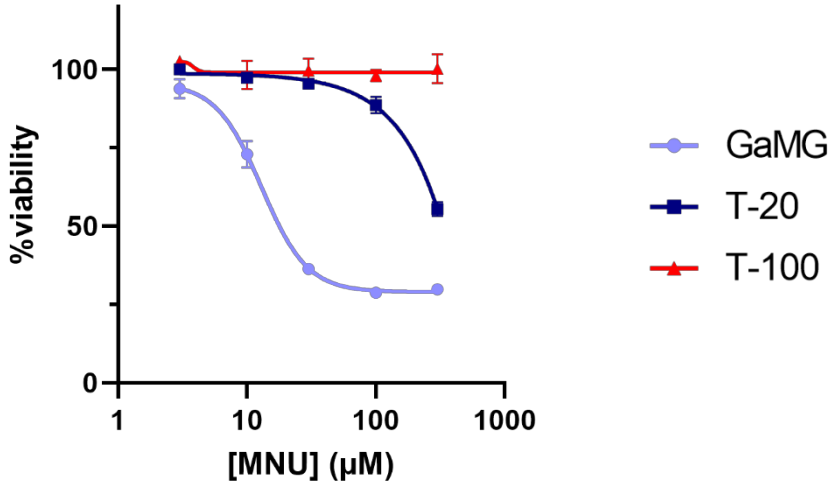
Tukey's multiple comparisons test	Significant?	Summary	Adjusted P value
0 µM			
GaMG vs. T-20	No	ns	>0.9999
GaMG vs. T-100	No	ns	>0.9999
T-20 vs. T-100	No	ns	>0.9999
3 µM			
GaMG vs. T-20	Yes	*	0.0473
GaMG vs. T-100	Yes	**	0.0036
T-20 vs. T-100	No	ns	0.4405
10 µM			
GaMG vs. T-20	Yes	****	<0.0001
GaMG vs. T-100	Yes	****	<0.0001
T-20 vs. T-100	No	ns	0.3857
30 µM			
GaMG vs. T-20	Yes	****	<0.0001
GaMG vs. T-100	Yes	****	<0.0001
T-20 vs. T-100	Yes	**	0.0041
100 µM			
GaMG vs. T-20	Yes	****	<0.0001
GaMG vs. T-100	Yes	****	<0.0001
T-20 vs. T-100	Yes	****	<0.0001
300 µM			
GaMG vs. T-20	Yes	**	0.0016
GaMG vs. T-100	Yes	****	<0.0001
T-20 vs. T-100	Yes	****	<0.0001

Table 3.1: Statistical testing of the TMZ dose response of GaMG, T-20 and T-100 cells. Results were from one representative experiment (Figure 3.1) and analysed by two-way ANOVA (*p < 0.05; **p < 0.01; ***p < 0.001; ****p < 0.0001).

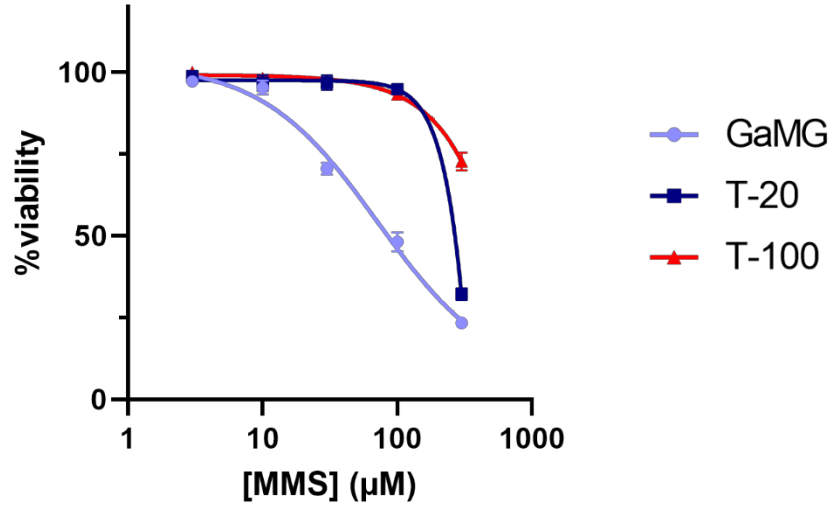
After exposure to similarly acting drugs, GaMG parental cells showed higher sensitivity towards MNU than MMS, with less than double the mean IC_{50}, and similar chemoresistance was observed in T-20 and T-100 cells (Figure 3.2A, B, D). At 10 μM MNU, T-20 and T-100 showed significantly higher viability than GaMG parental cells. At 100 μM MNU, the significant differences in viabilities between T-20 and T-100 cells as seen in TMZ-treated experiment (Figure 3.1) were also observed here, which suggested that the degree of acquired resistance towards MNU resembled that of TMZ (Table 3.2). The results suggest that the TMZ-resistant sublines are similarly resistant towards MNU. At 300 μM MNU, the viability of T-20 cells decreased but there was little change in the viability of T-100 cells (Figure 3.2A). Similarly, T-20 and T-100 cells were also resistant to MMS at concentrations up to 100 μM. At 300 μM MMS, the viability of T-20 cells was reduced to a level similar to GaMG parental cells. The viability of T-100 cells was also reduced by approximately 25% (Figure 3.2B). This suggested that T-20 cells were sensitive and T-100 cells were partially sensitive at 300 μM MMS.

In response to MMC, there was approximately 75% decrease in viabilities of all three cell lines at 1 μM and the viabilities further dropped to about 10% at 10 μM, which implied that they all responded to MMC with similar sensitivity (Figure 3.2C). Although there were some minor differences in viabilities between GaMG, T-20 and T-100 cells starting at 100 nM, the actual differences in percentages were less than 5% (Table 3.4).

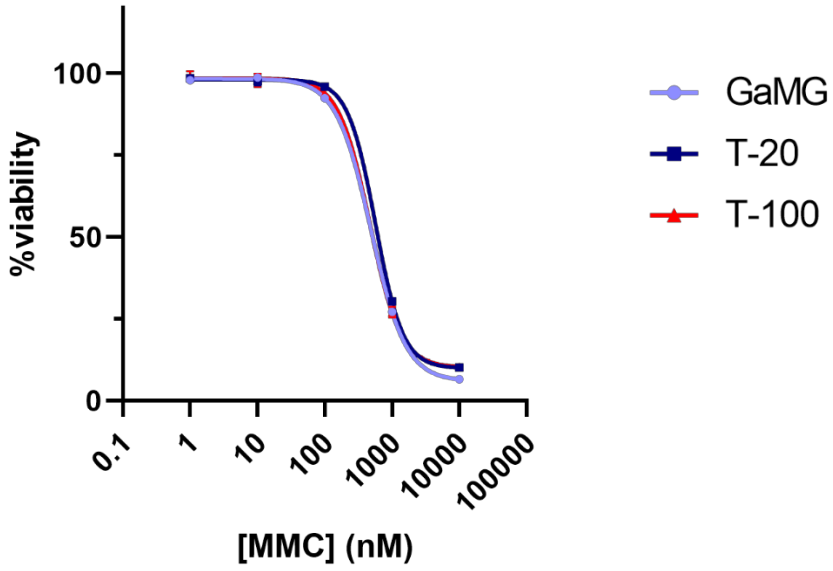
A


100
50
0
%viability
1
10
100
1000
[MNU] (µM)
GaMG
T-20
T-100

B


100
50
0
%viability
1
10
100
1000
[MMS] (µM)
GaMG
T-20
T-100

C


100
50
0
%viability
0.1
1
10
100
1000
10000
100000
[MMC] (nM)
GaMG
T-20
T-100

D

Cell Line	MNU IC_{50} (μM)	MMS IC_{50} (μM)	MMC IC_{50} (nM)
GaMG	33.62 ± 1.86	72.98 ± 11.21	500.72 ± 16.62
T-20	98.85 ± 14.88	267.11 ± 8.80	566.24 ± 58.78
T-100	>300	>300	733.08 ± 2.58

Figure 3.2: Dose response of GaMG and TMZ-resistant GaMG sublines towards MNU, MMS and MMC. Cells were seeded into 96-well plates and incubated overnight. The next day, triplicate or quadruplicate wells were treated with (A) MNU, (B) MMS or (C) MMC at indicated concentrations. Cell viability was tested after 5 days. Points on the graph are means ± SD of triplicate or quadruplicate technical replicates from one experiment. (D) IC_{50} values of each drug for each cell line (mean ± SD), calculated based on pooled triplicate values from three independent experiments.

Tukey's multiple comparisons test	Significant?	Summary	Adjusted P value
0 µM			
GaMG vs. T-20	No	ns	>0.9999
GaMG vs. T-100	No	ns	>0.9999
T-20 vs. T-100	No	ns	>0.9999
3 µM			
GaMG vs. T-20	Yes	*	0.0235
GaMG vs. T-100	Yes	**	0.0020
T-20 vs. T-100	No	ns	0.4818
10 µM			
GaMG vs. T-20	Yes	****	<0.0001
GaMG vs. T-100	Yes	****	<0.0001
T-20 vs. T-100	No	ns	0.9233
30 µM			
GaMG vs. T-20	Yes	****	<0.0001
GaMG vs. T-100	Yes	****	<0.0001
T-20 vs. T-100	No	ns	0.1604
100 µM			
GaMG vs. T-20	Yes	****	<0.0001
GaMG vs. T-100	Yes	****	<0.0001
T-20 vs. T-100	Yes	***	0.0004
300 µM			
GaMG vs. T-20	Yes	****	<0.0001
GaMG vs. T-100	Yes	****	<0.0001
T-20 vs. T-100	Yes	****	<0.0001

Table 3.2: Statistical testing of the MNU dose response of GaMG, T-20 and T-100 cells. Results were from one representative experiment (Figure 3.2A) and analysed by two-way ANOVA (*p < 0.05; **p < 0.01; ***p < 0.001; ****p < 0.0001).

Tukey's multiple comparisons test	Significant?	Summary	Adjusted P value
0 µM			
GaMG vs. T-20	No	ns	>0.9999
GaMG vs. T-100	No	ns	>0.9999
T-20 vs. T-100	No	ns	>0.9999
3 µM			
GaMG vs. T-20	No	ns	0.4745
GaMG vs. T-100	No	ns	0.1368
T-20 vs. T-100	No	ns	0.6357
10 µM			
GaMG vs. T-20	No	ns	0.5406
GaMG vs. T-100	No	ns	0.1178
T-20 vs. T-100	No	ns	0.5171
30 µM			
GaMG vs. T-20	Yes	****	<0.0001
GaMG vs. T-100	Yes	****	<0.0001
T-20 vs. T-100	No	ns	0.9226
100 µM			
GaMG vs. T-20	Yes	****	<0.0001
GaMG vs. T-100	Yes	****	<0.0001
T-20 vs. T-100	No	ns	0.4883
300 µM			
GaMG vs. T-20	Yes	****	<0.0001
GaMG vs. T-100	Yes	****	<0.0001
T-20 vs. T-100	Yes	****	<0.0001

Table 3.3: Statistical testing of the MMS dose response of GaMG, T-20 and T-100 cells. Results were from one representative experiment (Figure 3.2B) and analysed by two-way ANOVA (*p < 0.05; **p < 0.01; ***p < 0.001; ****p < 0.0001).

Tukey's multiple comparisons test	Significant?	Summary	Adjusted P value
0 µM			
GaMG vs. T-20	No	ns	>0.9999
GaMG vs. T-100	No	ns	>0.9999
T-20 vs. T-100	No	ns	>0.9999
1 nM			
GaMG vs. T-20	No	ns	0.7006
GaMG vs. T-100	No	ns	0.3037
T-20 vs. T-100	No	ns	0.7108
10 nM			
GaMG vs. T-20	No	ns	0.3125
GaMG vs. T-100	No	ns	0.5196
T-20 vs. T-100	No	ns	0.9515
100 nM			
GaMG vs. T-20	Yes	****	<0.0001
GaMG vs. T-100	No	ns	0.1556
T-20 vs. T-100	Yes	*	0.0311
1 µM			
GaMG vs. T-20	Yes	***	0.0004
GaMG vs. T-100	No	ns	0.9765
T-20 vs. T-100	Yes	***	0.0002
10 µM			
GaMG vs. T-20	Yes	****	<0.0001
GaMG vs. T-100	Yes	****	<0.0001
T-20 vs. T-100	No	ns	0.9331

Table 3.4: Statistical testing of the MMC dose response of GaMG, T-20 and T-100 cells. Results were from one representative experiment (Figure 3.2C) and analysed by two-way ANOVA (*p < 0.05; **p < 0.01; ***p < 0.001; ****p < 0.0001).

3.1.2 Response of GaMG and TMZ-resistant GaMG sublines to IR

As compared to the best supportive care only or chemotherapy without radiation, postoperative RT shows a statistically significant survival benefit in five out of six clinical trials (Andersen, 1978, Kristiansen et al., 1981, Michael et al., 1978, Sandberg-Wollheim et al., 1991, Shapiro et al., 1976, Walker et al., 1980). This establishes the importance of RT in GBM management.

Clonogenic assays are the gold standard for assessing radiosensitivity (Nuryadi et al., 2018). After irradiation, clonogenic assays were employed to investigate the ability of single cells to form colonies of 50 cells or more, and hence measure the survival and proliferation of GBM cells.

To determine the response of GaMG and TMZ-resistant GaMG sublines to irradiation, the cells were treated with the indicated doses (Figure 3.3). The clonogenicities of all three sublines were similar up to 4 Gy. There were some statistically significant differences at 6 Gy and above (Table 3.5), but the differences were small and unlikely to be biologically important. Overall, all three sublines exhibited radio-resistance, maintaining clonogenicity of more than 60% even after a single dose of 6 Gy and more than 10% post 10 Gy irradiation. These results were somewhat different to that of another study, where GaMG was radio-sensitive, showing less than 10% clonogenicity after 8 Gy irradiation (Kuger et al., 2013). The reason behind this inconsistency remains to be elucidated. Nevertheless, the little difference in

radiosensitivity between GaMG, T-20 and T-100 cells suggested that the acquisition of TMZ resistance did not affect the radiosensitivity of GBM cells.

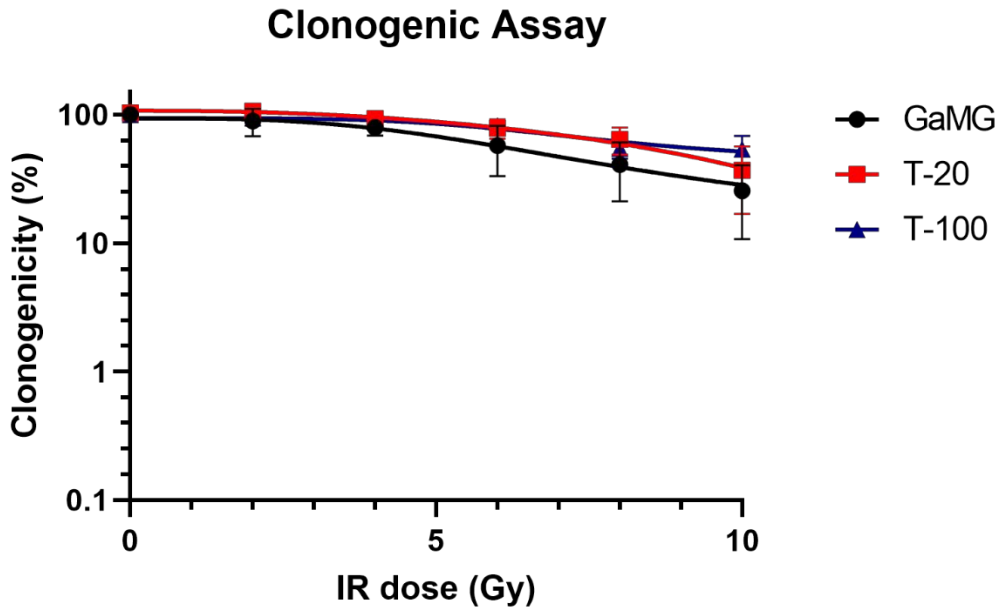


Figure 3.3: Radiation dose response of GaMG, T-20 and T-100 cells. The cells were seeded at 5000 single cells per 10cm plate in triplicate and incubated overnight. The next day, plates were irradiated at indicated doses (0-10 Gy) and subsequently incubated for 10 - 12 days until individual colonies of more than 50 cells were observed. The colonies were counted using GelCount™ software. Points on the graph are means ± SD of pooled triplicate values from three independent experiments.

Tukey's multiple comparisons test	Significant?	Summary	Adjusted P value
0 Gy			
GaMG vs. T-20	No	ns	0.9029
GaMG vs. T-100	No	ns	>0.9999
T-20 vs. T-100	No	ns	0.8907
2 Gy			
GaMG vs. T-20	No	ns	0.0542
GaMG vs. T-100	No	ns	0.7640
T-20 vs. T-100	No	ns	0.2103
4 Gy			
GaMG vs. T-20	No	ns	0.1509
GaMG vs. T-100	No	ns	0.4943
T-20 vs. T-100	No	ns	0.7041
6 Gy			
GaMG vs. T-20	Yes	**	0.0074
GaMG vs. T-100	Yes	**	0.0023
T-20 vs. T-100	No	ns	0.8869
8 Gy			
GaMG vs. T-20	Yes	**	0.0060
GaMG vs. T-100	No	ns	0.2014
T-20 vs. T-100	No	ns	0.4886
10 Gy			
GaMG vs. T-20	No	ns	0.2471
GaMG vs. T-100	Yes	***	0.0003
T-20 vs. T-100	Yes	*	0.0407

Table 3.5: Statistical testing of the radiation dose response of GaMG, T-20 and T-100. Results were from three independent experiments (Figure 3.3) and analysed by two-way ANOVA (*p < 0.05; **p < 0.01; ***p < 0.001; ****p < 0.0001).

3.1.3 Characterisation of mismatch repair proteins and MGMT in GaMG, T-20 and T-100 cells

MMR is required for the cytotoxicity of TMZ and MMR defects have been implicated in TMZ resistance (see section 1.2.1 and 1.3.2) (Tentori et al., 2009, Liu et al., 1996, McFaline-Figueroa et al., 2015). To investigate the role of MMR in the acquisition of TMZ resistance, the levels of major MMR proteins were examined by Western blotting. Experiments suggested that there was no significant difference in the level of MMR proteins between GaMG, T-20 and T-100 cells. All three sublines expressed similar levels of MSH6, MSH2 and MLH1 (Figure 3.4). These data suggested that MMR machinery might not contribute towards acquisition of TMZ resistance in GaMG cells.

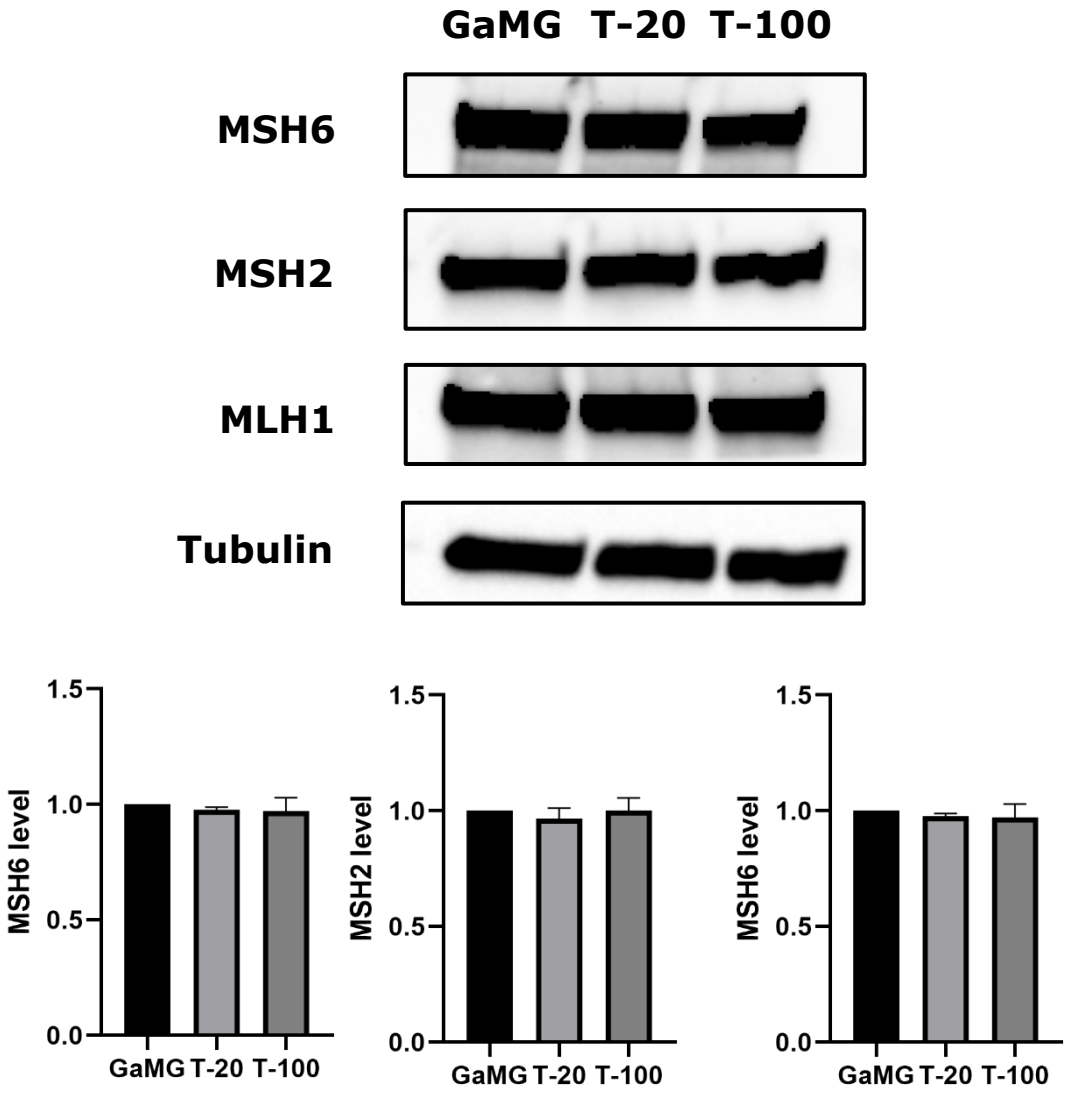


Figure 3.4: Characterisation of the MMR proteins in GaMG and TMZ-resistant GaMG sublines. Protein levels were studied in whole cell lysates extracted from thawed cell pellets. The bands were quantified using ImageJ and normalised using tubulin as the loading control. The protein levels were compared against GaMG cell lysates. The graphs were plotted as means ± SD based on pooled triplicate values from three independent experiments. Results were analysed using one-way ANOVA.

TMZ resistance has been largely attributed to MGMT overexpression (Hegi et al., 2005, Stupp et al., 2005). To determine whether MGMT was responsible for the TMZ resistance in T-20 and T-100 cells, MGMT expressions in all three cell lines was assessed. MGMT was not detected in GaMG parental cells but it was found that MGMT protein was clearly upregulated in T-20 and T-100 cells (Figure 3.5A). When compared to GaMG parental cells, MGMT protein level was more than 50 times higher in T-20 cells and more than 100 times higher in T-100 cells (Figure 3.5B).

Assessing the transcriptional differences between sublines also showed similar results, with almost 100 times more *MGMT* mRNA in T-20 cells and 150 times more in T-100 cells than in the GaMG parental cells (Figure 3.5C), perhaps suggesting a mechanism of MGMT-mediated acquired TMZ resistance.

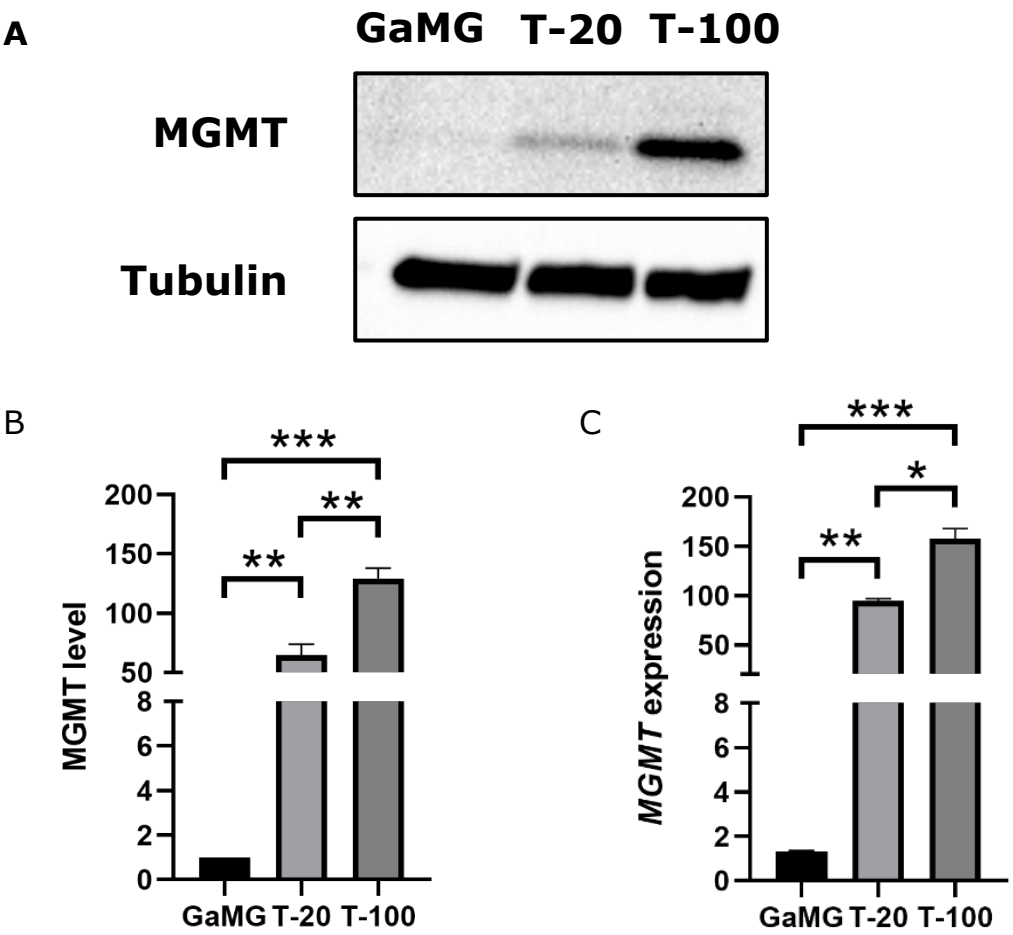


Figure 3.5: Characterisation of MGMT protein and mRNA expression in GaMG and GaMG sublines. (A) Western blot analysis of whole cell lysates showing MGMT levels in GaMG, T-20 and T-100 sublines. The blot was quantified using ImageJ and normalised using tubulin as the loading control. The protein levels were compared against GaMG cells. (B) The graphs were plotted as means ± SD. (C) Relative expression of *MGMT* in the three sublines plotted as means ± SD. The expressions were analysed for statistical significance using ordinary one-way ANOVA. Both graphs were plotted based on pooled triplicate values from three independent experiments.

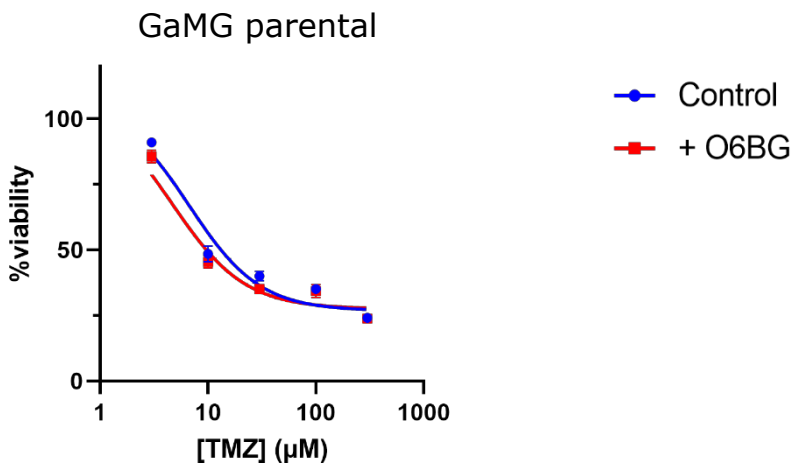
3.1.4 The effect of O6BG on the sensitivity of GaMG sublines to TMZ

To test whether MGMT was responsible for TMZ resistance in this model, O6BG was used. The O6BG concentration used here had been reported in the literature for human hematopoietic cells (Davis et al., 2001). Following pre-incubation with O6BG, there was no significant difference in sensitivity towards TMZ observed in GaMG parental and T-100 cells. However, there was a significant reduction in T-20 cell viability at increasing doses of TMZ, suggesting an increase in TMZ sensitivity (Figure 3.6). Although there was a significant decrease in the IC_{50} of T-20 cells after adding O6BG, the values were still approximately two times higher than that of the baseline level in the GaMG parental cells (Figure 3.6D). This result indicated that O6BG did not reverse TMZ resistance in T-100 cells and caused a partial reversal of TMZ resistance in T-20 cells.

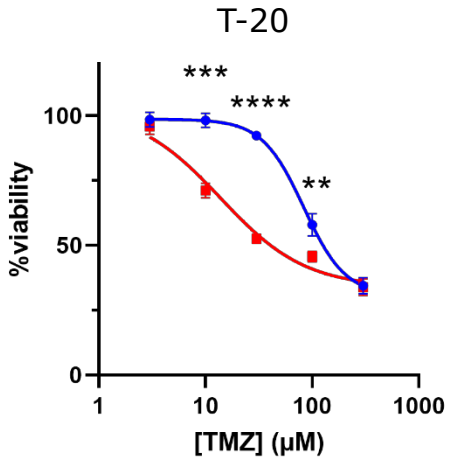
Similar to the aforementioned data, the results by the previous DPhil student Victoria Ma (Macaulay Group) also showed that acquired TMZ resistance of T-20 cells was partially reversed by O6BG as well as *MGMT* depletion by siRNA. These results supported data previously generated in the Macaulay lab showing that T-20 and T-100 cells had a different degree of acquired resistance towards TMZ depending on the TMZ concentration they were cultured in. The different response of T-20 and T-100 cells towards MGMT inhibition also implied different mechanism(s) of resistance.

Collectively, these results suggested that there are more mechanisms underlying acquired TMZ resistance that remain to be identified.

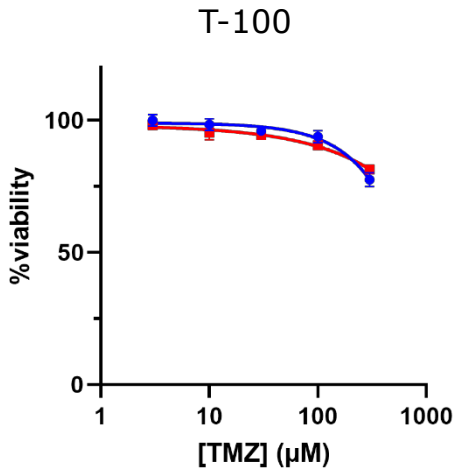
A


GaMG parental
Control
+ O6BG
%viability
100
50
0
1
10
100
1000
[TMZ] (µM)

B


T-20
***
****
**
%viability
100
50
0
1
10
100
1000
[TMZ] (µM)

C


T-100
%viability
100
50
0
1
10
100
1000
[TMZ] (µM)

D

Cell Line	Control IC_{50} (μM)	+ O6BG IC_{50} (μM)
GaMG	14.32 ± 0.98	23.34 ± 4.85
T-20	102.23 ± 4.51	42.67 ± 2.62
T-100	>300	>300

Figure 3.6: Investigation of the effect of O6BG on GaMG parental, T-20 and T-100 cell viability after TMZ treatment. Cells were seeded into 96-well plates and incubated overnight. The following day, cells were pre-incubated with 25 μM of O6BG for at least 2 hours, then TMZ was added into each well, diluting O6BG concentration to 20 μM. Cell viability was tested after 5 days. Graphs show the corresponding dose response curves of (A) GaMG parental, (B) T-20 and (C) T-100 cells. Points on the graph are means ± SD of triplicate values. (D) shows the IC_{50} for each cell line, calculated based on pooled triplicate values from three independent experiments. The results were analysed for statistical significance using unpaired student's t-tests (**p < 0.01; ***p < 0.001; ****p < 0.0001).

To investigate whether efflux pump played a role in this model, MGMT levels before and after TMZ exposure were examined. It was expected that MGMT would be consumed if TMZ was entering the cells as MGMT was degraded after receiving a methyl group from O^6-meG (Tolcher et al., 2003). Conversely, MGMT levels would be unaffected if TMZ was not able to enter the cells.

Herein, MGMT levels were significantly reduced in both T-20 and T-100 cells after treatment with TMZ and was further decreased with the addition of MGMT inhibitor O6BG (Figure 3.7). Depletion of MGMT after O6BG treatment has previously been reported in the literature (Kaina et al., 2010). Upon 100 μM TMZ treatment, MGMT level in T-20 cells were decreased, however T-100 cells displayed no changes to MGMT level. Exposure to 300 μM TMZ showed a further reduction in MGMT level in T-20 cells, and a decrease in T-100 cells.

These results suggested that TMZ was entering the cells and consumed MGMT. Therefore, an efflux pump mechanism of resistance was unlikely.

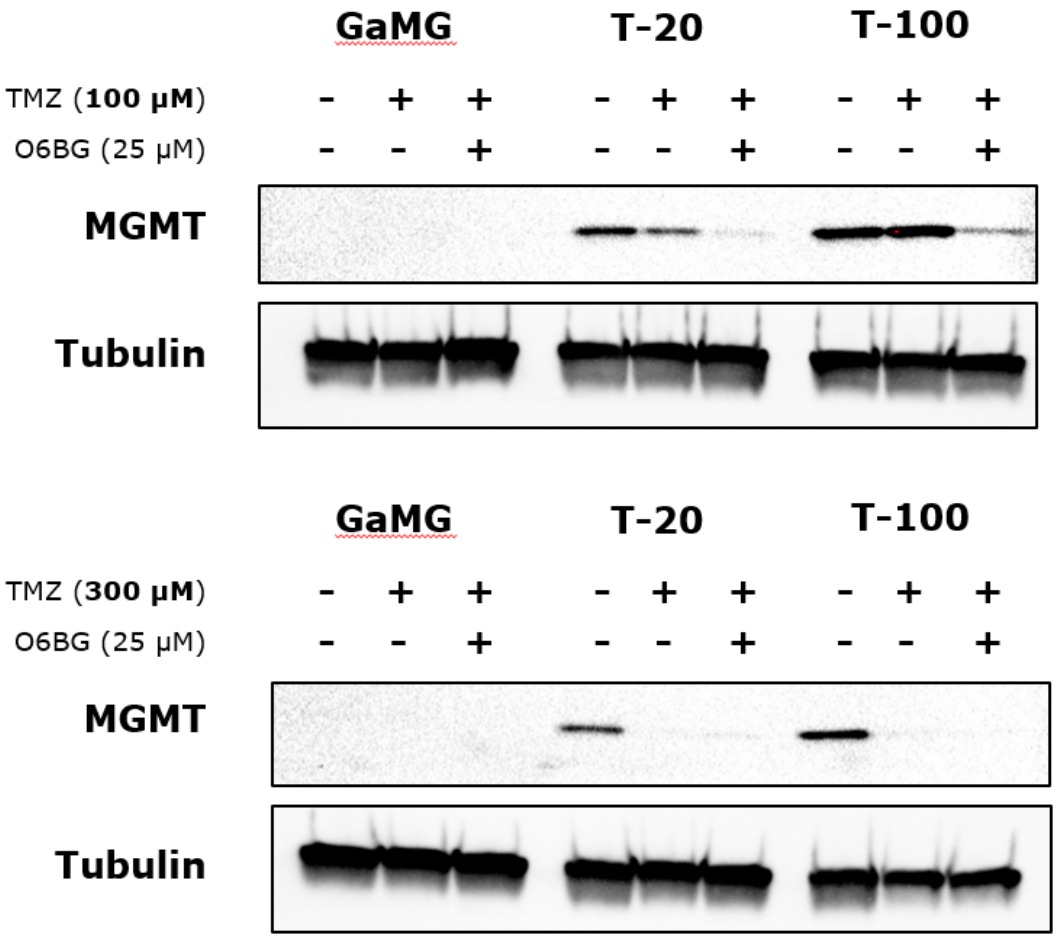


Figure 3.7: Level of MGMT protein after TMZ exposure. Western blot of whole cell lysates showing MGMT protein levels. The cells were treated with 100 µM and 300 µM of TMZ for 3 - 4 days with or without 25 µM of MGMT inhibitor O6BG before lysates were extracted as described previously. A similar result was obtained in a second independent experiment.

3.2 Discussion

The sensitivity of GaMG parental cells towards TMZ and the different extent of acquired resistance towards TMZ observed in T-20 and T-100 cells recapitulated the prior establishment of TMZ-resistant GBM cell sublines from a previously sensitive cell line.

Like TMZ, both MNU and MMS are methylating agents, which predominantly gives rise to N^7-methylguanine and N^3-methyladenine lesions, however MNU can also produce O^6-methylguanine (Beranek, 1990, Wurdeman et al., 1993). Therefore, the methylation pattern of MNU is quite similar to that of TMZ. In contrast, MMC interacts with the DNA by forming interstrand crosslinks and monoadducts (Fu et al., 2012) whereas irradiation induces mainly strand breaks (Toulany, 2019). The cross-resistance of the TMZ-resistant GaMG sublines T-20 and T-100 cells towards the methylating agents MNU and MMS but not the intercalating agent MMC and radiation indicated that the mechanisms of resistance were more likely to lie within, at least in part, the methylation pathway, for example, through enhanced repair of methylation rather than repair of the resulting strand breaks. To rule out the possibility that the apparent sensitivity of T-20 and T-100 cells towards MMC was due to overdose, the summary product characteristics of the drug was referred to. The MMC treatment concentrations used here were within the range of maximal serum concentrations after intravenous injections. This confirmed the clinical relevance of MMC concentrations used in the experiment.

As explained (section 1.2.1, Figure 1.3), cytotoxicity of TMZ requires a proficient MMR system. MMR deficiency plays a role in the acquisition of TMZ resistance in GBM cells (Stritzelberger et al., 2018) and causes GBM recurrence after current standards of care (Felsberg et al., 2011). Although it was shown here that there was no significant difference in the levels of key MMR proteins which suggested non-MMR mediated TMZ resistance, the amount of proteins present did not always represent activity. Therefore, further experiments would be needed to clarify the role of MMR in the acquisition of TMZ resistance in the resistant sublines. If time had allowed, MMR reporter experiments using fluorescence detection could have been performed (Ito et al., 2018). Briefly, the GaMG sublines are transformed with an expression plasmid containing a mismatch that generates a stop codon in the enhanced green fluorescent protein (eGFP) gene. MMR-proficient cells are able to recognise and repair the mismatch, hence eGFP is expressed and fluorescence can be detected in the cells using fluorescence microscopy. By comparing the fluorescence, the difference in MMR activity across GaMG parental and the resistant sublines could be assessed.

The expression of MGMT is an important component that renders the GBM tumours intrinsically more resistant to TMZ. It is a suicide protein that directly removes the cytotoxic O^6-methyl adducts from guanine residues. The MGMT promoter methylation status has been shown to be a strong prognostic factor that predicts survival in patients

with newly diagnosed GBM and a powerful predictor of TMZ sensitivity (Esteller et al., 2000, Gorlia et al., 2008, Hegi et al., 2004, Weller et al., 2009). The reduction of MGMT levels displayed in the resistant sublines after treatment with TMZ (Figure 3.7) could suggest that TMZ was entering the cells and causing O^6 methylation lesions, which were then repaired by MGMT and the protein was consumed, hence making an efflux pump mechanism unlikely. Further work such as pulse chase analysis or cycloheximide experiments could be undertaken to confirm MGMT protein consumption.

O6BG is a potent inhibitor of MGMT, which acts as a pseudo-substrate and transfers its benzyl group to the active site-cysteine of MGMT, thereby irreversibly inactivating and depleting the demethylating protein (Friedman et al., 2002, Kaina et al., 2010). The observation of MGMT levels being further reduced after combination treatment with TMZ and O6BG indicated satisfactory inhibition and then depletion of the demethylating protein, thereby validating the viability results observed after MGMT inhibition (Figure 3.7). Nevertheless, O6BG inhibition has not been found to be clinically effective in reversing TMZ resistance (see section 1.3.1).

GaMG cells, which did not express endogenous MGMT, were sensitive towards TMZ. However, despite the pre-inhibition of MGMT, O6BG only partially restored the sensitivity of T-20 cells towards TMZ and did not exert any detectable effect on T-100 cells, although MGMT was significantly upregulated in T-100 cells. This suggested that MGMT

might only partially mediate the acquisition of TMZ resistance in the T-20 cells. Furthermore, clonal analyses of patient tumours revealed that the expression of the biomarker MGMT did not always correlate with TMZ resistance (Meyer et al., 2015), which was consistent with the results reported here and therefore highlighting a limitation of this marker. Collectively, the results suggested that new mechanisms or biomarkers underlying TMZ responsiveness remained to be found. It should be noted that there were several limitations of the experiments. Firstly, MGMT presence did not represent its enzymatic activity. Therefore, an *in vitro* biochemical MGMT activity assay utilising radiolabelled oligodeoxynucleotides could be used to assess the functional activity of MGMT in the cells and hence determining the efficacy of O6BG (Nagel et al., 2019). Additionally, it would be informative to measure γH2A.X foci or p53-binding protein 1 (53BP1) to assess the degree of DNA damage observed, and apoptosis assays to check whether differences in viability observed in GaMG and the TMZ-resistant sublines were due to delayed growth or cell death in GaMG sublines.

In summary, this work suggested that TMZ-resistant GaMG sublines were cross-resistant towards other methylating agents. Further, TMZ resistance might not involve defects in MMR machinery or an efflux pump mechanism and could be only partially mediated by MGMT. Additional work is needed to identify the novel mechanisms of TMZ resistance in GBM cells.

Chapter 4: Investigation of genetic alterations underlying acquired temozolomide resistance in GBM

4.1 Results

4.1.1 Differential expression analysis across GaMG sublines

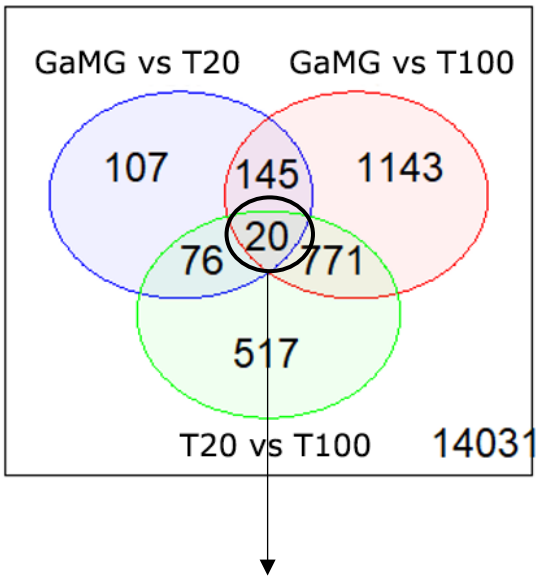
The induced TMZ resistance in T-20 and T-100 could be due to multiple mechanisms. To begin with, GaMG and its sublines were sorted by Victoria Ma (Macaulay group) into 96-well plates using fluorescence-activated cell sorting (FACS) (Ma, 2019) and the scRNA-seq analysis was performed by Dr Neil Ashley from the Weatherall Institute of Molecular Medicine in Oxford. Sequencing data from 96 single cells were analysed for each subline. Then, the bioinformatic data analysis was done by Dr Dimitrios Voukantsis from Prof. Francesca Buffa lab.

GBM tumours are well known for their heterogeneous nature (Inda et al., 2014), and performing scRNA-seq can be informative as it allows quantitative and unbiased characterisation of cellular heterogeneity and account for cell-to-cell variability.

A differentially expressed (DE) gene is defined as gene that showed $\log_2$-fold change of 1.0 (i.e. two-fold change in expression) and a p-value of less than 0.05. The scRNA-seq data analyses performed by Dr Voukantsis revealed that there was a total of 2779 DE genes while comparing GaMG, T-20 and T-100 cells, where the greatest number of DE genes fell in the comparison between GaMG

versus T-100, with 2079 DE genes (Figure 4.1A). There were 20 genes that were differentially expressed between the 3 sublines, and each of their relative expression levels are presented in Figure 4.1B. The top half of the heat map showed the DE genes that were overexpressed in the TMZ-resistant sublines, which included *MGMT*, *RRAD*, *BCAT1*, *CT83* and *CPNE8*, whereas the bottom half showed the DE genes which were overexpressed in the GaMG parental cells, for instance *EBF1* and *MEST*. From these 20 DE genes, several candidates were chosen for validation based on the discussion between me and Dr Voukantsis, as it was hypothesised that the potential mechanisms underlying the resistance could be differentially expressed between the TMZ-sensitive GaMG parental cells and TMZ-resistant GaMG sublines.

A



B

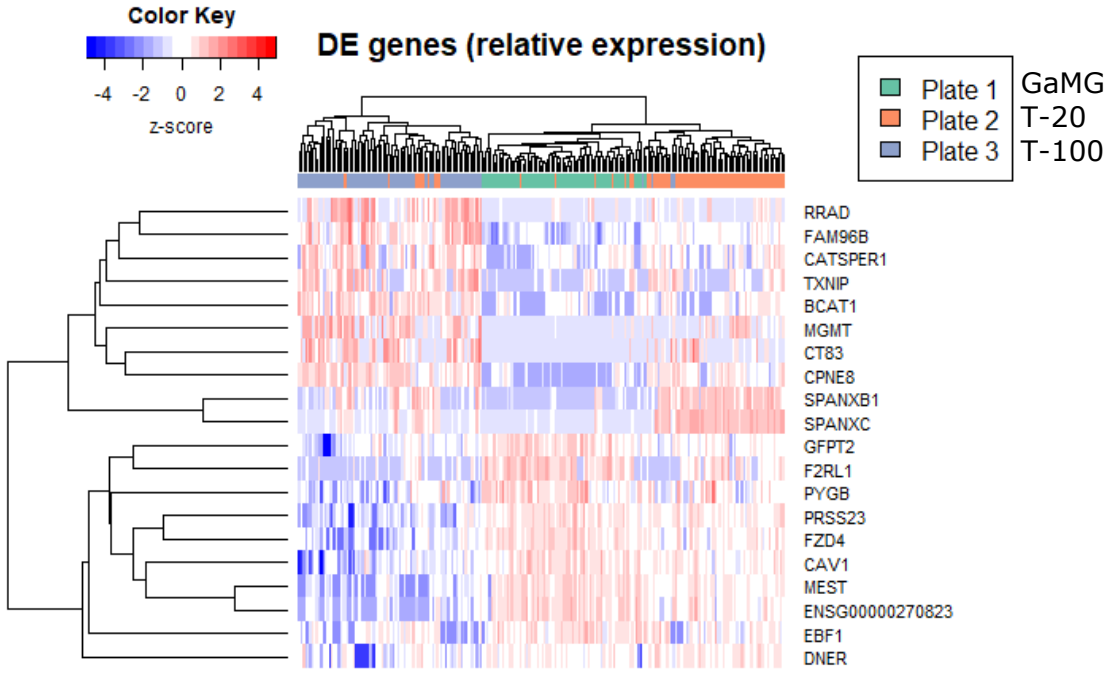


Figure 4.1: Differential expression analyses between GaMG, T-20 and T-100 (by Dr Voukantsis). (A) Comparison of number of DE genes across the three sublines. Methods used include Wilcox/Mann-Whitney-U Test, edgeR and MAST. (B) Heat map showing the relative expression of each of the 20 DE genes that was shared across the 3 sublines.

In addition, all the DE genes were tested by Dr Voukantsis for the Gene Ontology (GO) terms and Kyoto Encyclopedia of Genes and Genomes (KEGG) pathways that were enriched, which identified many terms and pathways associated with the DE genes such as Notch signalling, regulation of the inflammatory response and NF-κB signalling pathway (Figure 4.2, Figure 4.3, Figure 4.4).

Although the GO over-representation analysis had identified many enriched GO terms for the DE genes between GaMG and T-20 cells as well as GaMG and T-100 cells, there was no enriched GO term between T-20 and T-100 cells. On the other hand, there were only enriched KEGG pathways between GaMG and T-20 cells, whereas analysis of the DE genes for GaMG vs T-100 cells and T-20 vs T-100 cells did not show any KEGG pathways to be enriched. In other words, there were no common pathways in all three sublines.

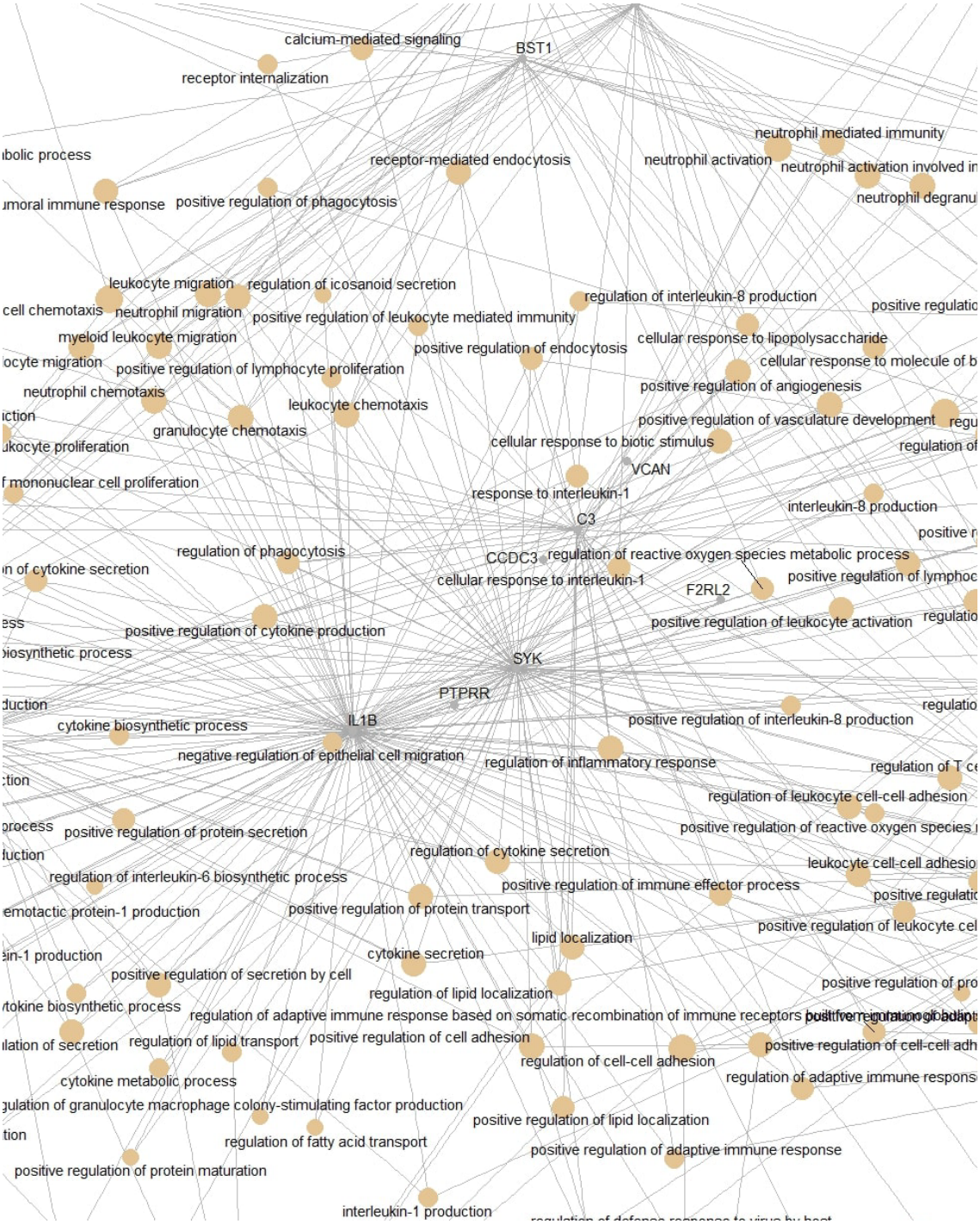


Figure 4.2: The enriched GO terms for the DE genes between GaMG and T-20 cells (by Dr Voukantsis). Image was cropped for improved legibility. The size of dots represents the count of genes in each term.

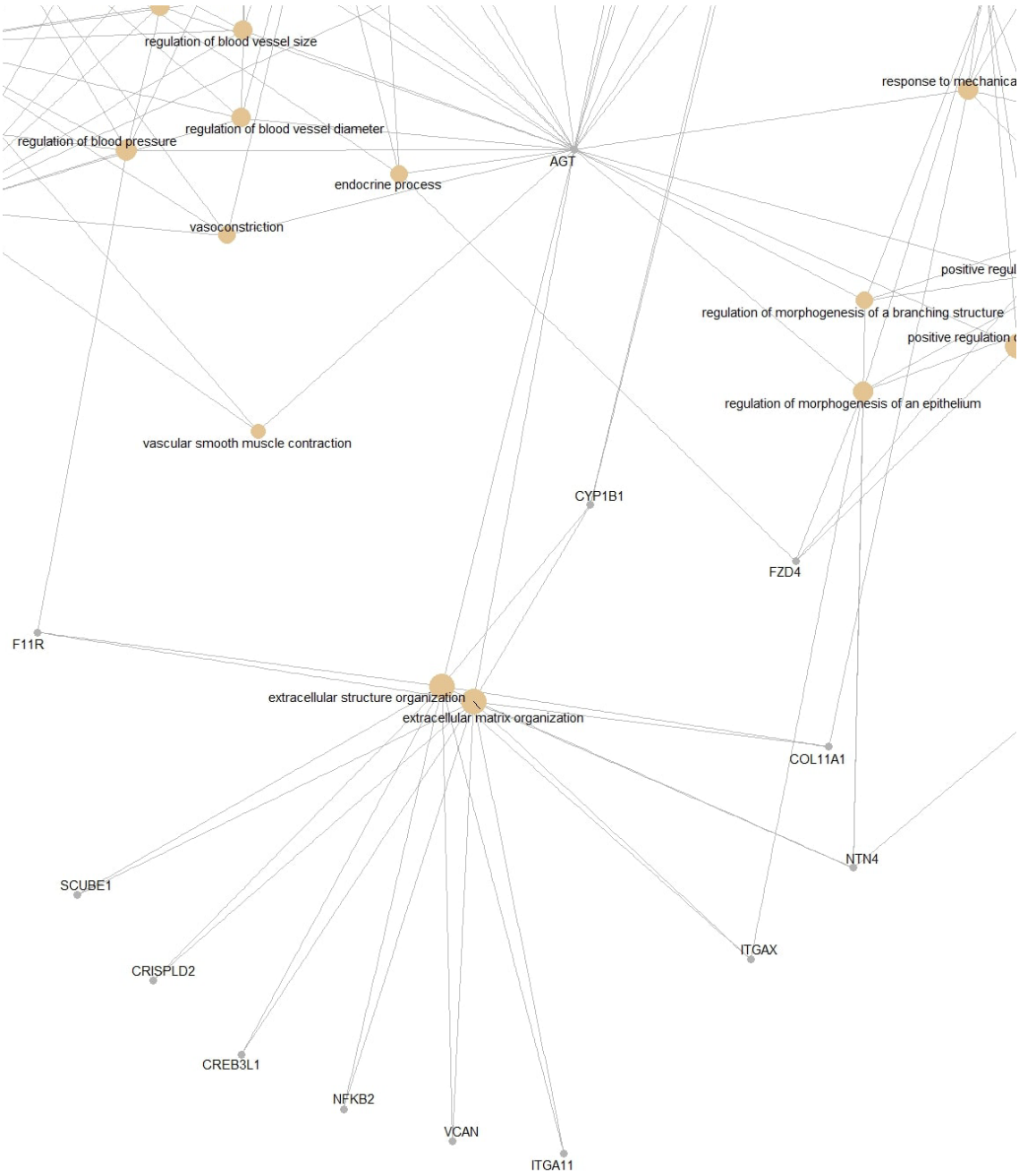


Figure 4.3: The enriched GO terms for the DE genes between GaMG and T-100 cells (by Dr Voukantsis). Image was cropped for improved legibility. The size of dots represents the count of genes in each term.

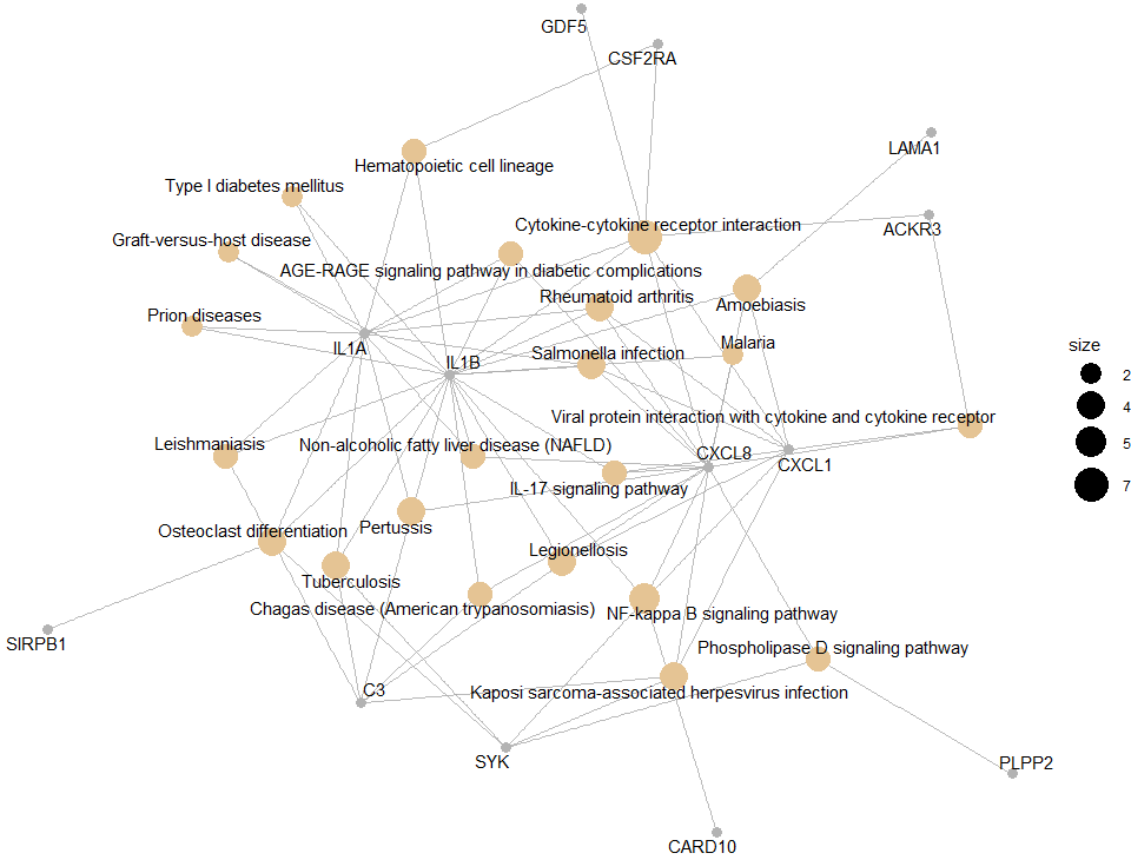


Figure 4.4: The enriched KEGG pathways for the DE genes between GaMG and T-20 cells (by Dr Voukantsis). The size of the dots represents the gene count enriched in the associated pathway.

4.1.2 Heterogeneity of GaMG and TMZ-resistant GaMG sublines

To understand more about the heterogeneity of GaMG sublines, t-distributed stochastic neighbour embedding (t-SNE) analysis was performed by Dr Voukantsis, where cells with similar multi-dimensional phenotypes are plotted close to each other (Kobak et al., 2019). The analysis indicated that all three of the GaMG sublines were heterogeneous but T-20 cells were more heterogeneous than GaMG and T-100 cells, appearing to have three separate clusters, one more than its two counterparts (Figure 4.5).

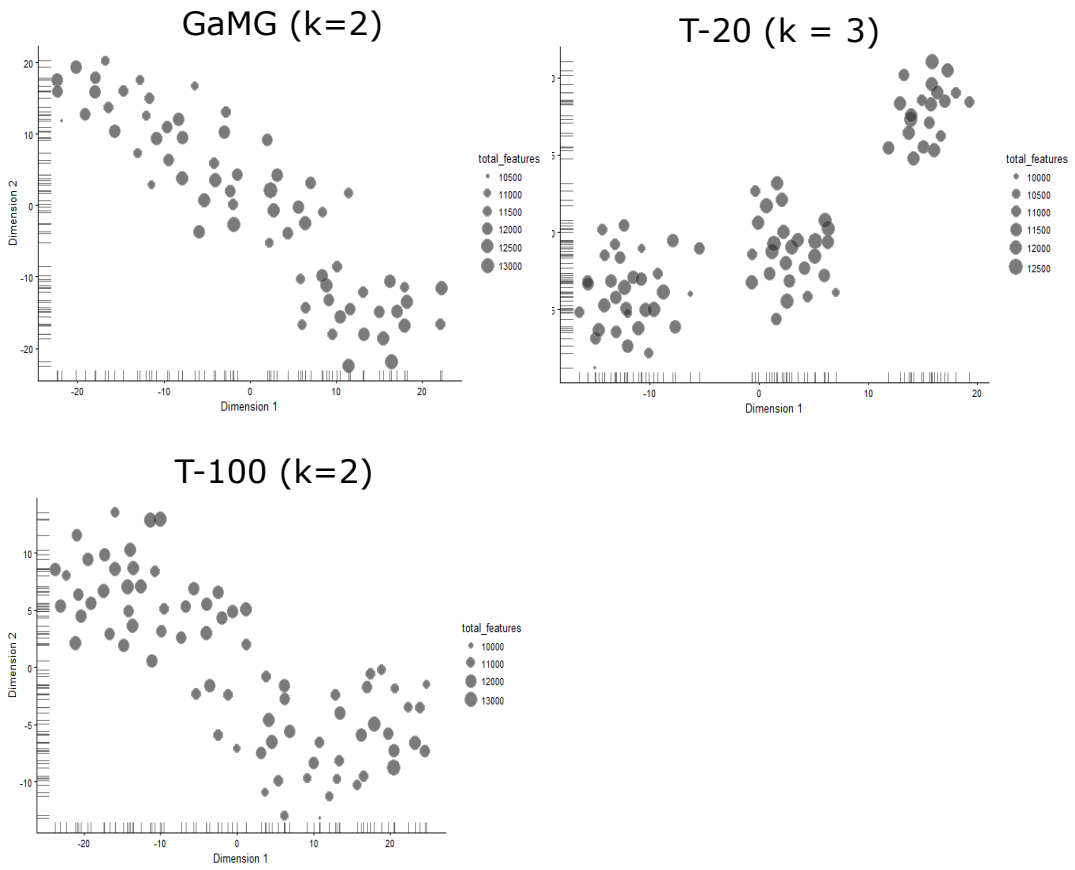


Figure 4.5: t-SNE plots showing the heterogeneity analysis of GaMG, T-20 and T-100 cells (by Dr Voukantsis).

Despite being the most frequently used approach in single-cell analysis, there are limitations in t-SNE analysis which include being computationally expensive, the inability to be used in very large datasets, as well as the loss of global structure such as inter-cluster relationships and distances, leading to potentially misleading visualisations (Kobak et al., 2019). Therefore, uniform manifold approximation and projection (UMAP) analysis was also utilised by Dr Voukantsis in this heterogeneity analysis as it preserves local and global structure of the data (Becht et al., 2019). There was a total of four different clusters in the three sublines where cluster 0 appeared in mostly GaMG parental cells and some in T-20 cells whereas cluster 2 occurred mostly in T-20 cells and only a few in the GaMG plate. Cluster 1 and 3 were exclusively in T-100 cells. These analyses indicated a different composition of cells across the three sublines, especially between T-20 and T-100 cells (Figure 4.6).

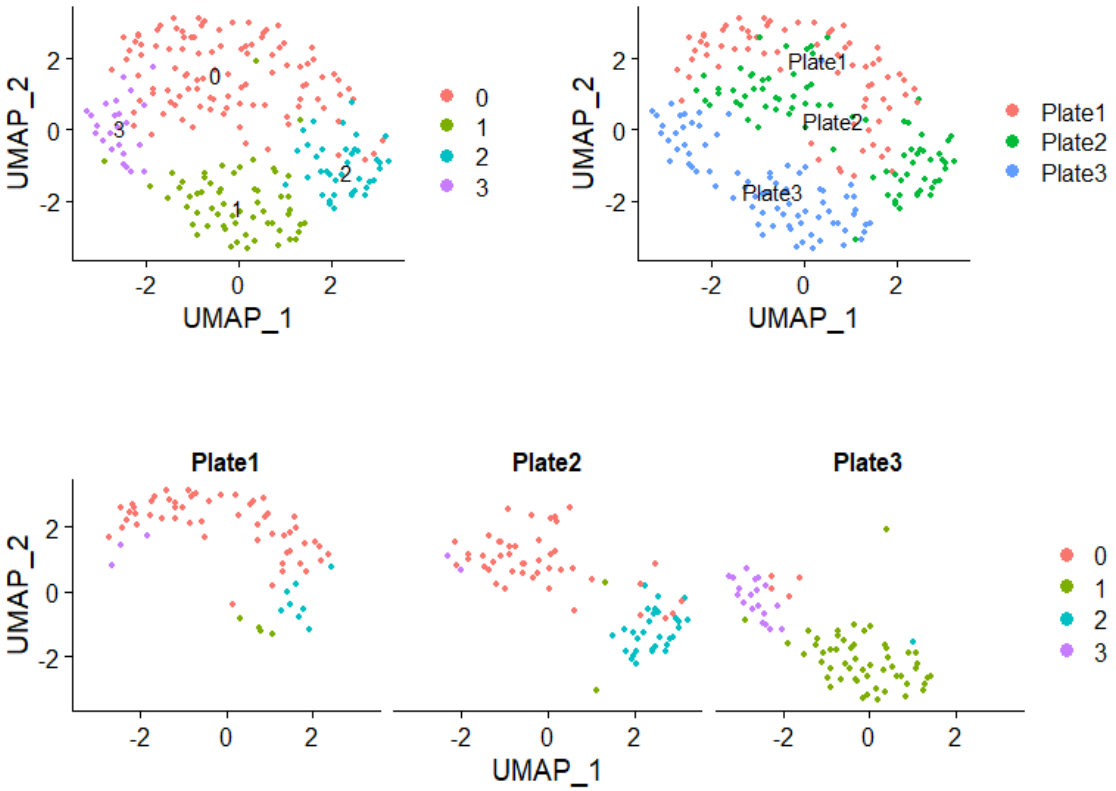


Figure 4.6: UMAP projections showing different clusters of GaMG sublines (by Dr Voukantsis). Plate 1 is GaMG parental cells, plate 2 and 3 represent T-20 and T-100 cells respectively.

A pseudotime analysis was then performed by Dr Voukantsis using Slingshot to understand the relationship between the identified clusters. Slingshot is a programming tool for lineage branching reconstruction and pseudotime inference from scRNA-seq data (Street et al., 2018). The result suggested that there were two trajectories originating from the initial population of cluster 0, which mainly occurred in GaMG parental cells (Figure 4.7). One branching trajectory evolved from cluster 0 into cluster 2 and then cluster 1 whereas the other trajectory showed cluster 0 developing into cluster 3. This seemed to suggest that T-20 cells were directly descended from GaMG parental cells and T-100 cells were made up of clusters evolved from both GaMG and T-20 sublines.

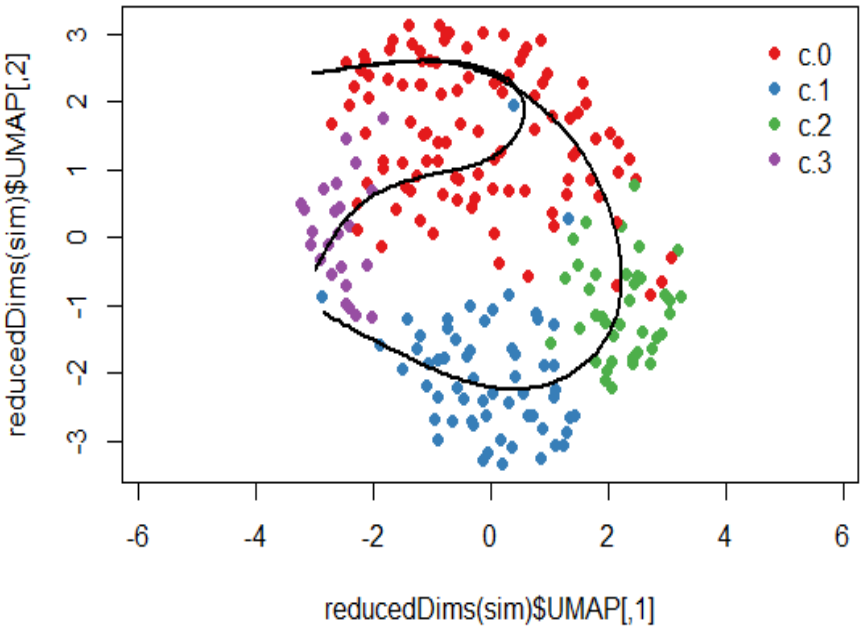


Figure 4.7: Pseudotime trajectories of the four different clusters (by Dr Voukantsis).

Next, the differential expression between the two trajectory paths was investigated by Dr Voukantsis. The greatest number of DE genes occurred in the comparison between cluster 2 and 0 with 276 of DE genes, and there were no shared DE genes among the four clusters. (Figure 4.8). The list of DE genes was also tested by Dr Voukantsis for enriched Gene Ontology terms as well as KEGG pathways and the pathways associated with the DE genes were identified, including DNA replication and Fanconi anaemia pathway (Figure 4.9 - Figure 4.17).

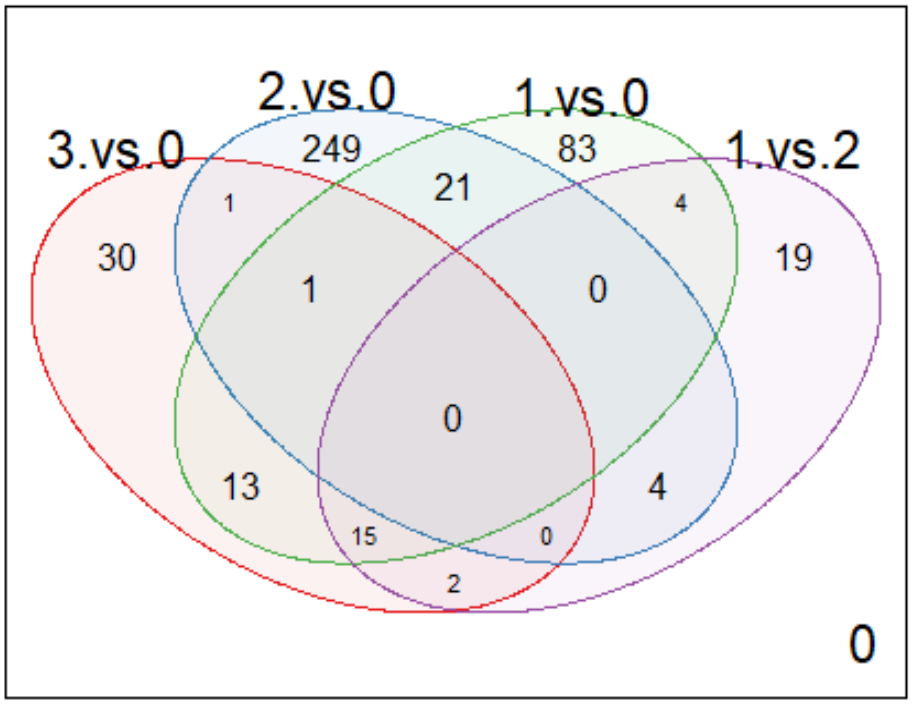


Figure 4.8: Comparison of number of DE genes between the four clusters (by Dr Voukantsis).

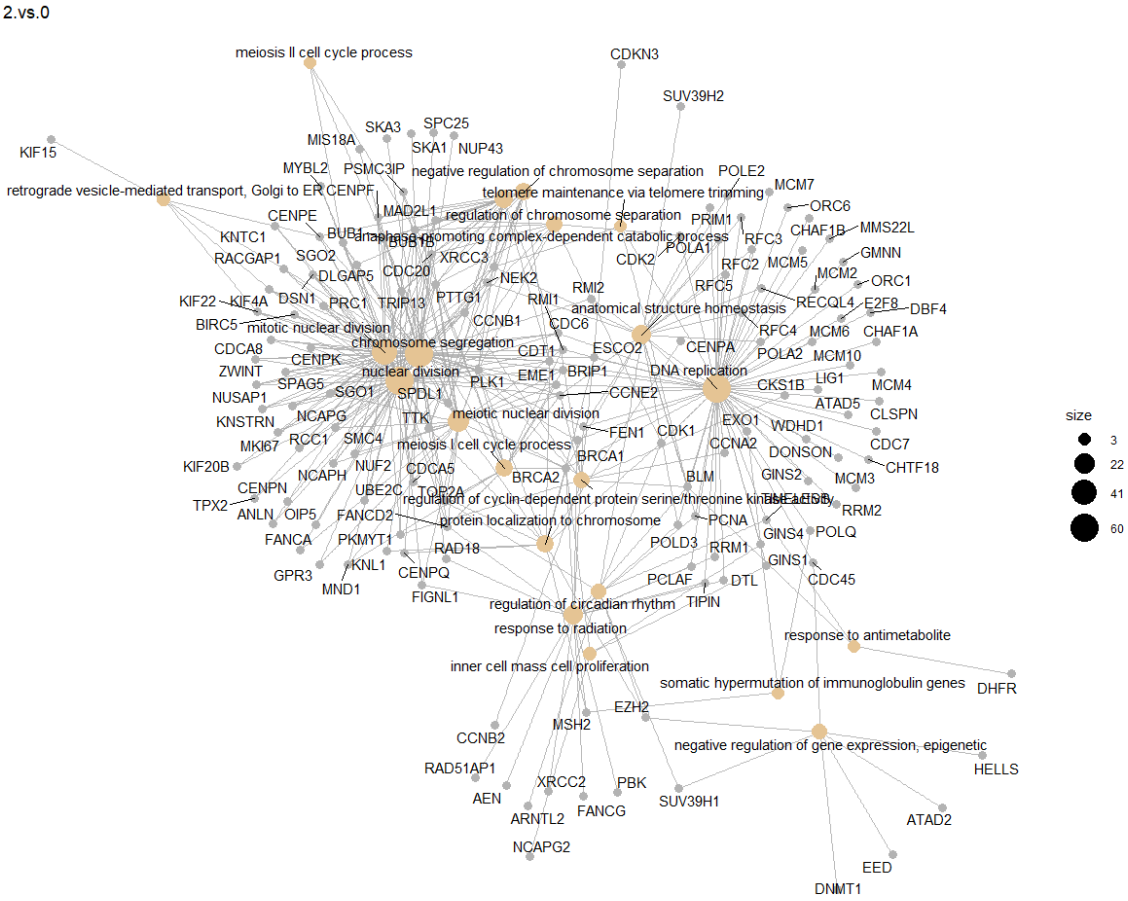


Figure 4.9: The enriched GO terms for the DE genes between cluster 2 and 0 (by Dr Voukantsis).

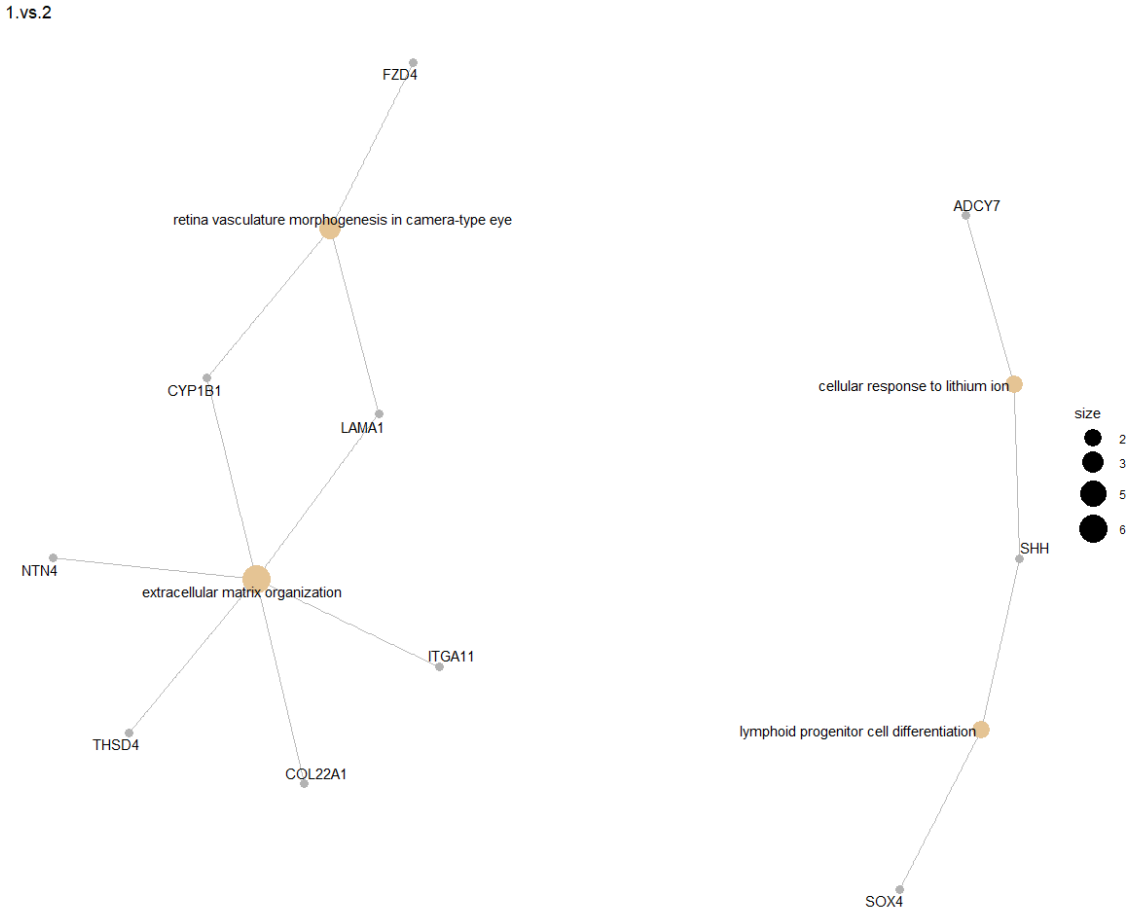


Figure 4.10: The enriched GO terms for the DE genes between cluster 1 and 2 (by Dr Voukantsis).

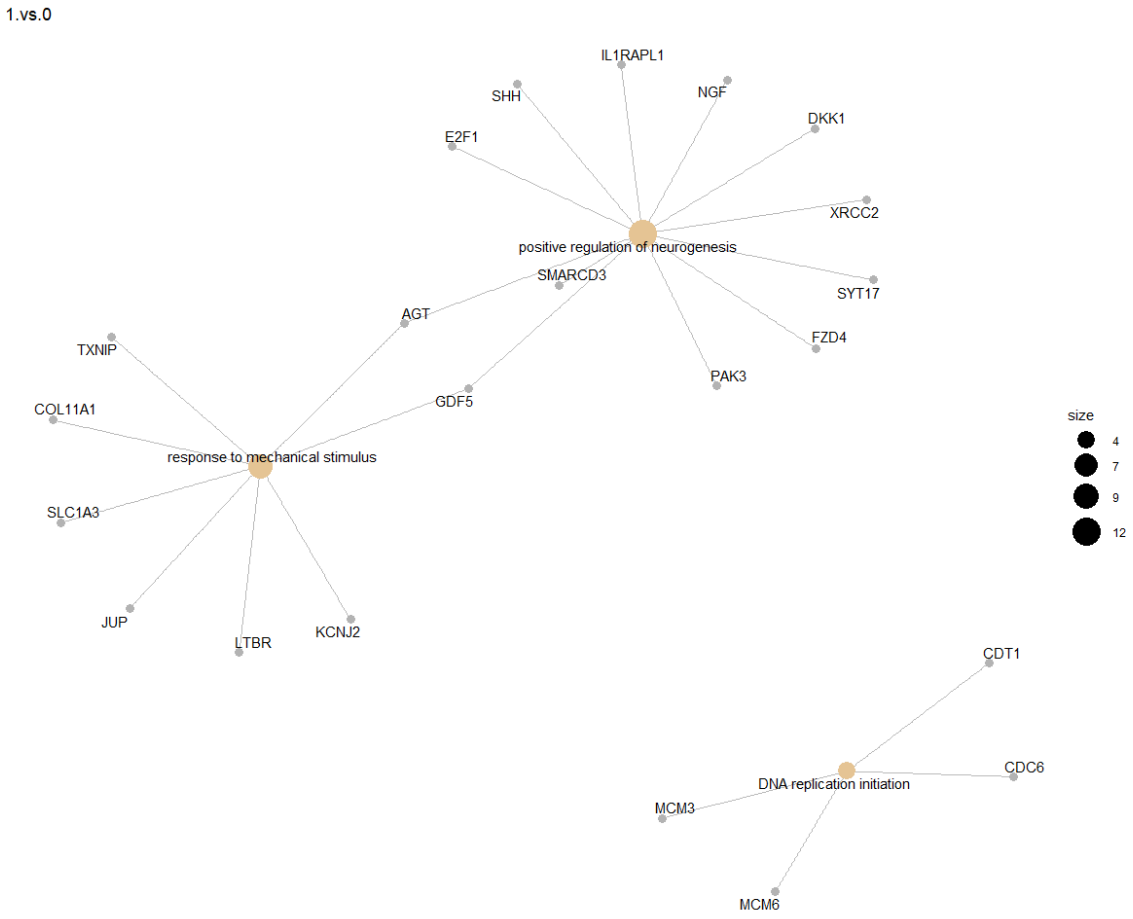


Figure 4.11: The enriched GO terms for the DE genes between cluster 1 and 0 (by Dr Voukantsis).

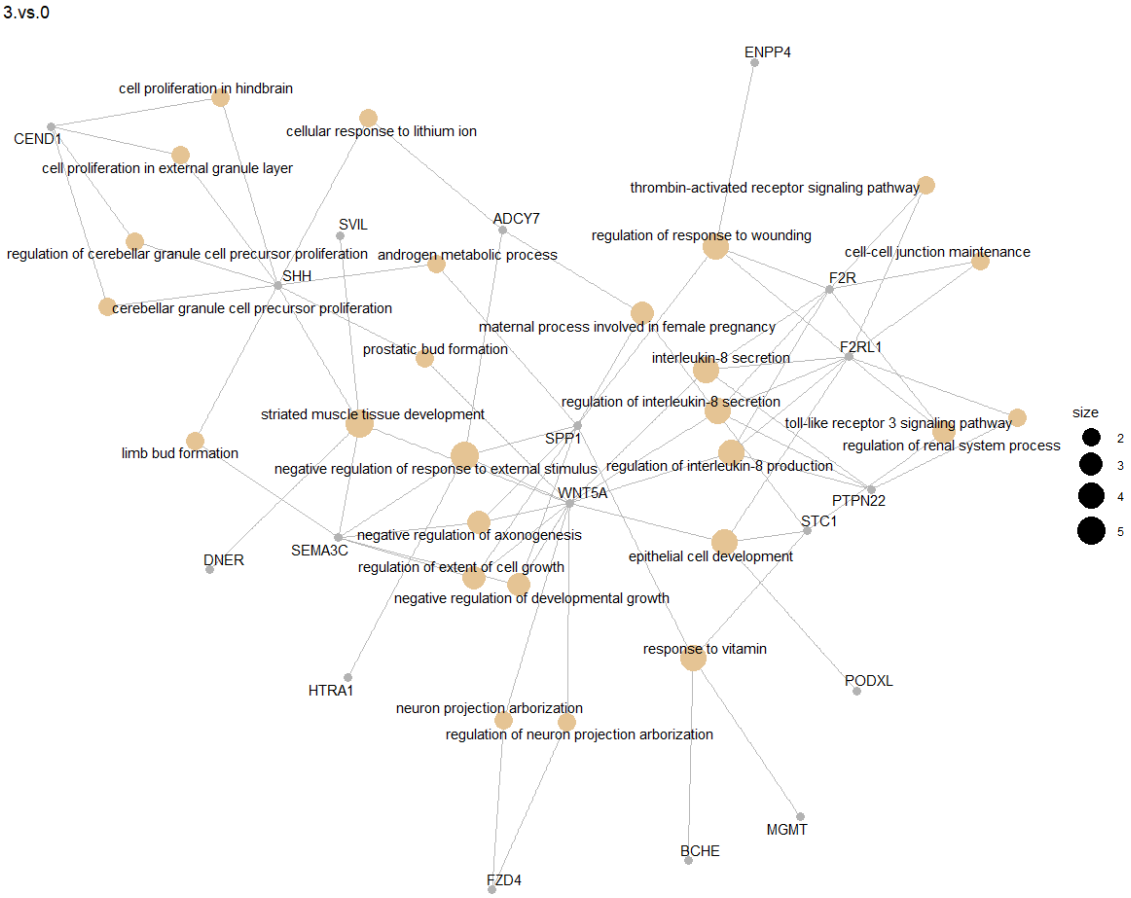


Figure 4.12: The enriched GO terms for the DE genes between cluster 3 and 0 (by Dr Voukantsis).

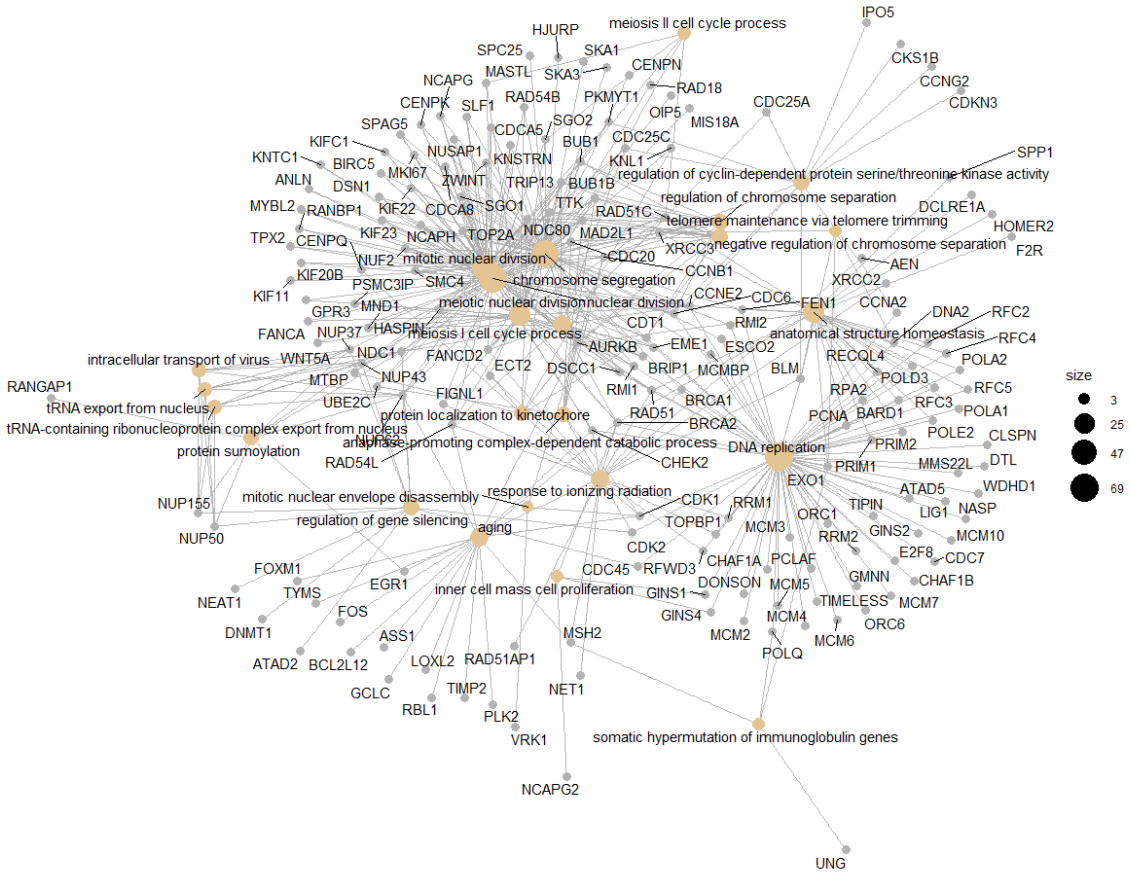


Figure 4.13: The enriched GO terms for the DE genes between cluster 2 and 3 (by Dr Voukantsis).

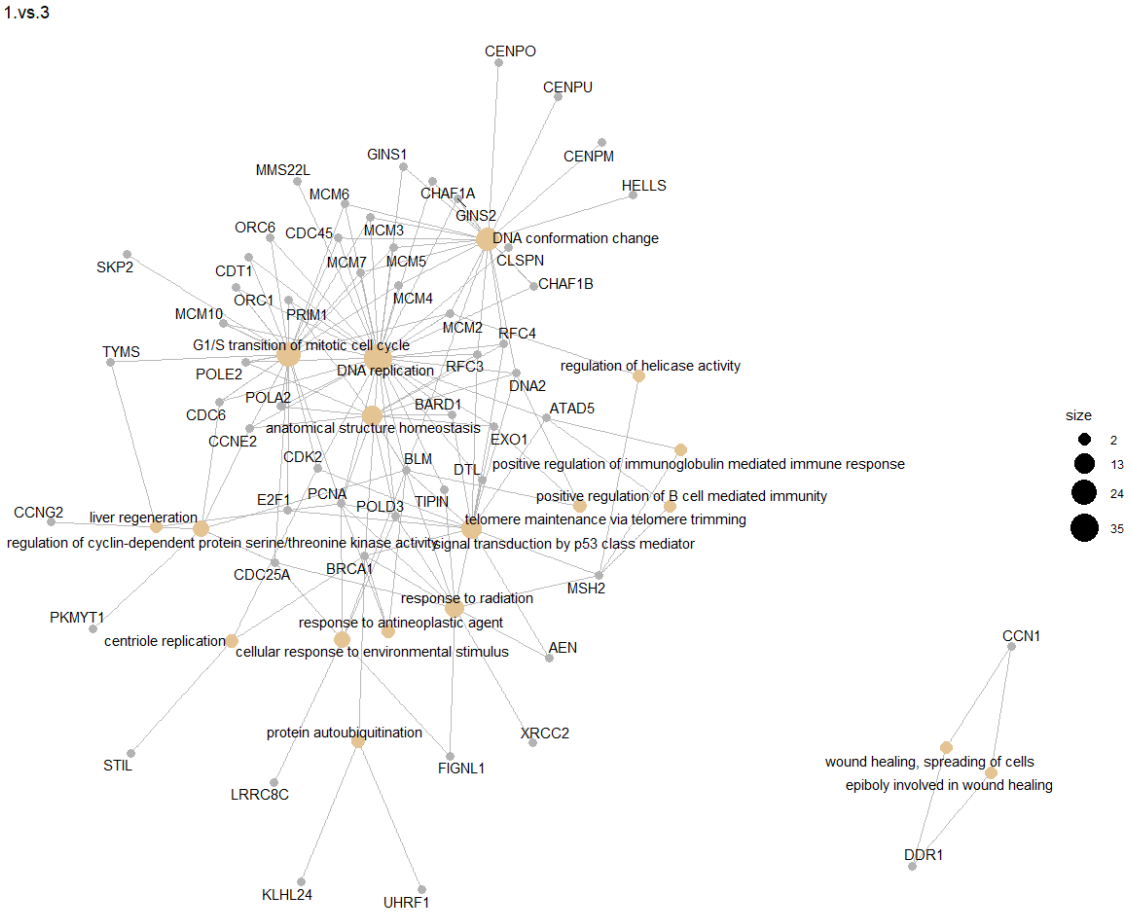


Figure 4.14: The enriched GO terms for the DE genes between cluster 1 and 3 (by Dr Voukantsis).

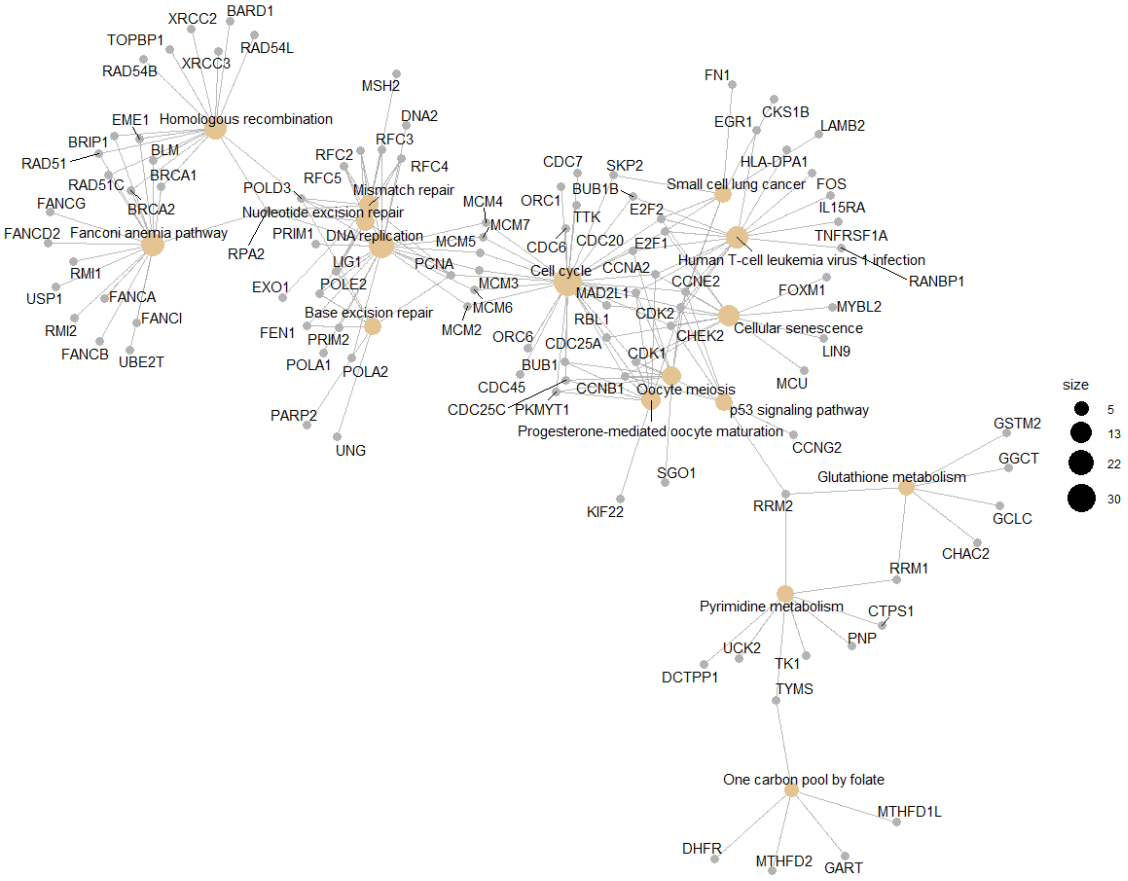


Figure 4.15: The enriched KEGG pathways for the DE genes between cluster 2 and 3 (by Dr Voukantsis).

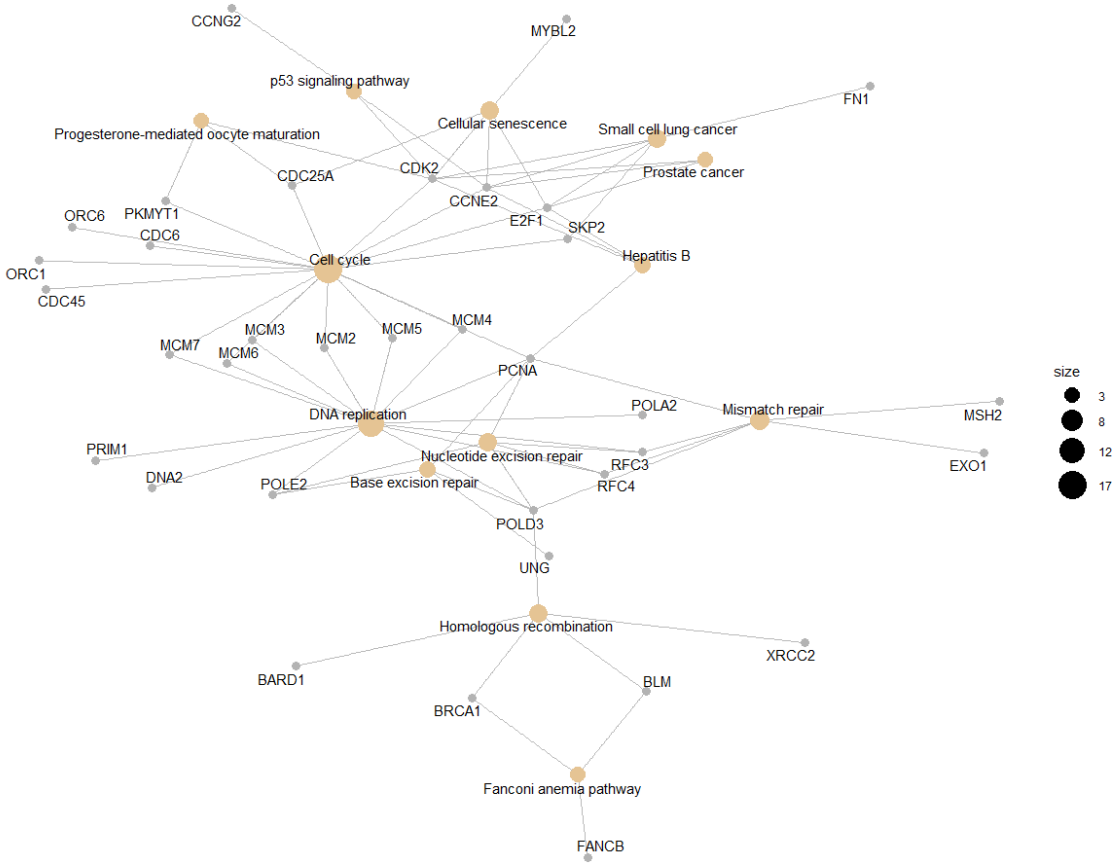


Figure 4.16: The enriched KEGG pathways for the DE genes between cluster 1 and 3 (by Dr Voukantsis).

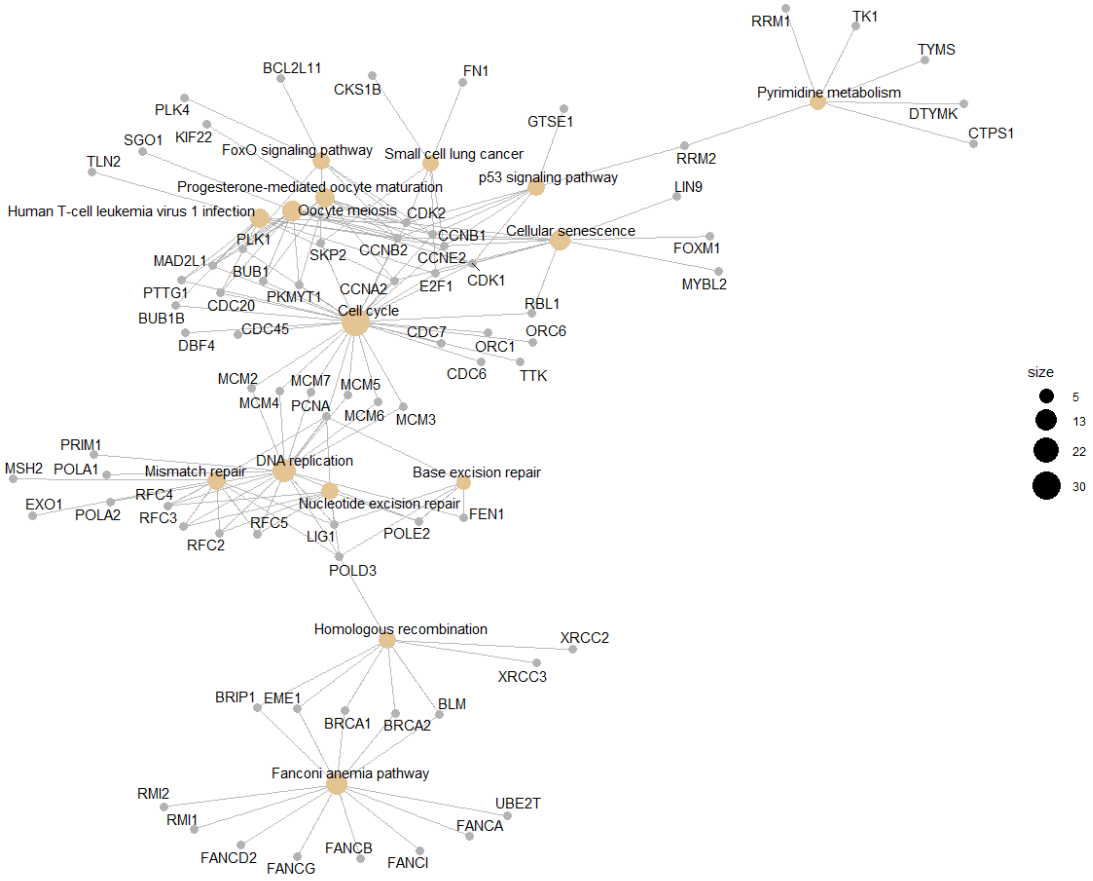


Figure 4.17: The enriched KEGG pathways for the DE genes between cluster 2 and 0 (by Dr Voukantsis).

4.1.3 Validation of Differentially Expressed Genes

Due to the high number of DE genes being identified from plate-based and cluster-based analyses, it was practically not feasible to validate all their expression using qRT-PCR. Therefore, DE genes were selected based on several factors. Firstly, the significance of their differential expression from violin plots data were examined. Secondly, their associated pathways from GO or KEGG over-representation analysis were checked, and thirdly their levels of novelty were established from a review of the literature.

Some of the DE genes identified from the scRNA-seq analysis have been reported in the literature to play a role in TMZ resistance, such as *RRAD*, hepatocyte growth factor (*HGF*), cyclin dependent kinase 1 (*CDK1*), forkhead box M1 (*FoxM1*) and polo like kinase 4 (*PLK4*) (Gil Del Alcazar et al., 2016, Jun et al., 2007, Peng et al., 2017, Yeom et al., 2014, Zhang et al., 2019b). As mentioned in the Introduction, *RRAD* had previously been validated as differentially expressed by previous student Victoria Ma (Macaulay group). Therefore, most of these genes were not selected for validation.

Firstly, *MGMT* was overexpressed in the resistant sublines (Figure 4.18). This overexpression not only correlated with the prediction from violin plot created by Dr Voukantsis, but also the protein expression from Figure 3.5. These results showed that the scRNA-seq data did reveal changes that had already been observed in bulk cultures.

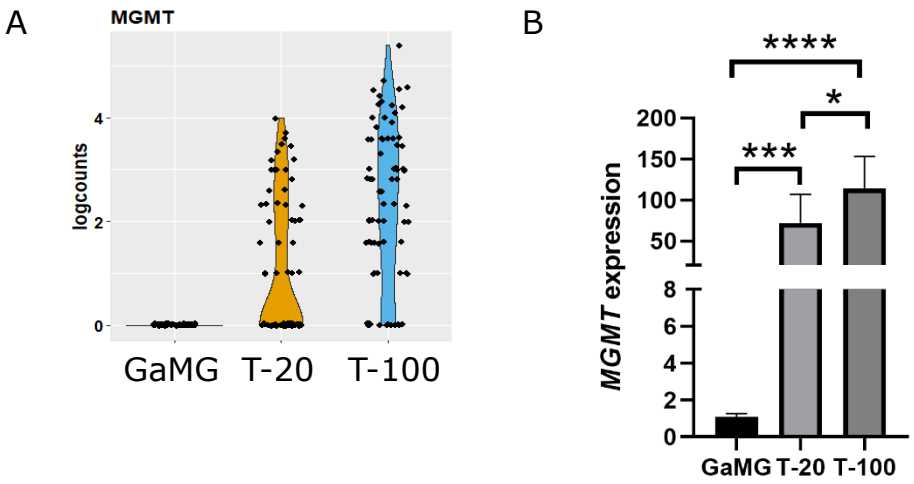


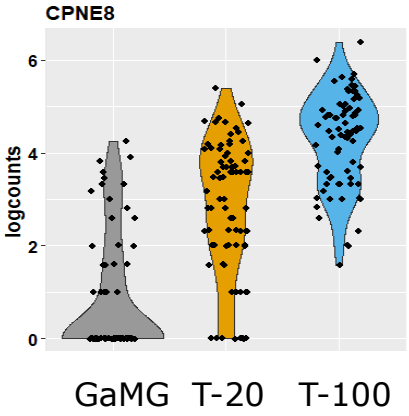
Figure 4.18: Validation of *MGMT* expression in GaMG, T-20 and T-100 cells. (A) Violin plot from scRNA-seq analysis for *MGMT* (by Dr Voukantsis). (B) qPCR result showed relative expression of *MGMT* in the GaMG sublines (by me). Graph was plotted as means ± SD based on pooled data from three independent experiments, each with triplicate technical replicates. The expressions were analysed for statistical significance using ordinary one-way ANOVA (*p < 0.05; **p < 0.01; ***p < 0.001; ****p < 0.0001).

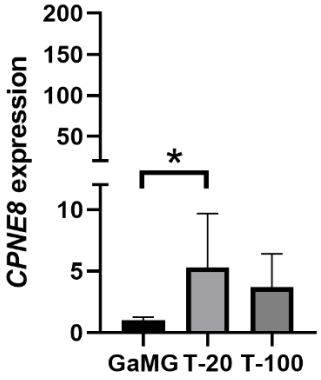
From the top twenty genes that were differentially expressed between the three sublines in Figure 4.1, seven of them had been validated. The violin plots created by Dr Voukantsis based on scRNA-seq analysis predicted that *CPNE8*, *CT83*. *BCAT1*, *CATSPER1* and *FAM96B* were upregulated in the TMZ-resistant sublines.

Based on the pooled data from three independent experiments, *CPNE8* was upregulated by approximately 5 times in the TMZ-resistant sublines. Meanwhile, the expressions of *CT83* in T-20 and T-100 cells were approximately 50 and 100 times higher than GaMG parental cells respectively. There was little difference in *BCAT1* expression between GaMG and T-20 cells, but the gene was overexpressed by approximately 5 times in T-100 cells. The expressions of *CATSPER1* and *FAM96B* were only validated in two independent experiments as the differential expressions were insignificant and inconsistent (Figure 4.19).

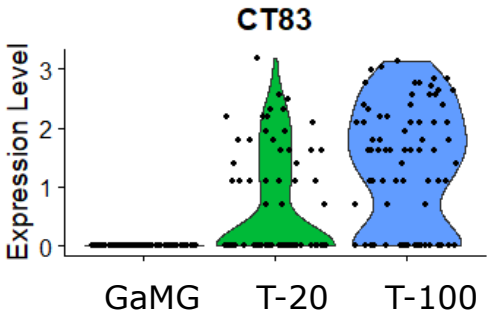
From these results, there were three genes that showed consistent and significant upregulation across three independent experiments, and at the same time correlated with the violin plots, namely: *CPNE8*, *CT83* and *BCAT1*. Although the overexpression of *BCAT1* and *CPNE8* in the resistant sublines was not as marked as *CT83*, the differential expressions were still consistent and significant.

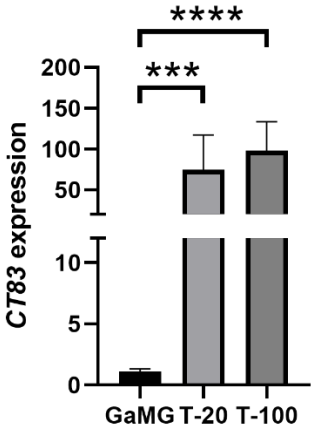
CPNE8



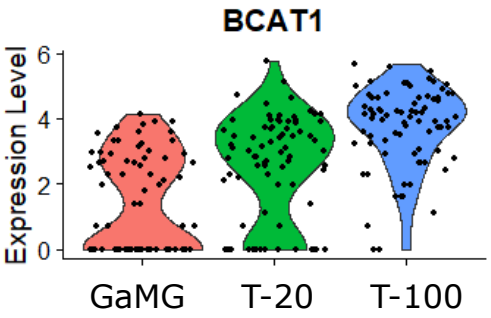


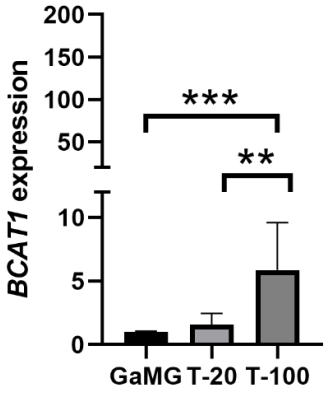
CT83



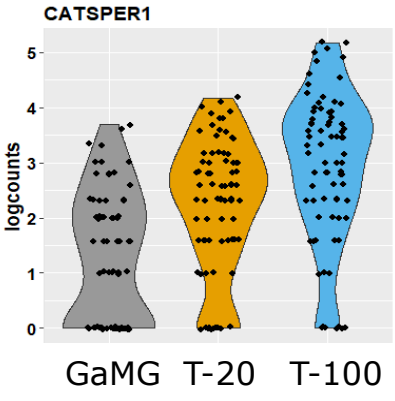


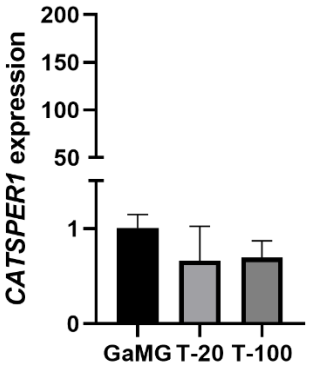
BCAT1





CATSPER1





FAM96B

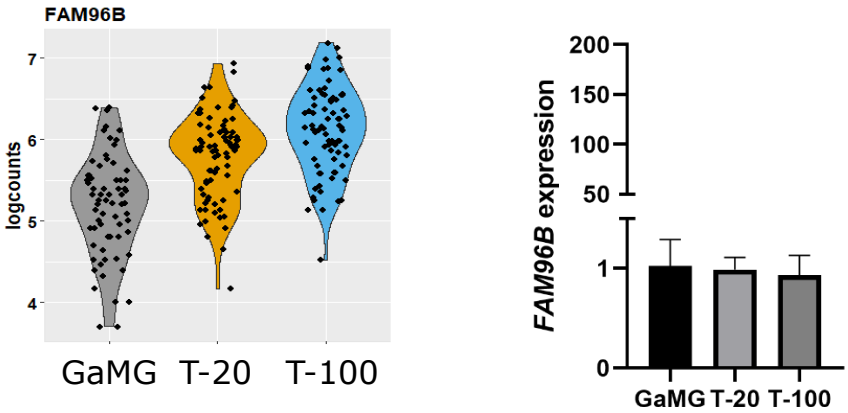


Figure 4.19: Validation of the upregulated genes from the 20 genes that were differentially expressed between all three sublines. Violin plots were created by Dr Voukantsis, qRT-PCR validations were performed by me. Graph was plotted as means ± SD based on pooled data from three independent experiments, each with triplicate technical replicates. The expressions were analysed for statistical significance using ordinary one-way ANOVA (*p < 0.05; **p < 0.01; ***p < 0.001; ****p < 0.0001).

On the contrary, it was predicted from the violin plots made by Dr Voukantsis that *MEST* and *EBF1* were downregulated in the TMZ-resistant sublines.

Similar to the violin plot, *EBF1* showed significant downregulation in the resistant sublines. The expression of *EBF1* in T-100 cells was approximately half to that of the GaMG parental cells. Meanwhile, the differential expressions of *MEST* were not significant in all three sublines. Its expression in T-100 cells was higher than GaMG parental cells, which was opposite to the depiction from the violin plot (Figure 4.20).

In summary, the differential expressions of *CPNE8*, *CT83*, *BCAT1* and *EBF1* correlated with the violin plot data from scRNA-seq data but *CATSPER1*, *FAM96B* and *MEST* did not prove to be DE in bulk cultures.

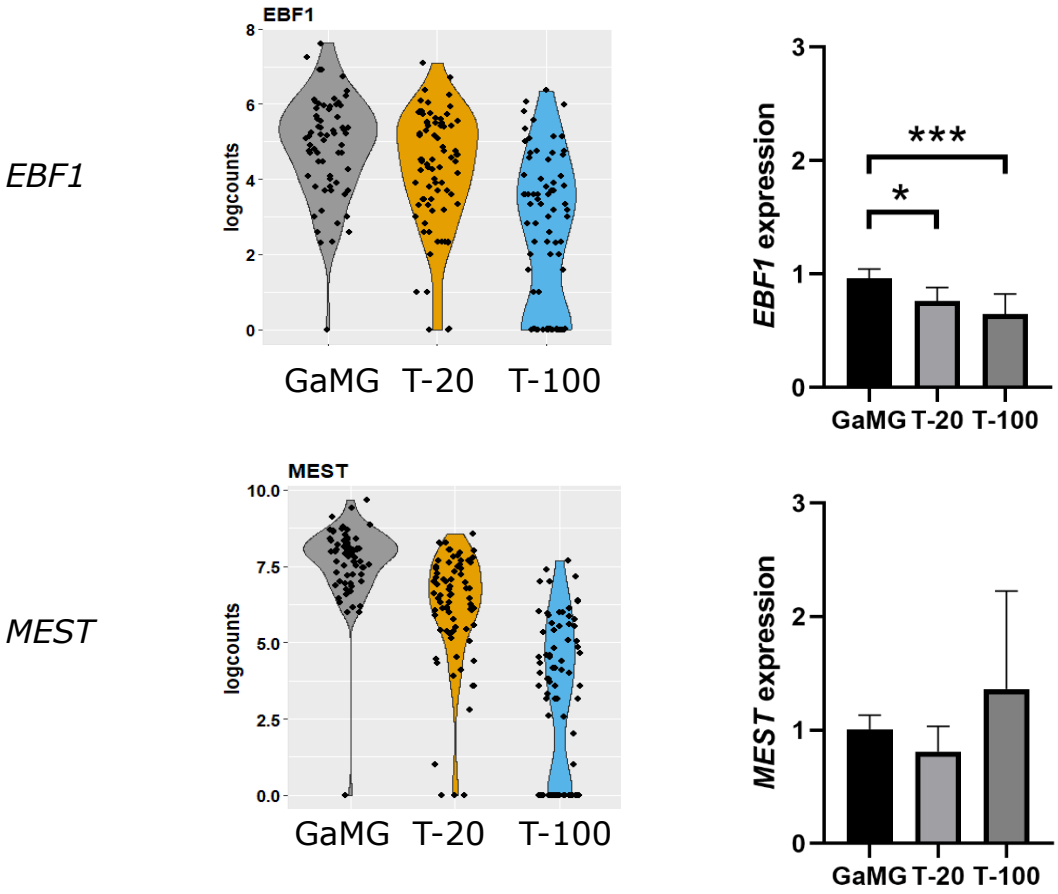


Figure 4.20: Validation of the downregulated genes from the 20 genes that were differentially expressed between all three sublines. Violin plots were created by Dr Voukantsis, qRT-PCR validations were performed by me. Graph was plotted as means ± SD based on pooled data from three independent experiments, each with triplicate technical replicates. The expressions were analysed for statistical significance using ordinary one-way ANOVA (*p < 0.05; **p < 0.01; ***p < 0.001; ****p < 0.0001).

As *HGF* and *E2F1* had been implicated in TMZ resistance (Meng et al., 2020, Jun et al., 2007), checking their expressions would verify their relevance in this model. Corresponding to the scRNA-seq data, *E2F1* was downregulated by approximately 50% in T-20 and to a greater extent in T-100 cells. Conversely, *HGF* was upregulated in T-20 cells, which was different to the violin plot (Figure 4.21).

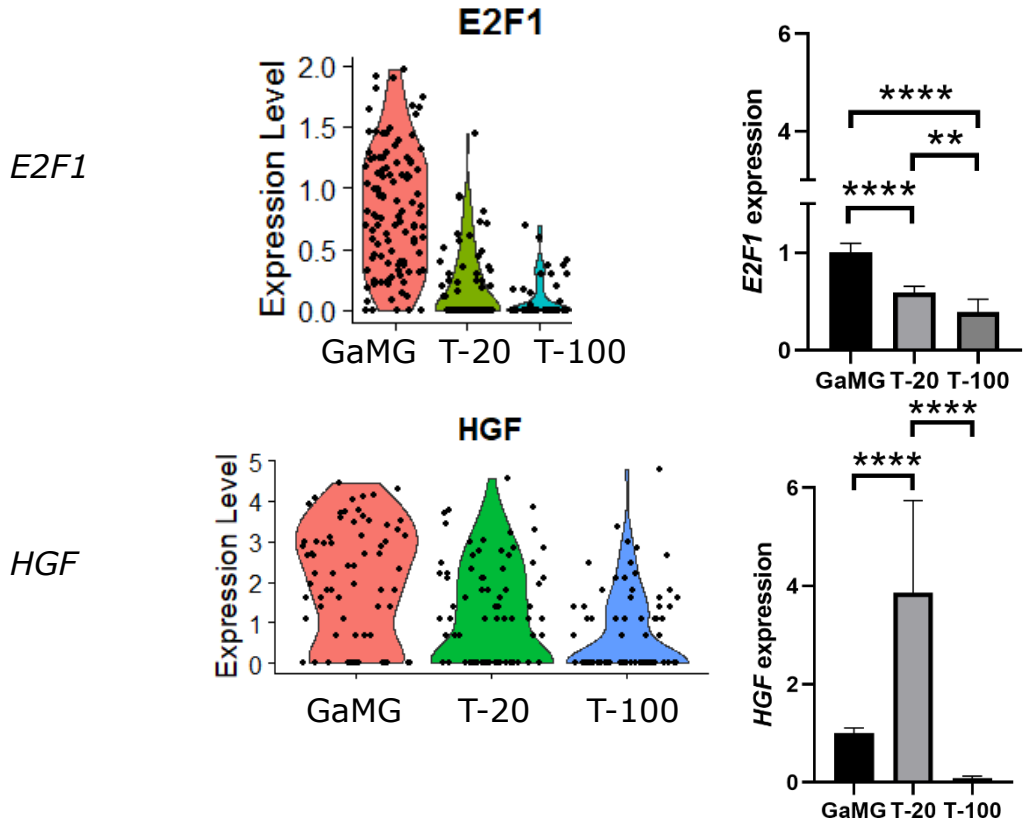


Figure 4.21: Validation of the DE genes that had been reported to drive TMZ resistance. Violin plots were created by Dr Voukantsis, qRT-PCR validations were performed by me. Graph was plotted as means ± SD based on pooled data from three independent experiments, each with triplicate technical replicates. The expressions were analysed for statistical significance using ordinary one-way ANOVA (*p < 0.05; **p < 0.01; ***p < 0.001; ****p < 0.0001).

In the GO and KEGG over-representation analysis done by Dr Voukantsis, DNA replication had been repeatedly shown to be enriched (Figure 4.13 - Figure 4.17). Ribonucleotide reductase (RNR) is an important enzyme in genome maintenance (Sagawa et al., 2017). It catalyses the formation of deoxyribonucleotides from ribonucleotides, hence regulating the deoxyribonucleoside triphosphates (dNTPs) pools (Aye et al., 2015). Therefore, the expressions of its large catalytic subunit *RRM1* and small regulatory subunit *RRM2* were examined.

The expression of *RRM2* in T-20 cells was approximately half to the GaMG parental cells, and a quarter in T-100 cells. These expressions correlated to the prediction from the violin plot. However, *RRM1* did not show any significant change in expression across the GaMG sublines (Figure 4.22).

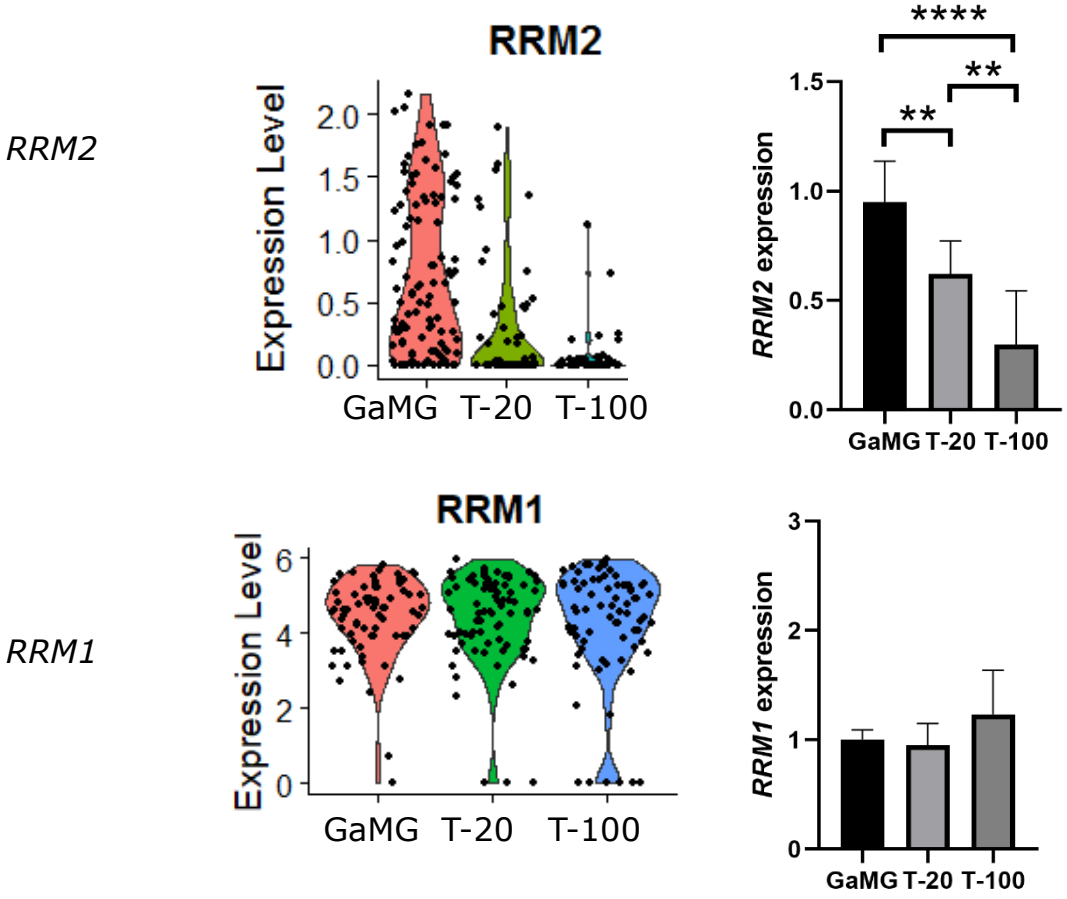
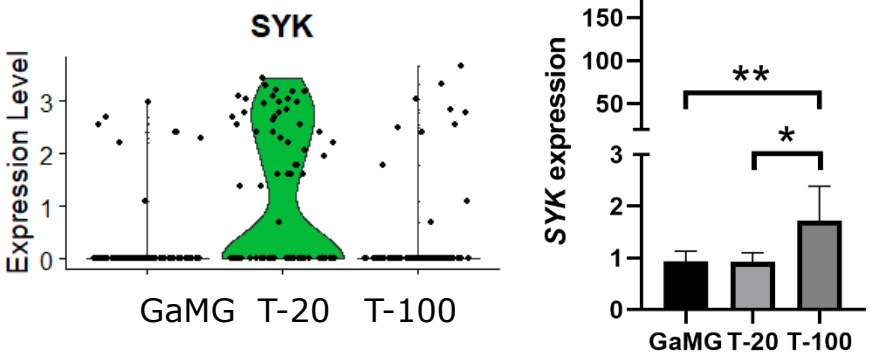


Figure 4.22: Validation of the genes encoding ribonucleotide reductase subunits. Violin plots were created by Dr Voukantsis, qRT-PCR validations were performed by me. Graphs were plotted as means ± SD based on pooled data from three independent experiments, each with triplicate technical replicates. The expressions were analysed for statistical significance using ordinary one-way ANOVA (*p < 0.05; **p < 0.01; ***p < 0.001; ****p < 0.0001).

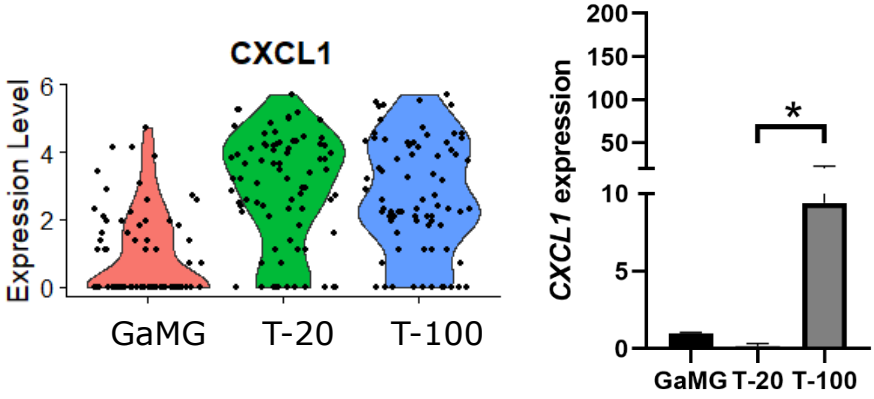
Several other DE genes had also been selected for qRT-PCR validations based on the aforementioned factors. For instance, spleen tyrosine kinase (*SYK*) expression was validated as it was shown that the gene was involved in the invasion and proliferation of GBM (Moncayo et al., 2018). However, the qRT-PCR result of *SYK* did not correspond to the violin plot from scRNA-seq analysis. In addition, KIT proto-oncogene receptor tyrosine kinase (*KIT*) was chosen for validation as the violin plot showed significant downregulation in the resistant sublines. Other genes that were validated include Shugoshin 1 (*SGO1*), minichromosome maintenance complex component 7 (*MCM7*) and proliferating cell nuclear antigen (*PCNA*), which played a role in cellular replication and DNA repair. After three independent experiments, all these genes did not show significant difference in expressions nor correlated with the prediction from the violin plots (Figure 4.23).

In total, 22 genes were validated using qRT-PCR. There were 6 genes that showed consistent and significant differential expression across three independent repeats and at the same time correlated with the violin plots from scRNA-seq analysis, namely: *MGMT*, *CT83*, *BCAT1* and *CPNE8* being overexpressed in the resistant sublines and *EBF1*, *E2F1* being downregulated. Therefore, these genes except *MGMT* were selected for testing of functional contribution as the contribution of *MGMT* in TMZ resistance had been repeatedly reported in the literature (Hegi et al., 2005, Kaina et al., 2010).

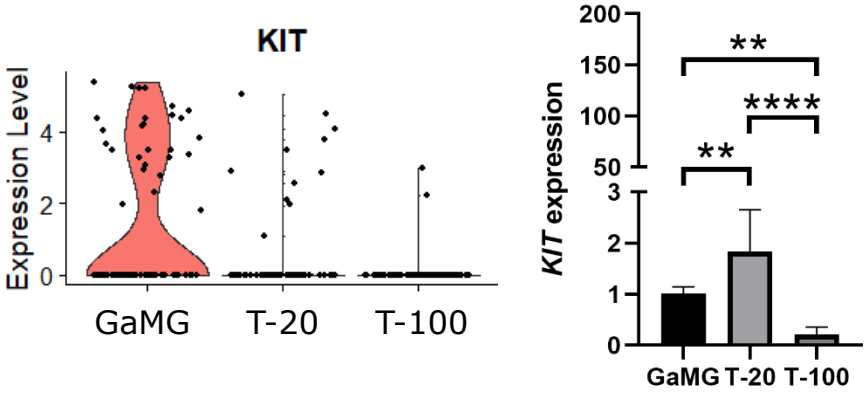
SYK



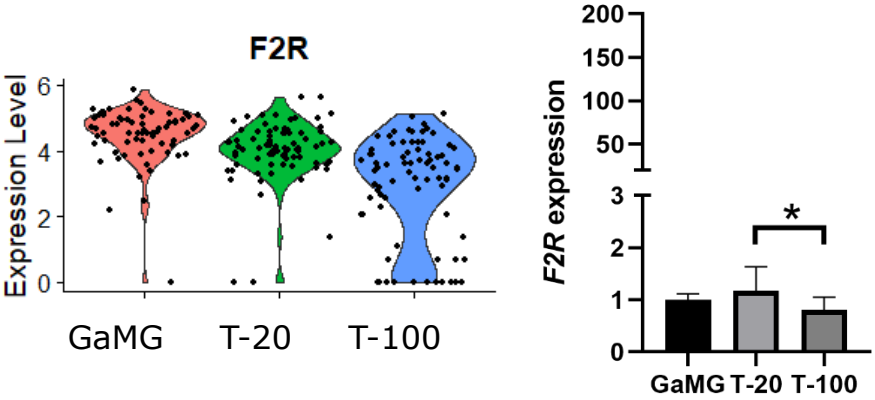
CXCL1



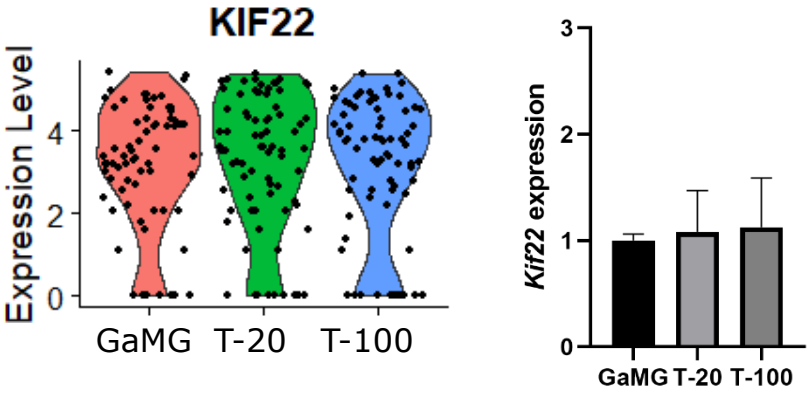
KIT



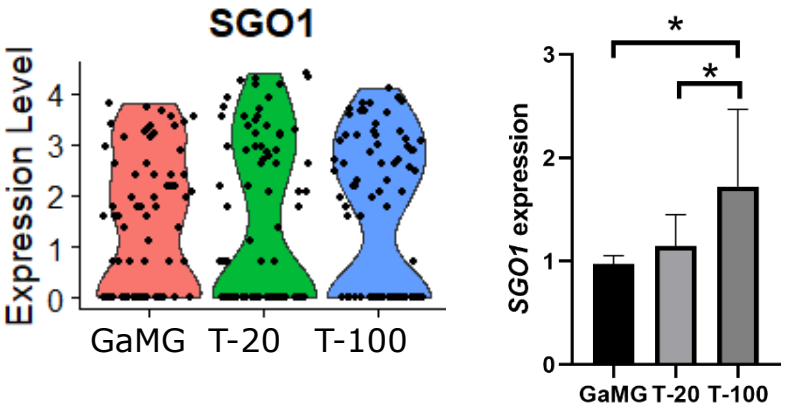
F2R



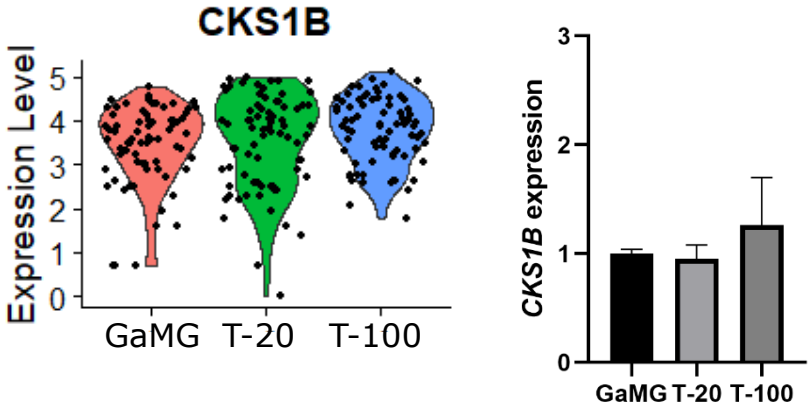
Kif22



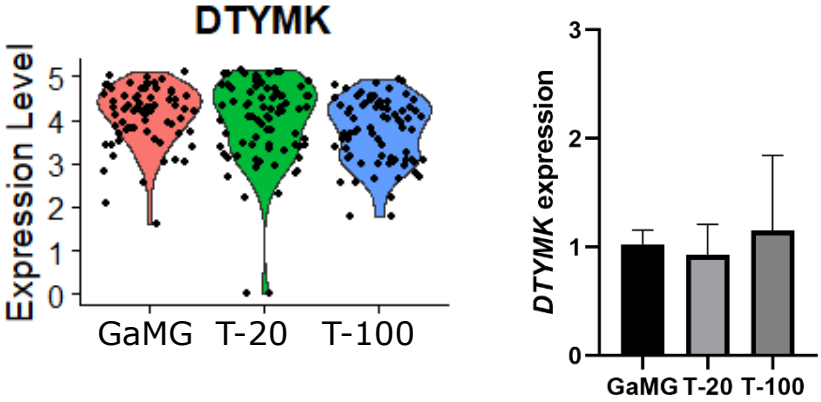
SGO1

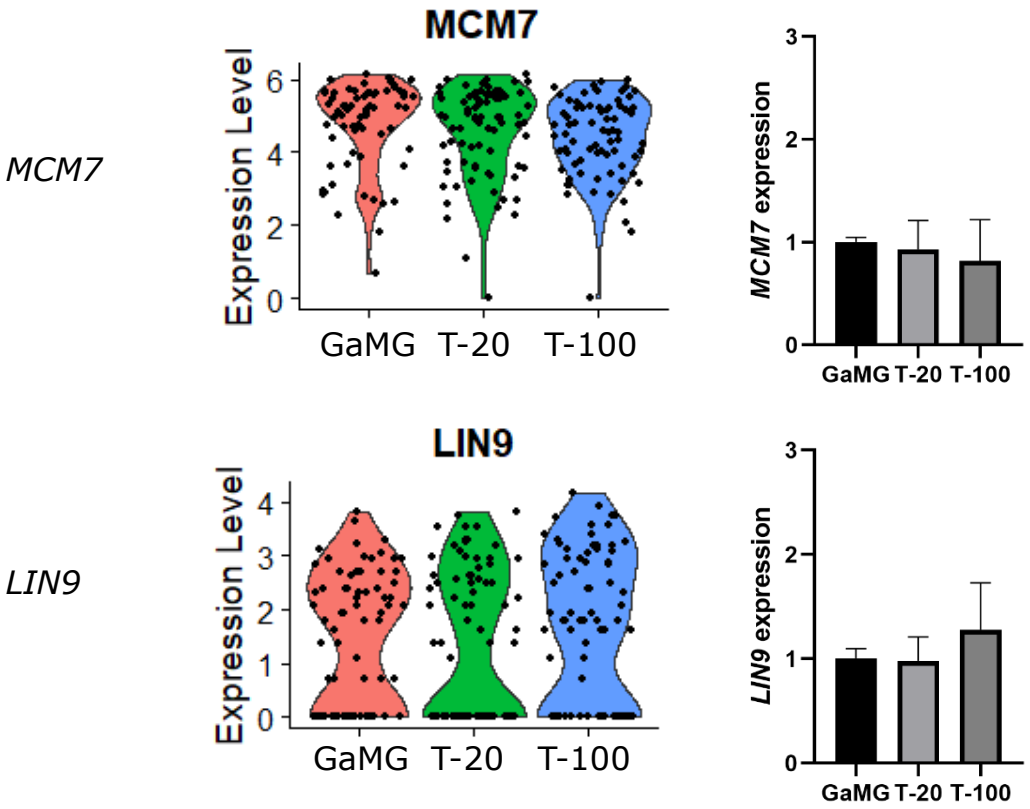


CKS1B



DTYMK





MCM7

LIN9

Figure 4.23: Validation of other selected genes. Violin plots were created by Dr Voukantsis, qRT-PCR validations were performed by me. Graphs were plotted as means ± SD based on pooled data from three independent experiments, each with triplicate technical replicates. The expressions were analysed for statistical significance using ordinary one-way ANOVA (*p < 0.05; **p < 0.01; ***p < 0.001; ****p < 0.0001).

4.2 Discussion

To avoid duplication of similar work, a literature review was carried out to check if associations between genes of interest and TMZ resistance had been established. Some genes identified from the scRNA-seq analysis had been reported to contribute to TMZ resistance in human GBM cell lines, including U87, LN-229, U251 and U138, although not previously in GaMG. Each cell line has different mutations and gene expression patterns. For instance, GaMG expresses wildtype *PTEN* and mutant *TP53*, however U87 expresses mutant *PTEN*, wildtype *TP53* and *EGFRvIII* (Huang et al., 2010, Kuger et al., 2013). Nevertheless, identification of resistance drivers that have already been published can serve to validate the direction of the scRNA-seq analysis in this project.

The expression of *MGMT* was validated at the mRNA level, paralleling the differential expression of MGMT protein found in Figure 3.5. However, as observed in T-100 cells after MGMT inhibition (Figure 3.6), differential expression did not necessarily imply a role as a chemoresistance driver. The expressions of other genes implicated in TMZ resistance, including *RRAD*, *CDK1*, *FoxM1* and *PLK4* were not validated by qRT-PCR and hence not investigated further. Instead, the emphasis was placed on *CT83*, *BCAT1*, *CPNE8*, *EBF1* and *E2F1*.

In terms of novelty, *CT83*, *BCAT1*, *CPNE8* and *EBF1* had not been reported to drive TMZ resistance in the literature. Although *E2F1* had been reported, the improvement in TMZ sensitivity was achieved via

downregulation of the gene in induced TMZ-resistant GBM cells of LN229, U87MG and patient-derived GBM cell HG9 (Meng et al., 2020). Furthermore, the differential expression of *E2F1* was not shown in the resistant and sensitive cells. From the qPCR result in Figure 4.21, *E2F1* was downregulated in the resistant sublines, which was opposite to that reported in the published article. Therefore, *E2F1* was still investigated.

CT83, the Cancer/testis antigen 83, is a relatively novel gene and there is limited information about its function in the literature. Under normal condition, expression of *CT83* is restricted to male germ cells in the testis (Fagerberg et al., 2014), but it is also detected in different cancers such as gastric and breast cancer (Futawatari et al., 2017, Kondo et al., 2018). In addition, more than half of triple-negative breast cancer patients were found to express *CT83* in at least 30% of their tumour cells. It was shown that both *in vivo* vaccination and *in vitro* CD8+ T cells priming were able to stimulate a strong *CT83*-specific immune response, which suggested that CT83 could be targeted in T-cell based immunotherapies (Paret et al., 2015).

BCAT1 is the first enzyme that initiates the branched-chain amino acid degradation pathway. It was shown that *BCAT1* was overexpressed in wild-type IDH1 GBM and it promoted cell proliferation through amino acid catabolism (Tönjes et al., 2013). *CPNE8* is a calcium-dependent membrane-binding protein that belongs to the Copine family, with unclear physiological functions (Maitra et al.,

2003). Meanwhile, *EBF1* is a transcription factor that is important for activating lineage specification during early B cell development (Nechanitzky et al., 2013). Lastly, *E2F1* encodes the protein which belongs to the E2F family of transcription factors. It is crucial in the regulation of cell cycle progression and cell proliferation (DeGregori et al., 2006).

Advances in single-cell technologies have allowed the investigation of gene expression down to individual cells level. Although measuring mRNA expressions has often been used to estimate the associated protein abundance, such approximation may be inaccurate (Gygi et al., 1999). This may be due to the delay between transcription and translation, energy constraints, localisation of mRNA and protein in the cell, limited number of RNA polymerases and ribosomes, and their inhomogeneous spatial distribution in the cells (Liu et al., 2016). By using integrative analyses, global proteomics and phospho-proteomics profiling could complement the scRNA-seq to improve the accuracy of finding potential novel mediators, minimising the probabilities of identifying false positives (Kumar et al., 2016).

In summary, the scRNA-seq analysis had identified significant transcriptional differences between GaMG, T-20 and T-100 cells. The differential expression of 22 genes was tested, *MGMT*, *CT83*, *BCAT1*, *CPNE8*, *EBF1* and *E2F1* were validated as DE and 5 of these were chosen for further testing to investigate their functional contribution to GBM viability and TMZ resistance.

Chapter 5: Investigation of differentially expressed genes as potential novel drivers of acquired temozolomide resistance in GBM

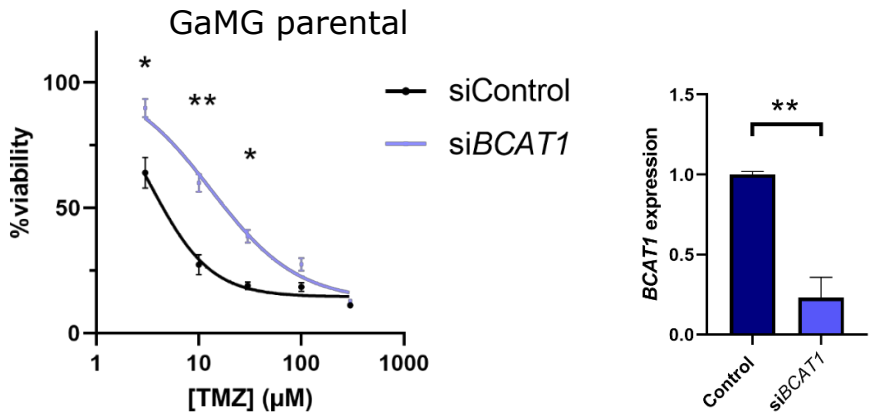
5.1 Results

5.1.1 The effects of individual gene knockdown on TMZ resistance

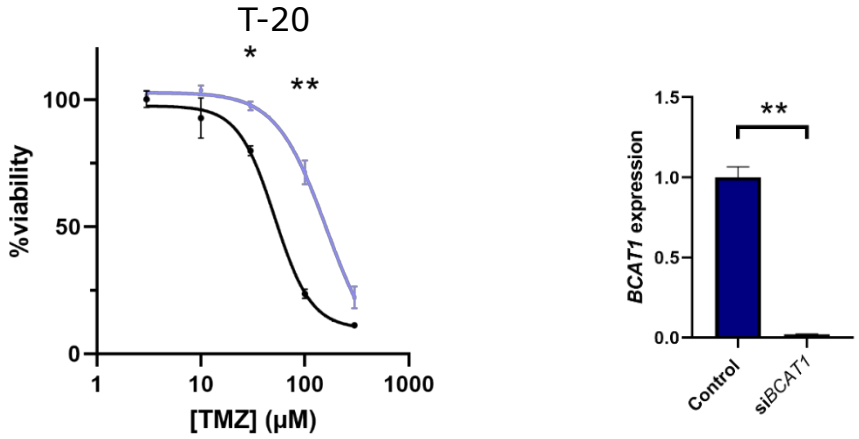
To examine the potential role of the five genes identified from qPCR validation, each of these genes were depleted using siRNAs. It was hypothesised that the acquired TMZ resistance in T-20 and T-100 cells could be reversed by depleting *BCAT1*, *CT83* and *CPNE8*, which were overexpressed in the resistant sublines; whereas GaMG parental cells would develop TMZ resistance after knocking down *EBF1* and *E2F1*, which were downregulated in the resistant sublines.

The first experiments tested effects of knocking down the genes that were confirmed to be overexpressed in the TMZ-resistant sublines. After confirmation of effective knockdown, depletion of *BCAT1* and *CT83* caused GaMG and T-20 cells to become more not less resistant towards TMZ and no significant effect was observed in T-100 cells (Figure 5.1 and Figure 5.2). After *CPNE8* knockdown, there was a slight improvement in the sensitivity of T-20 cells towards TMZ at 30 μM and 100 μM and about 50% reduction in IC_{50} (Figure 5.3). However, this difference might not be meaningful physiologically because the IC_{50} value was still above the TMZ concentrations achieved in circulation and CSF.

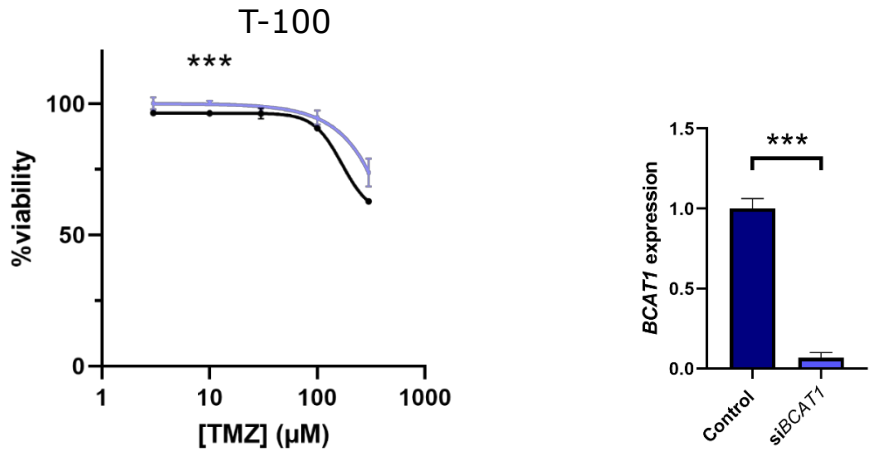
A



B



C

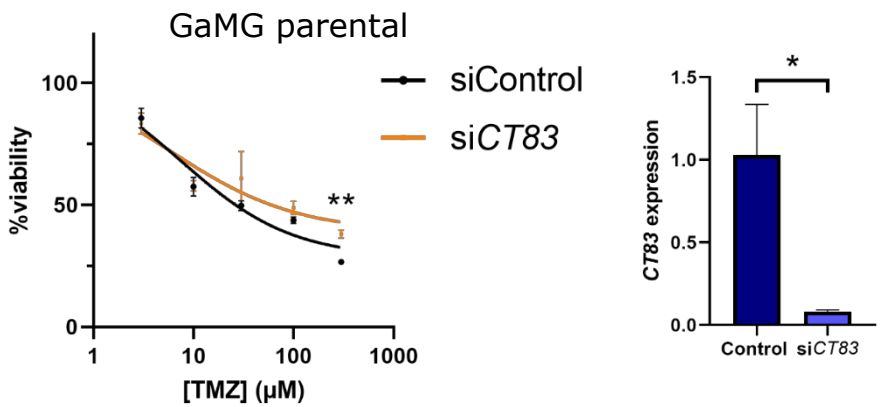


D

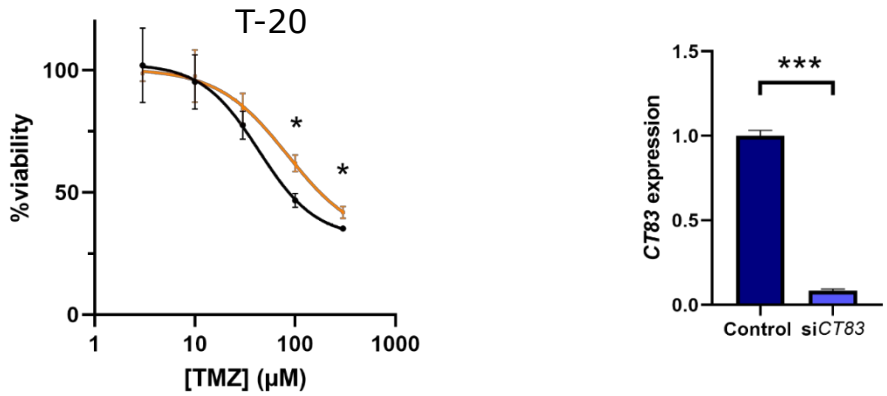
Cell Line	siControl IC_{50} (μM)	si*BCAT1* IC_{50} (μM)
GaMG	21.41 ± 23.92	44.28 ± 36.95
T-20	156.36 ± 143.20	197.72 ± 54.09
T-100	>300	>300

Figure 5.1: Effect of *BCAT1* knockdown on dose response of GaMG parental, T-20 and T-100 to TMZ. Cells were transfected with 25 nM of siControl or si*BCAT1*, treated with TMZ as described in section 2.11.2, and cell viability was tested after 5 - 7 days. Results were from one representative experiment. Points on the graph were means ± SD of triplicate values. The results were analysed for statistical significance using unpaired student's t-tests (**p < 0.01; ***p < 0.001; ****p < 0.0001). The bar graphs were qPCR results associated with the representative experiment, showing efficiency of knockdown. Graphs were plotted as means ± SD, each with triplicate technical replicates; statistical significance was tested using Welch's t-test. (D) shows the IC_{50} for each cell line, calculated based on pooled triplicate values from two independent experiments.

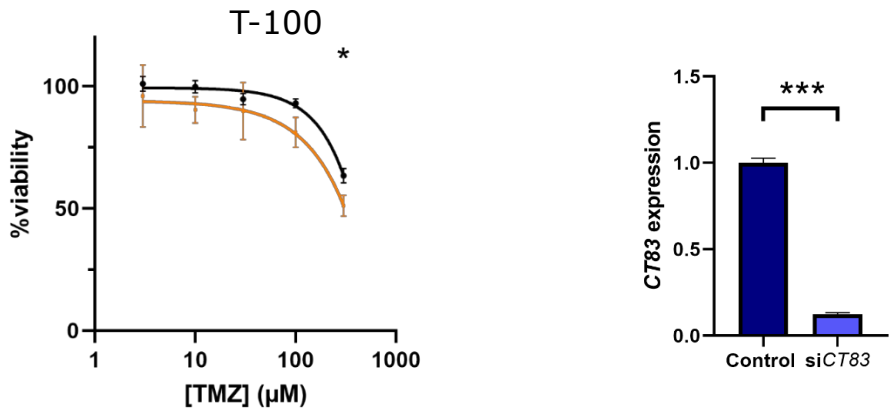
A



B



C

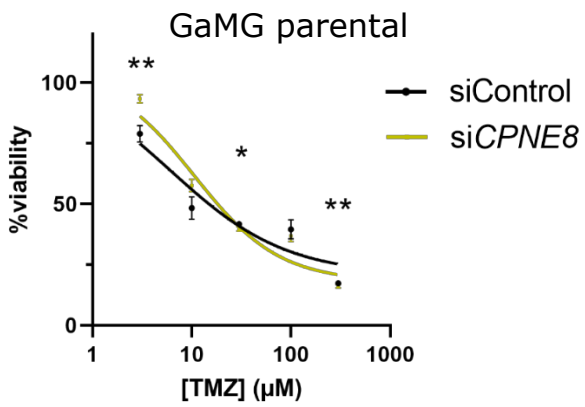


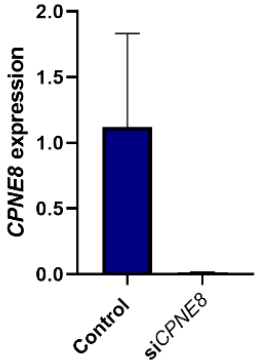
D

Cell Line	siControl IC_{50} (μM)	si*CT83* IC_{50} (μM)
GaMG	17.59 ± 12.53	38.76 ± 30.53
T-20	100.47 ± 19.61	163.83 ± 19.2
T-100	>300	>300

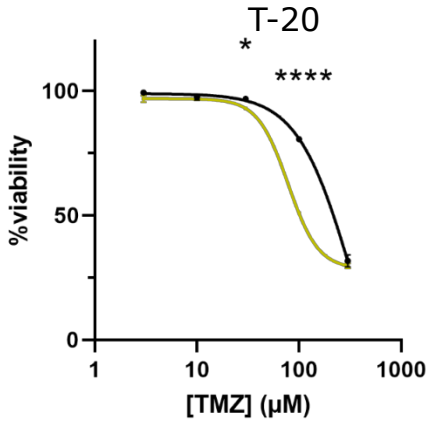
Figure 5.2: Effect of *CT83* knockdown on dose response of GaMG parental, T-20 and T-100 to TMZ. Cells were transfected with 50 nM of siControl or si*CT83*, treated with TMZ as described in section 2.11.2, and cell viability was tested after 5 - 7 days. Results were from one representative experiment. Points on the graph were means ± SD of triplicate values. The results were analysed for statistical significance using unpaired student's t-tests (**p < 0.01; ***p < 0.001; ****p < 0.0001). The bar graphs were qPCR results associated with the representative experiment, showing efficiency of knockdown. Graphs were plotted as means ± SD, each with triplicate technical replicates; statistical significance was tested using Welch's t-test. (D) shows the IC_{50} for each cell line, calculated based on pooled triplicate values from two independent experiments.

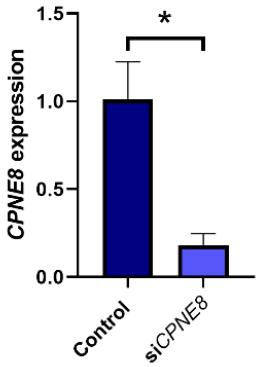
A



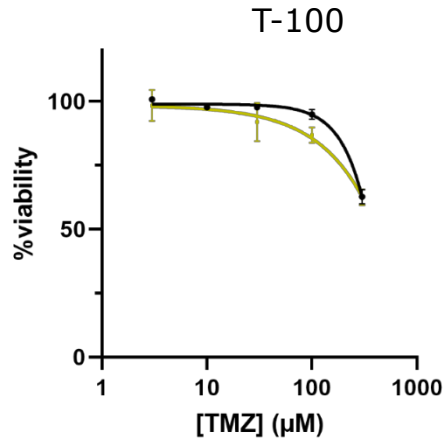


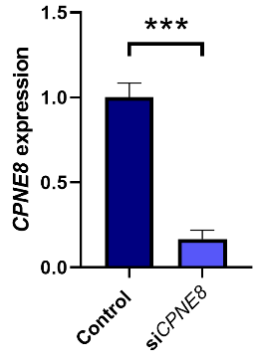
B





C





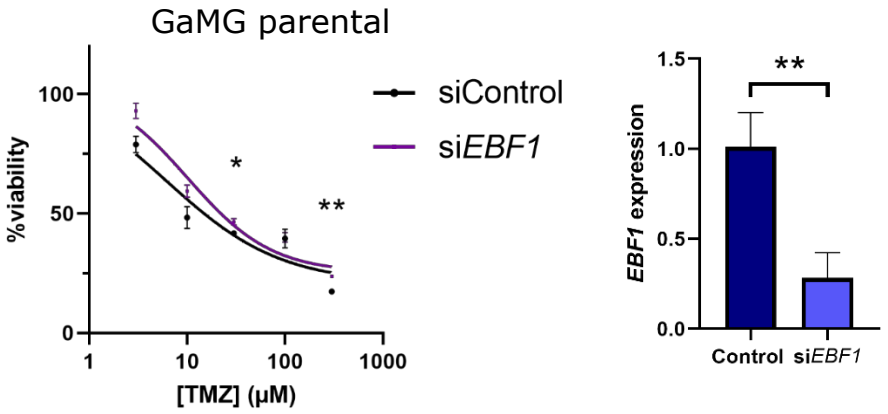
D

Cell Line	siControl IC_{50} (μM)	si*CPNE8* IC_{50} (μM)
GaMG	55.25 ± 56.96	47.91 ± 41.90
T-20	183.69 ± 48.15	98.93 ± 4.48
T-100	337.20 ± 18.38	354.62 ± 89.05

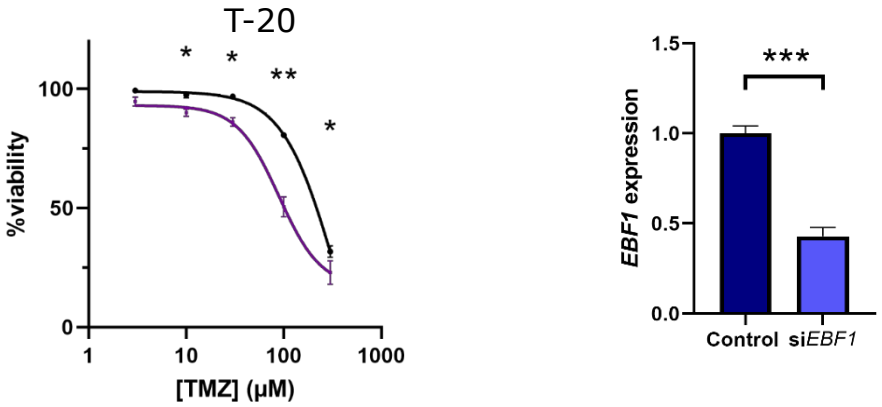
Figure 5.3: Effect of *CPNE8* knockdown on dose response of GaMG parental, T-20 and T-100 to TMZ. Cells were transfected with 25 nM of siControl or si*CPNE8*, treated with TMZ as described in section 2.11.2, and cell viability was tested after 5 - 7 days. Results were from one representative experiment. Points on the graph were means ± SD of triplicate values. The results were analysed for statistical significance using unpaired student's t-tests (**p < 0.01; ***p < 0.001; ****p < 0.0001). The bar graphs were qPCR results associated with the representative experiment, showing efficiency of knockdown. Graphs were plotted as means ± SD, each with triplicate technical replicates; statistical significance was tested using Welch's t-test. (D) shows the IC_{50} for each cell line, calculated based on pooled triplicate values from two independent experiments.

Secondly, experiments were conducted to knockdown genes found to be overpexressed in GaMG parental cells. There was no significant change in viability indicative of TMZ resistance observed upon *EBF1* depletion (Figure 5.4). Although there was an increased resistance towards TMZ observed in GaMG parental cells, the effect was minimal and not reproducible. In contrast to what was hypothesised, T-20 cells were less TMZ-resistant after *EBF1* knockdown, but again the effect was nominal.

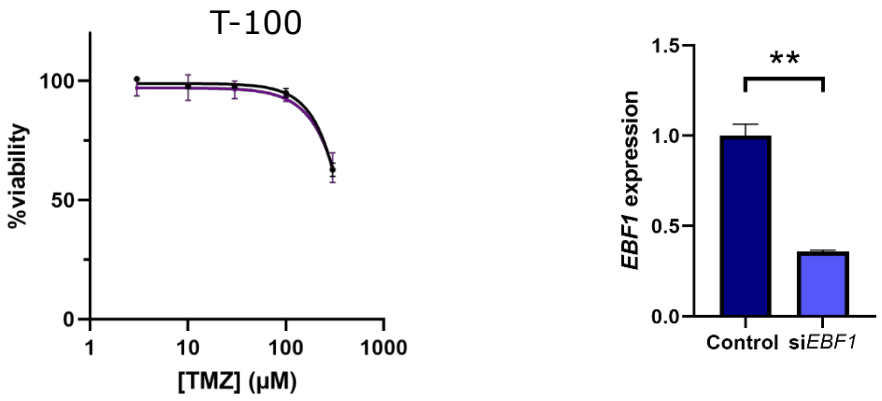
A



B



C



D

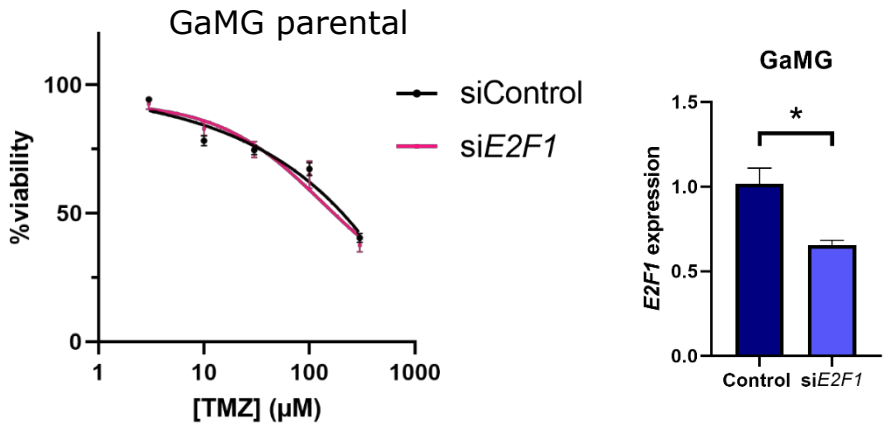
Cell Line	siControl IC_{50} (μM)	si*EBF1* IC_{50} (μM)
GaMG	11.36 ± 5.11	15.86 ± 8.96
T-20	147.27 ± 99.67	96.35 ± 7.98
T-100	372.73 ± 31.87	374.35 ± 15.89

Figure 5.4: Effect of *EBF1* knockdown on dose response of GaMG parental, T-20 and T-100 to TMZ. Cells were transfected with 25 nM of siControl or si*EBF1*, treated with TMZ as described in section 2.11.2, and cell viability was tested after 5 - 7 days. Results were from one representative experiment. Points on the graph were means ± SD of triplicate values. The results were analysed for statistical significance using unpaired student's t-tests (**p < 0.01; ***p < 0.001; ****p < 0.0001). The bar graphs were qPCR results associated with the representative experiment, showing efficiency of knockdown. Graphs were plotted as means ± SD, each with triplicate technical replicates; statistical significance was tested using Welch's t-test. (D) shows the IC_{50} for each cell line, calculated based on pooled triplicate values from two independent experiments.

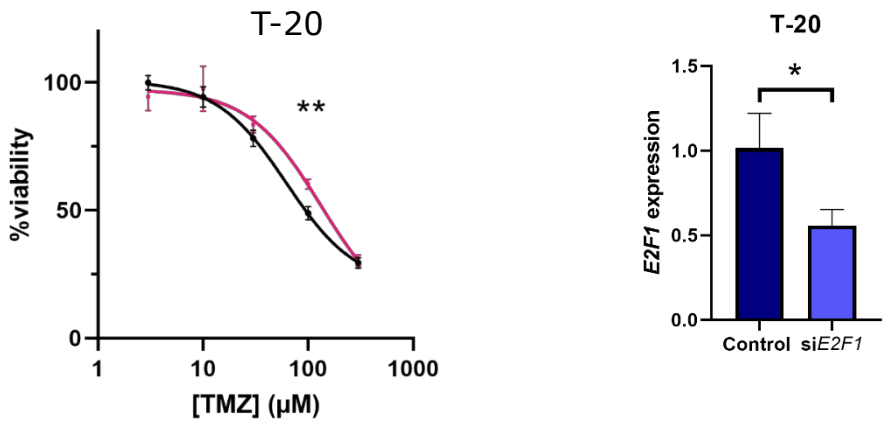
Similar to *EBF1* knockdown, *E2F1* depletion did not cause any significant change in TMZ resistance (Figure 5.5). However, the IC_{50} value of the TMZ-sensitive GaMG parental cells was 206.4 μM (Figure 5.5D), approximately 30-times higher than the experiment from Figure 3.1. This is not currently understood but might be due to the fluctuations of cell seeding density or some technical complications in the plate reader. This variation in the TMZ sensitivity did not relate to the passage number as the differences in the IC_{50} values were sometimes observed with simultaneous seeding of two plates. Moreover, the same preparation of TMZ had been used each time. Transfection with si*E2F1* caused T-20 cells to be marginally more resistant at 100 μM but made T-100 cells slightly more sensitive to TMZ at the concentration of 300 μM. Although there were statistical differences based on analysis of triplicate technical replicates from two independent experiments (i.e. 6 data points), most of the differences were small. Additional experiments would have been done if time allowed, to repeat these experiments, aiming to draw conclusions from these conflicting results.

In summary, the depletion of any individual gene did not lead to any significant change in the sensitivity towards TMZ.

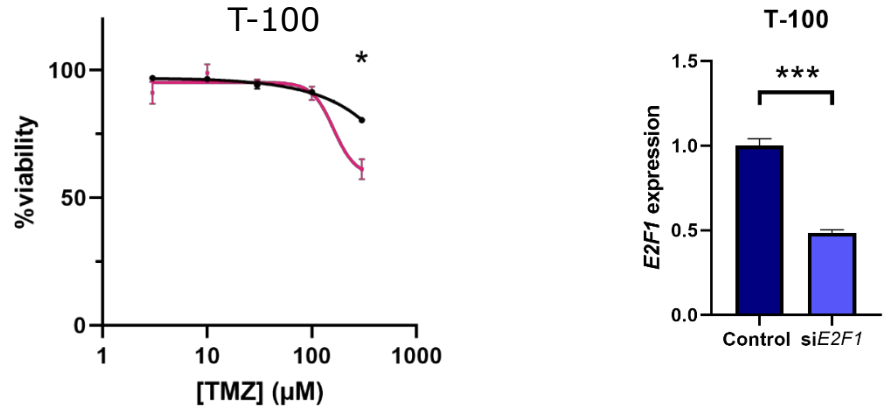
A



B



C



D

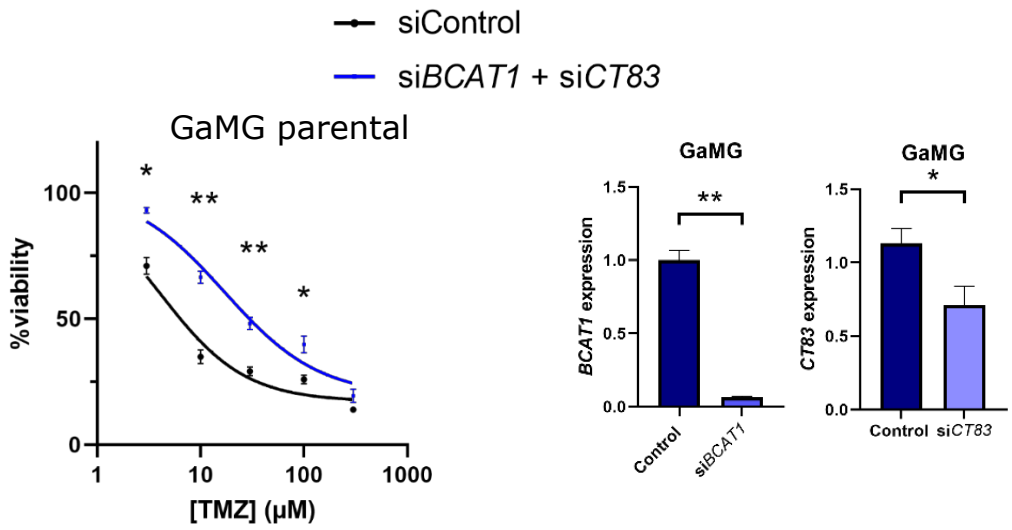
Cell Line	siControl IC_{50} (μM)	si*E2F1* IC_{50} (μM)
GaMG	206.4	170.8
T-20	94.4	141.7
T-100	>300	>300

Figure 5.5: Effect of *E2F1* knockdown on dose response of GaMG parental, T-20 and T-100 to TMZ. Cells were transfected with 50 nM of siControl or si*E2F1*. After treatment with TMZ, cell viability was tested after 5 - 7 days. Points on the graph are means ± SD of triplicate values. The results were analysed for statistical significance using unpaired student's t-tests (**p < 0.01; ***p < 0.001; ****p < 0.0001). The bar graphs were qPCR results associated with the representative experiment, showing efficiency of knockdown. Graphs were plotted as means ± SD, each with triplicate technical replicates; statistical significance was tested using Welch's t-test. (D) shows the IC_{50} for each cell line, calculated based on triplicate values from one independent experiment.

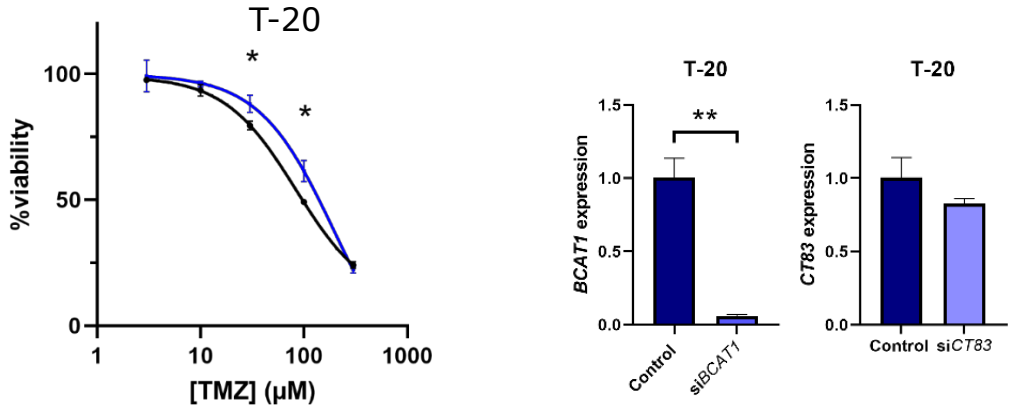
5.1.2 The effects of dual depletion of candidate genes on TMZ resistance in GaMG sublines

Recognising that TMZ resistance may be driven by multiple mediators, the effects of depleting any two of these genes were tested. Herein, the emphasis was placed on the genes that were overexpressed in the resistant sublines, i.e. *BCAT*, *CT83* and *CPNE8*, because it was hypothesised that the novel drivers of TMZ resistance were upregulated. Similar to what was observed in individual knockdown of *BCAT1* and *CT83* (Figure 5.1 and Figure 5.2), co-depletion of these two genes resulted in a more TMZ-resistant phenotype in GaMG and T-20 cells (Figure 5.6A, B), and the IC_{50} values of the co-depletion group were higher than those of the control group (Figure 5.6D), conflicting with the hypothesis. In contrast, there was a small reduction in TMZ resistance at 300 μM observed in T-100 cells. To investigate whether *BCAT1*:*CT83* co-depletion had any effect on cell viability in the absence of TMZ, the viability data from the '0 μM' TMZ conditions in the co-depletion experiments (Figure 5.6A-C) were analysed. The cell viability at 0 μM of TMZ was reduced after *BCAT1*:*CT83* co-depletion and the percentage change in viability in T20 and T100 cells was greater (reduction to 55±3% and 68±3% of non-silencing controls) than in parental cells (86±1%) (Figure 5.6E). These observed effects might be due to *BCAT1* depletion alone as the efficiency of *CT83* knockdown was poor in this experiment.

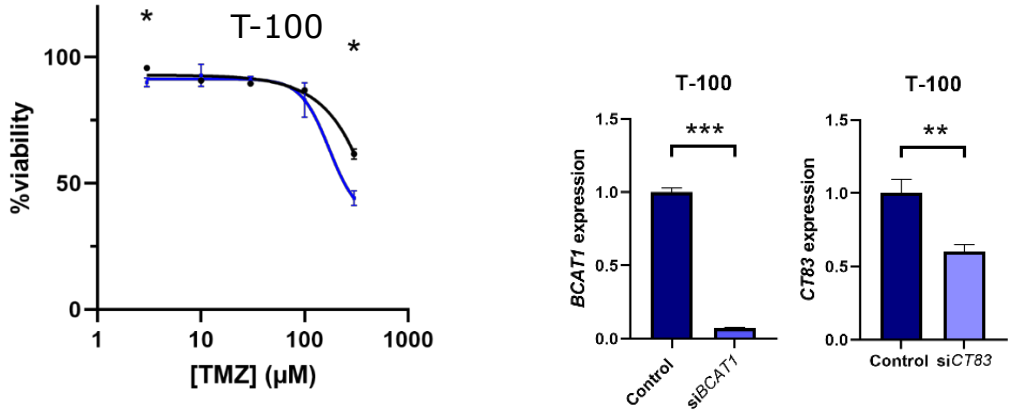
A



B



C



D

Cell Line	siControl IC_{50} (μM)	si*BCAT1* + si*CT83* IC_{50} (μM)
GaMG	6.4	29.8
T-20	96.8	140.4
T-100	385.7	243.1

E

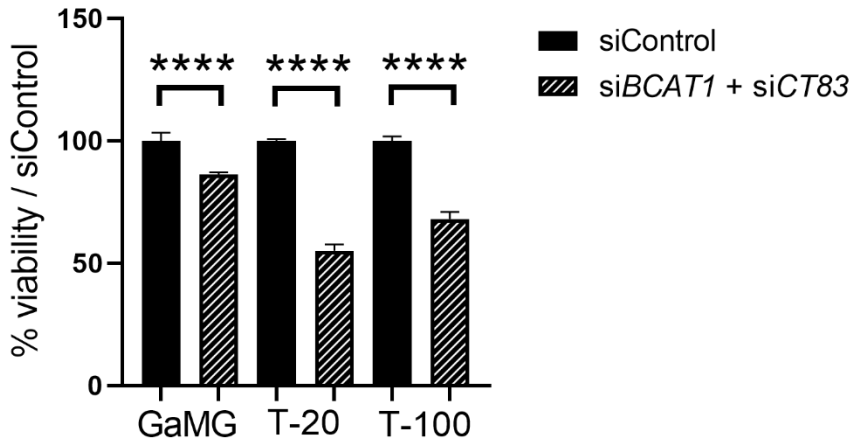
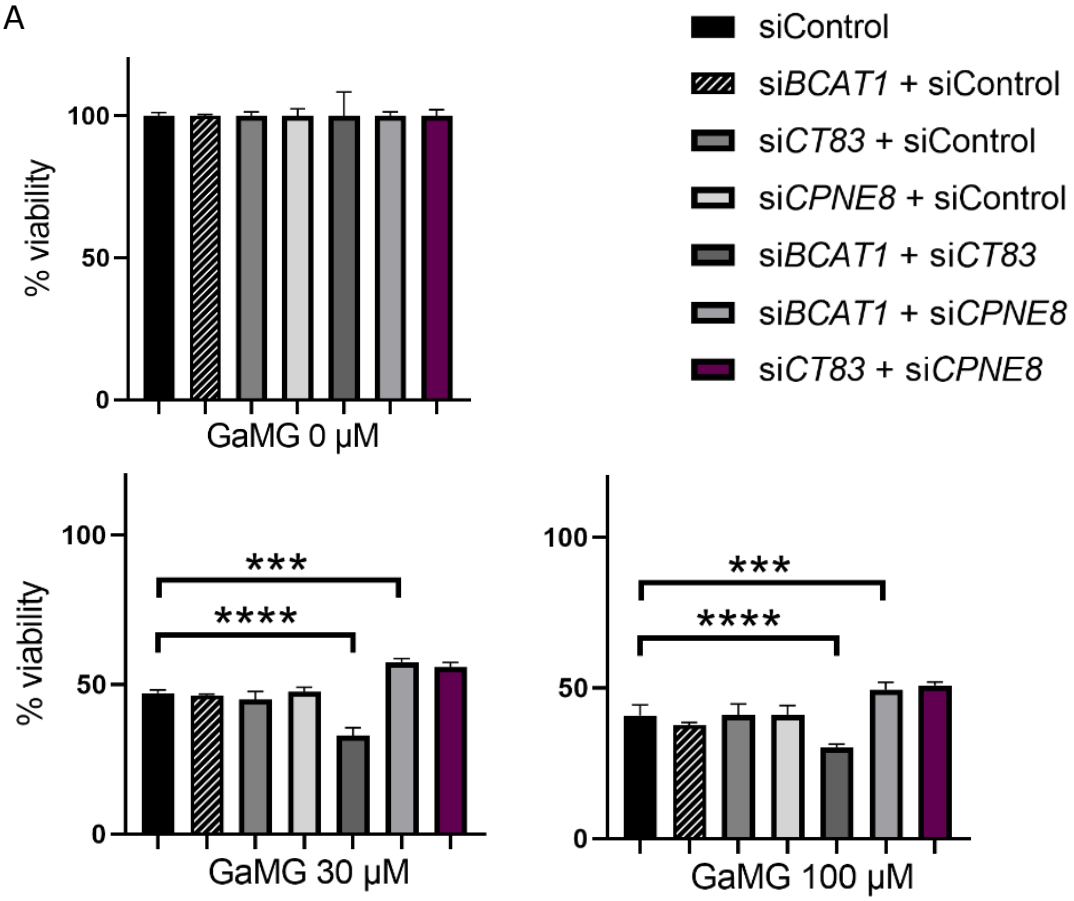


Figure 5.6: Effect of *BCAT1* and *CT83* co-depletion on dose response of GaMG parental, T-20 and T-100 to TMZ. Cells were transfected with 50 nM of si*BCAT1* and si*CT83*. After treatment with TMZ, cell viability was tested after 5 days. Points on the graph are means ± SD of triplicate values. The results were analysed for statistical significance using unpaired student's t-tests (**p < 0.01; ***p < 0.001; ****p < 0.0001). The bar graphs were qPCR results associated with the experiment, showing efficiency of knockdown. Graphs were plotted as means ± SD, each with triplicate technical replicates; statistical significance was tested using Welch's t-test. (D) shows the IC_{50} for each cell line, calculated based on pooled triplicate values from one experiment. (E) Viabilities of GaMG sublines in the absence of TMZ.

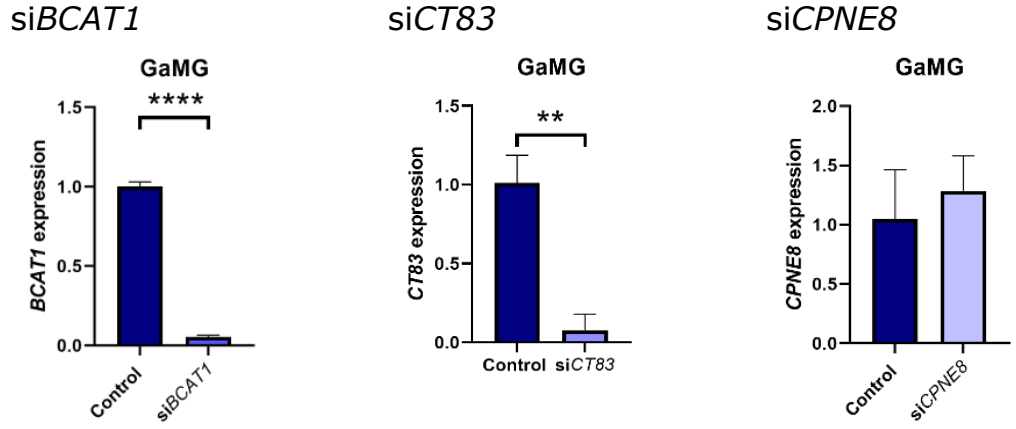
Further work was then carried out to test other combinations of siRNAs. However, depleting any two of the three upregulated genes did not lead to any significant effect on TMZ resistance (Figure 5.7 - Figure 5.9). At 0 μM TMZ, there was no significant change in the viabilities of GaMG sublines even with effective *BCAT1*:*CT83* co-depletion (Figure 5.7A, Figure 5.8A, Figure 5.9A). This was different to what was observed in Figure 5.6E. Despite previous success in individual depletion, the efficiency of knocking down *CPNE8* using Oligofectamine in these dual-depletion experiments was poor due to unknown reasons. Further attempts were carried out using DharmaFECT but with no success. The effort had to be aborted because of time constraints.

In summary, it was concluded that *BCAT1* and *CT83*, both alone and together, did not contribute to the acquisition of TMZ resistance in GaMG cells.

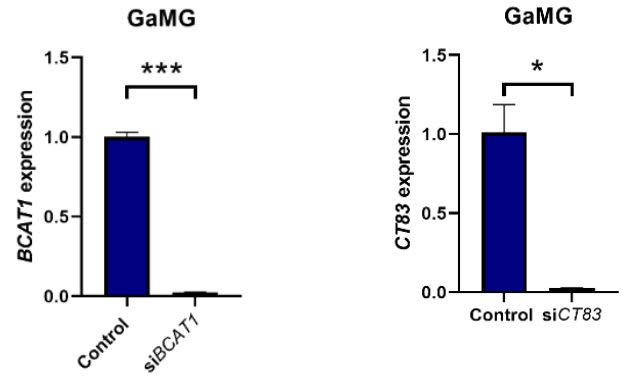
A


siControl
siBCAT1 + siControl
siCT83 + siControl
siCPNE8 + siControl
siBCAT1 + siCT83
siBCAT1 + siCPNE8
siCT83 + siCPNE8
% viability
100
50
0
GaMG 0 µM
***
****
GaMG 30 µM
GaMG 100 µM

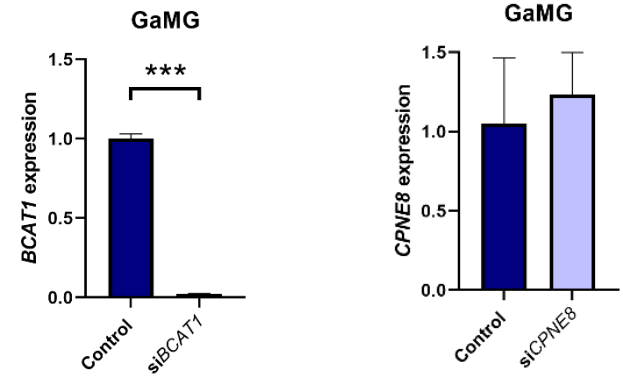
B


siBCAT1
siCT83
siCPNE8
GaMG
****
**
BCAT1 expression
CT83 expression
CPNE8 expression
1.5
1.0
0.5
0.0
2.0
Control
siBCAT1
siCT83
siCPNE8

si*BCAT1* + si*CT83*



si*BCAT1* + si*CPNE8*



si*CT83* + si*CPNE8*

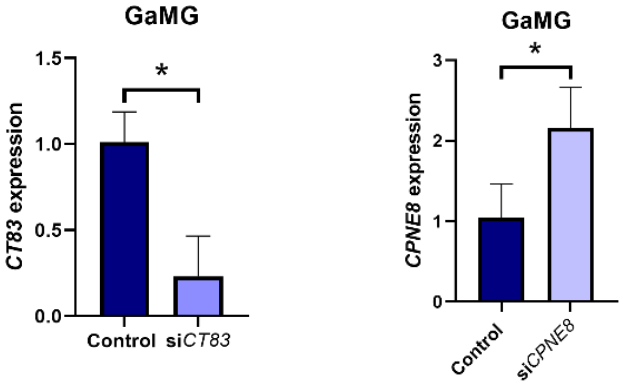
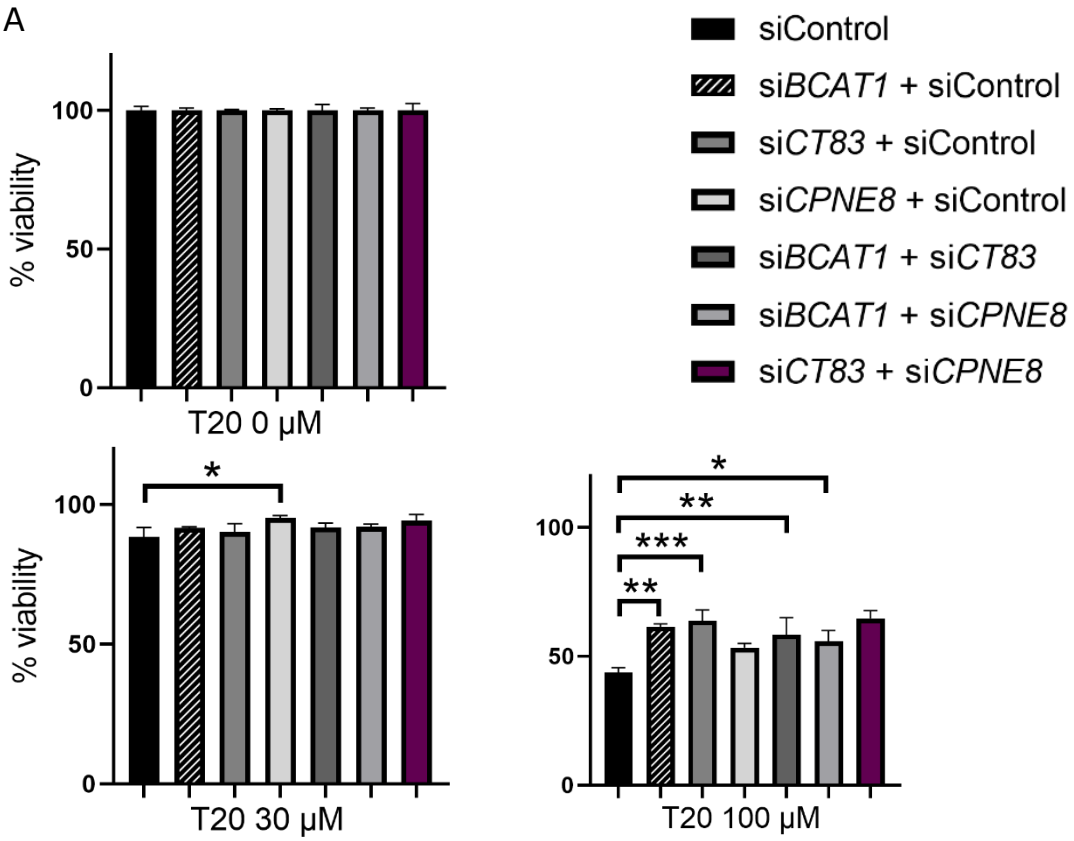
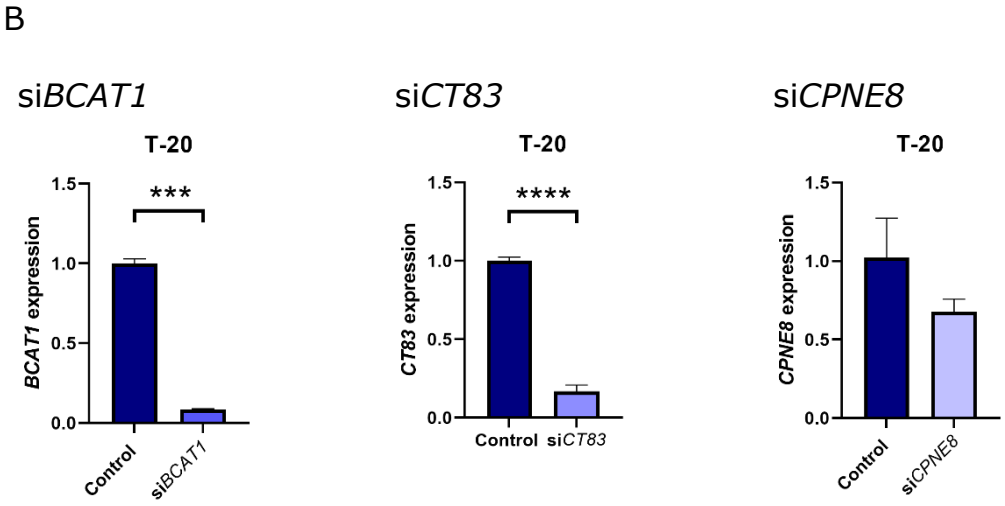
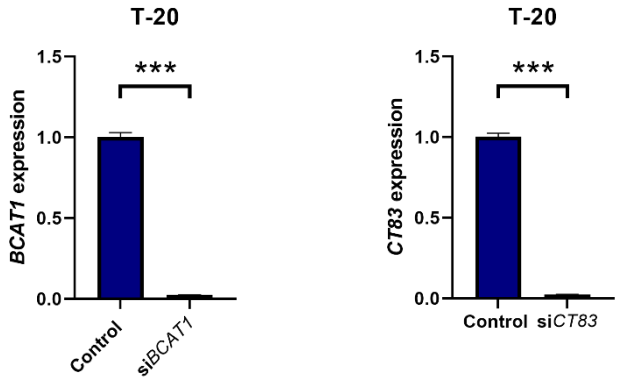


Figure 5.7: Effect of co-depleting two genes on TMZ resistance in GaMG. (A) GaMG cells were transfected with 25 nM of each siRNAs. After treatment with TMZ, cell viability was tested after 5-7 days. Bars on the graph are means ± SD of triplicate values from one independent experiment. The results were analysed for statistical significance using one-way ANOVA. (B) qPCR results as means ± SD showing efficiency of knockdown; statistical significance was tested using Welch's t-test.

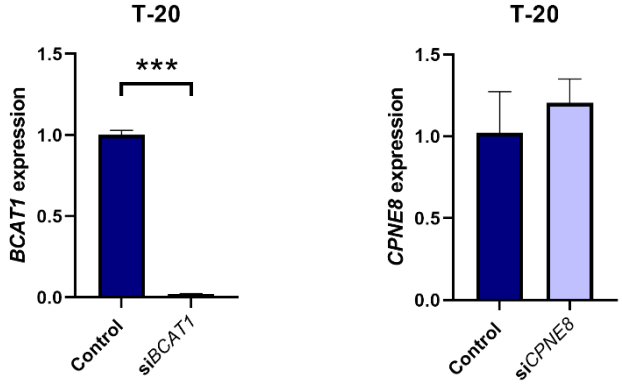

A
siControl
siBCAT1 + siControl
siCT83 + siControl
siCPNE8 + siControl
siBCAT1 + siCT83
siBCAT1 + siCPNE8
siCT83 + siCPNE8
% viability
100
50
0
T20 0 µM
*
T20 30 µM
*
**
***
**
T20 100 µM


B
siBCAT1
siCT83
siCPNE8
T-20
***
BCAT1 expression
1.5
1.0
0.5
0.0
Control
siBCAT1
T-20
****
CT83 expression
Control
siCT83
T-20
CPNE8 expression
Control
siCPNE8

si*BCAT1* + si*CT83*



si*BCAT1* + si*CPNE8*



si*CT83* + si*CPNE8*

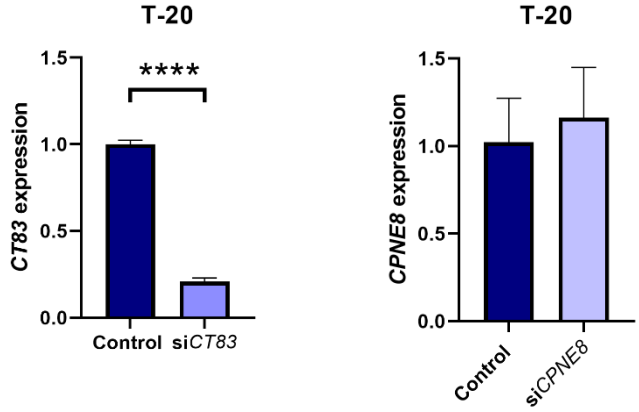
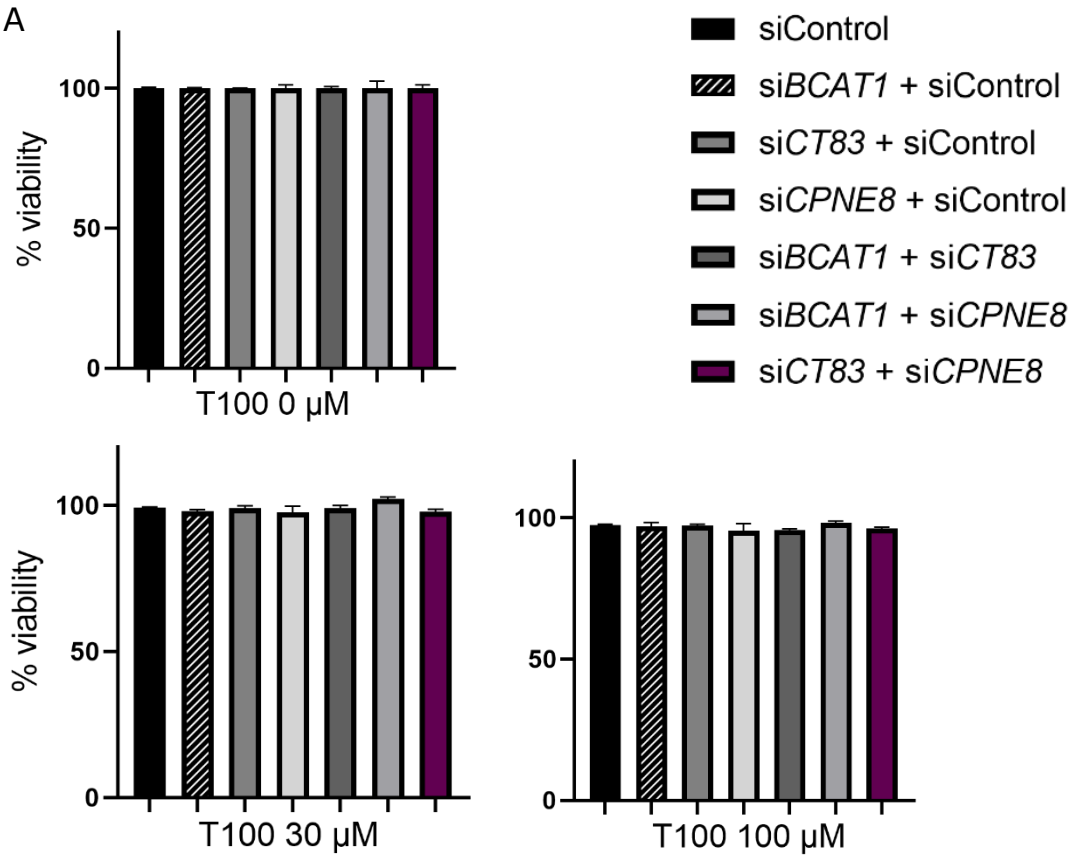
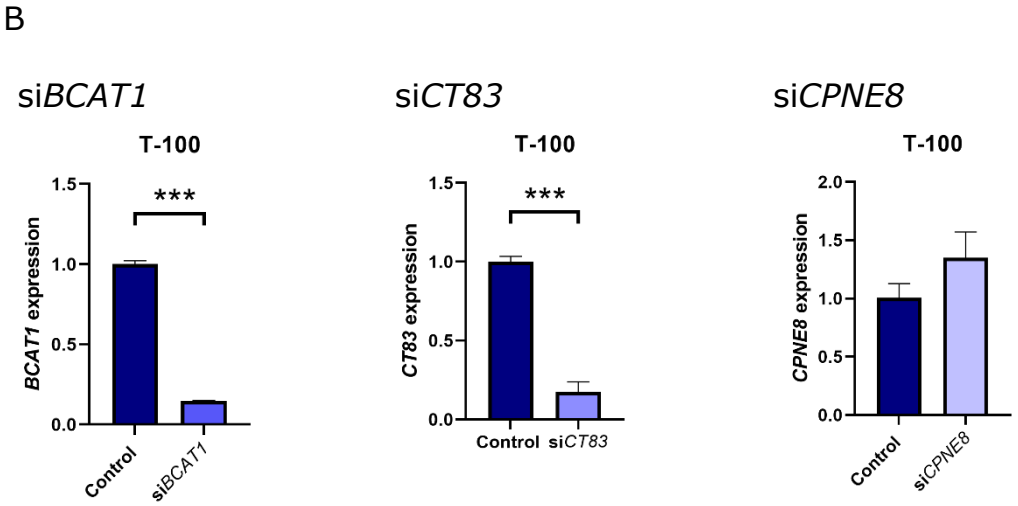
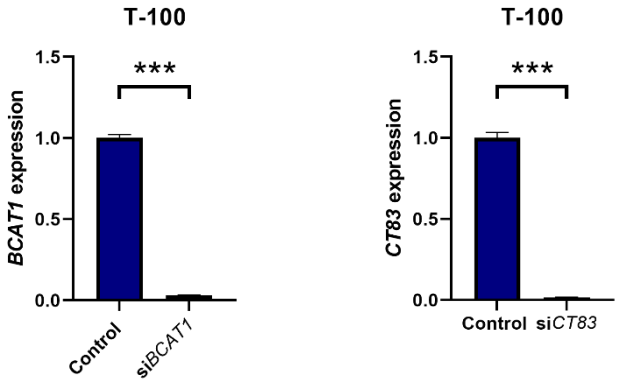


Figure 5.8: Effect of co-depleting two genes on TMZ resistance in T-20. (A) T-20 cells were transfected with 25 nM of each siRNAs. After treatment with TMZ, cell viability was tested after 5-7 days. Bars on the graph are means ± SD of triplicate values from one independent experiment. The results were analysed for statistical significance using one-way ANOVA. (B) qPCR results as means ± SD showing efficiency of knockdown; statistical significance was tested using Welch's t-test.

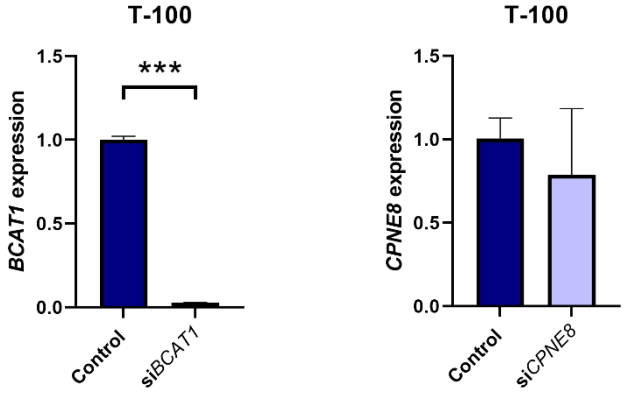

A
siControl
siBCAT1 + siControl
siCT83 + siControl
siCPNE8 + siControl
siBCAT1 + siCT83
siBCAT1 + siCPNE8
siCT83 + siCPNE8
% viability
100
50
0
T100 0 µM
T100 30 µM
T100 100 µM


B
siBCAT1
siCT83
siCPNE8
T-100
***
BCAT1 expression
CT83 expression
CPNE8 expression
Control
siBCAT1
siCT83
siCPNE8

si*BCAT1* + si*CT83*



si*BCAT1* + si*CPNE8*



si*CT83* + si*CPNE8*

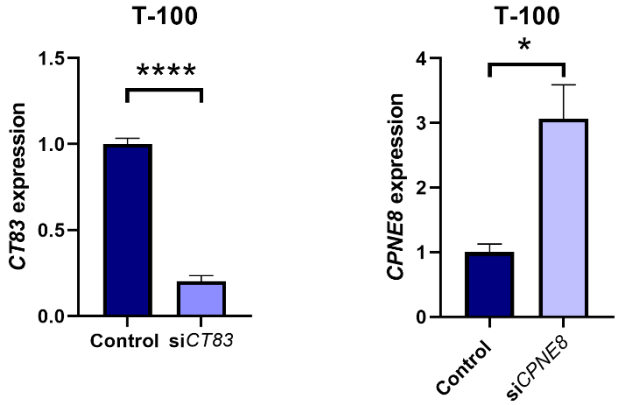
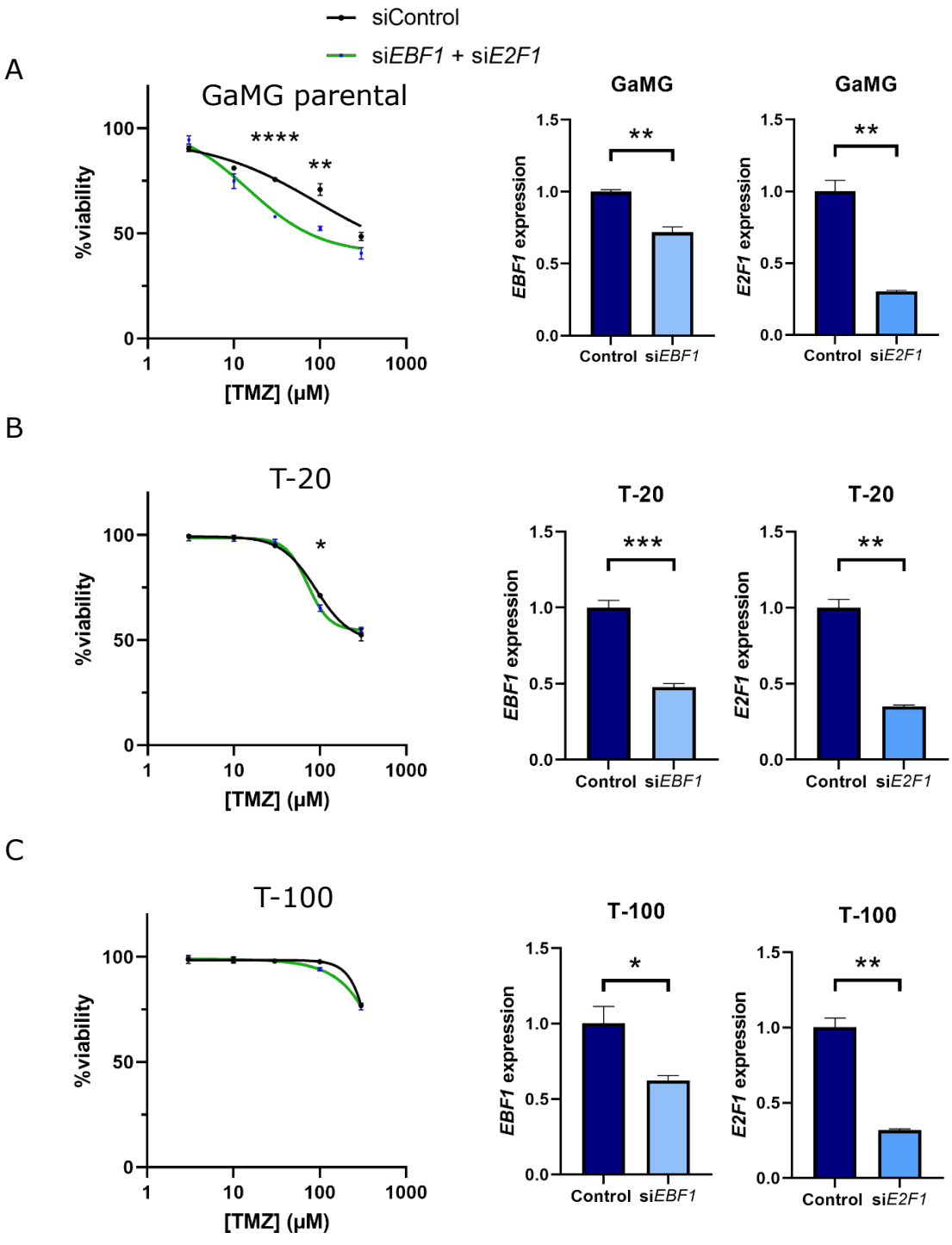


Figure 5.9: Effect of co-depleting two genes on TMZ resistance in T-100. (A) T-100 cells were transfected with 25 nM of each siRNAs. After treatment with TMZ, cell viability was tested after 5-7 days. Bars on the graph are means ± SD of triplicate values from one independent experiment. The results were analysed for statistical significance using one-way ANOVA. (B) qPCR results as means ± SD showing efficiency of knockdown; statistical significance was tested using Welch's t-test.

Next, co-depletion of targets that were found to be expressed more highly in the GaMG parental cells was tested. After *EBF1* and *E2F1* co-depletion, there was a slight improvement in GaMG parental cells' sensitivity towards TMZ whereas no effect was observed in both T-20 and T-100 cells (Figure 5.10).



D

Cell Line	siControl IC_{50} (μM)	si*EBF1* + si*E2F1* IC_{50} (μM)
GaMG	>300	74.45
T-20	>300	>300
T-100	>300	>300

Figure 5.10: Effect of *EBF1* and *E2F1* co-depletion on dose response of GaMG parental, T-20 and T-100 to TMZ. Cells were transfected with 50 nM of si*EBF1* and si*E2F1*. After treatment with TMZ, cell viability was tested after 5 days. Points on the graph are means ± SD of triplicate values. The results were analysed for statistical significance using unpaired student's t-tests (**p < 0.01; ***p < 0.001; ****p < 0.0001). The bar graphs were qPCR results associated with the experiment, showing efficiency of knockdown. Graphs were plotted as means ± SD, each with triplicate technical replicates; statistical significance was tested using Welch's t-test. (D) shows the IC_{50} for each cell line, calculated based on pooled triplicate values from one independent experiment.

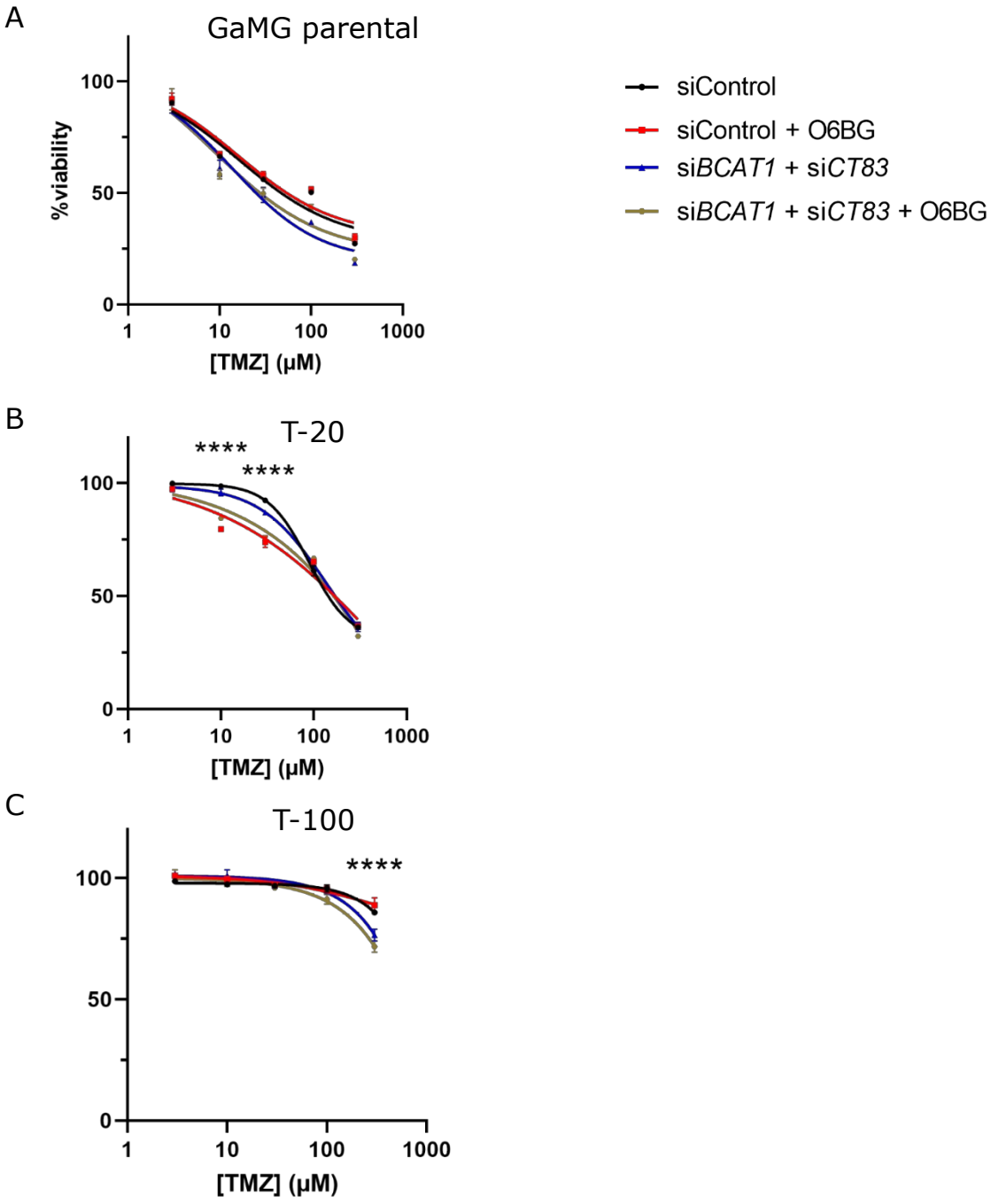
5.1.3 The effect of *BCAT1*:*CT83* co-depletion with MGMT inhibition

Since TMZ resistance in T-20 cells was partially dependent on MGMT (Figure 3.6), the effect of co-depleting *BCAT1*:*CT83* and MGMT inhibition using O6BG was investigated.

Similar to results in Figure 5.6, no significant change in TMZ resistance after depleting *BCAT1* and *CT83* together was observed. After the addition of 20 μM of O6BG to the depleted cells, a small reduction in TMZ resistance at 10-30 μM of TMZ in T20 cells was observed, but the effect might be due to MGMT inhibition as a similar result was observed with O6BG alone (Figure 5.11). These results were similar to Figure 3.6 where O6BG partially reversed TMZ resistance in T-20 cells.

At 300 μM of TMZ in T100 cells, there was also a slight increase in TMZ sensitivity after depletion of *BCAT1* and *CT83*, with or without MGMT inhibition (Figure 5.11C). This effect might be attributed to *BCAT1*:*CT83* co-depletion as O6BG alone did not lead to any change in viability and the results were similar to Figure 5.6C.

Overall, there was statistical significance in some conditions but unlikely to be biologically significant, despite effective target depletion using siRNAs.


A
GaMG parental
%viability
100
50
0
1
10
100
1000
[TMZ] (μM)
siControl
siControl + O6BG
siBCAT1 + siCT83
siBCAT1 + siCT83 + O6BG
B
T-20
****
****
100
50
0
1
10
100
1000
[TMZ] (μM)
C
T-100
****
100
50
0
1
10
100
1000
[TMZ] (μM)
D
GaMG parental
T-20
T-100
GaMG
**
BCAT1 expression
1.5
1.0
0.5
0.0
Control
siBCAT1
GaMG
**
CT83 expression
Control
siCT83
T-20
****
BCAT1 expression
Control
siBCAT1
T-20
***
CT83 expression
Control
siCT83
T-100
***
BCAT1 expression
Control
siBCAT1
T-100
*
CT83 expression
Control
siCT83

E

IC_{50}	GaMG	T-20	T-100
AllStar	47.20	143.28	>300
AllStar + O6BG	54.38	168.66	>300
si*BCAT1*+si*CT83*	25.02	170.40	>300
si*BCAT1*+si*CT83*+O6BG	27.65	163.78	>300

Figure 5.11: Effect of BCAT1 and CT83 co-depletion, with or without O6BG, on dose response of GaMG parental, T-20 and T-100 to TMZ. Cells were transfected with 50 nM of si*BCAT1* and si*CT83*. After treatment with 20 μM of O6BG plus TMZ, cell viability was tested after 5-7 days. Points on the graph are means ± SD of triplicate values. The results were analysed for statistical significance using unpaired student's t-tests (**p < 0.01; ***p < 0.001; ****p < 0.0001). (D) qPCR results as means ± SD showing efficiency of knockdown; statistical significance was tested using Welch's t-test. (E) shows the IC_{50} for each cell line, calculated based on pooled triplicate values from one independent experiment.

5.2 Discussion

The relatively novel status of several of these DE genes explained the lack of available inhibitors. Therefore, depletion of candidate DE genes was used to test their functional contribution to TMZ resistance. Generation of permanent DE gene deletion clones using gene editing techniques such as the CRISPR/Cas9 system could have been more accurate in testing the effect of these genes due to the off-target activity of siRNAs and variable knockdown efficiencies, but given the time constraints of this project, siRNAs were chosen.

No reversal of TMZ resistance was observed upon depletion of the candidate DE genes, either alone or together, in the resistant sublines. The rationale for only knocking down two genes rather than more, was to avoid generating excessive and unnecessary cellular stress, but still be able to test if TMZ resistance was mediated by multiple drivers. Although there was a small reduction observed at 300 μM of TMZ in T-100 cells after *E2F1* and *BCAT1*:*CT83* depletion (Figure 5.5 and Figure 5.6), achieving this concentration in the CSF would mean even higher concentrations in the plasma, which could lead to significantly higher risk of toxic side effects.

After *BCAT1* and *CT83* co-depletion, the viabilities of T-20 and T-100 cells were lower than that of GaMG parental cells in the absence of TMZ (Figure 5.6E). This suggests that even if *BCAT1* and *CT83* are not on their own driving TMZ resistance, the cells may be more dependent on these genes for viability. However, similar results were

not observed across different repeats. This inconsistency might be due to inaccurate cell-counting while seeding the cells post siRNAs transfection as the number of cells were sometimes below the accurate range of the cell counter machine.

Statistical analyses indicated that the standard deviations for all the IC_{50} values might have been large due to inconsistent phenotypes. The sensitivity of the GaMG sublines towards TMZ seemed to change in between experiments, with GaMG sometimes being more resistant and T-20 being more sensitive. Nonetheless, conclusions could still be drawn from these results, which suggested that these genes are not driving TMZ resistance.

The hypothesis that knocking down overexpressed genes in the resistant sublines would reverse TMZ resistance and downregulated genes would increase resistance might be oversimplified, as the cellular compensatory mechanisms are neglected. For instance, an upregulated gene can be an effect of a compensatory process that is evoked in response to other mutations (El-Brolosy et al., 2017). Further investigation of the difference between GaMG parental and TMZ-resistant sublines in cell cycle response, apoptosis and DNA damage induction after TMZ exposure may shed light on the mechanisms of TMZ resistance. Additionally, T-20 and T-100 cells are made up of different clusters (Figure 4.6), meaning the drivers of TMZ resistance in the two resistant sublines could be different. The different mediators can possibly be identified by validating and testing the

functional contribution of the top ten DE genes between the clusters in T-20 and T-100 cells, i.e. cluster 2 vs 1 and 2 vs 3. This could also be compared against the top twenty DE genes between the three sublines from Figure 4.1, which may reveal some useful insights.

Chapter 6: Conclusion

The aim of this project was to investigate potential novel drivers contributing to TMZ resistance in adult GBM. However, there were several practical constraints in this project. Firstly, the cell viabilities were estimated using CellTiter-Blue®, which measured the metabolic capacity of viable cells, but this might not reflect the true changes in cell number as the conversion from resazurin to resorufin could be impacted by changes in intracellular metabolic activity that did not directly affect overall cell viability (Rai et al., 2018). In addition, there were only 96 cells being analysed in scRNA-seq for each subline and the number of cells was limited by cost. This might have reduce the statistical power and opportunity to observe relationships between transcriptomes (Haque et al., 2017).

Despite following the same protocol, changes in the TMZ-resistant phenotype between different experiments was frequently observed especially in the GaMG parental cells. Without a consistent TMZ sensitivity, the investigation was very challenging as the real effects of any intervention might not have been observed. Another limitation of this project has been the time constraint, resulting in insufficient repeats of data. For instance, certain depletion experiments with poor transfection efficiency were not able to be repeated, with fine-tuned and optimised transfection conditions. The COVID-19 pandemic has certainly worsened the situation as the lab was shut for more than three months during the spring-summer national lockdown.

Although retrospective suspension was approved and more time was granted, the bench work did not return to full capacity, limiting the number of people in the department and the maintenance of social distancing.

Although several relatively novel DE genes have been identified and validated (i.e. *BCAT1*, *CT83*, *CPNE8*, *EBF1* and *E2F1*), they did not seem to contribute towards acquisition of TMZ resistance in the GaMG sublines using the experimental methods documented above, to deplete target proteins singly or in pairs. Nevertheless, *BCAT1*, which affected metabolism of branched-chain amino acid, was found to be upregulated in IDH1-wildtype GBM (Cho et al., 2017). It was also shown that GBM cells entered a transient state with decreased growth and distinctive metabolic properties during the acquisition of TMZ resistance (Rabé et al., 2020). Therefore, the role of *BCAT1* in this shift of metabolism could be investigated further. Besides, the transcription factor E2F1 might not on its own mediate TMZ resistance in this model, but another transcription factor nuclear factor I A (NFIA) had been shown to be upregulated and contributed to acquisition of TMZ resistance in GBM cells via activation of NF-κB pathway (Yu et al., 2019). As mentioned previously, TMZ resistance might be mediated by multiple drivers and it had been shown that TMZ resistance was successfully overcome through combined inhibition of NAD^+ biosynthesis and BER pathway (Goellner et al., 2011). Although targeting multiple genes with siRNAs might cause toxicity in the cells,

the availability of more inhibitors would allow higher number of targets being simultaneously blocked. For instance, a cytosolic BCAT inhibitor (#9002002, Cayman Chemical) could be used simultaneously with si*CT83* and si*CPNE8*.

Further work that can be done if time permits to firm up the evidence and improve the accuracy of identifying novel drivers have been described in the discussion section of each chapter, such as the proteomics analysis. A previous DPhil student from the Macaulay Group, Victoria Ma had found that after treatment with TMZ there were significantly reduced γH2AX foci in T-20 and there were even fewer foci in TMZ-treated T-100 cells. After TMZ-induced methylation, at least two cycles of replication are needed to generate strand breaks (Quiros et al., 2010), but the resistant sublines were still proliferating similarly to the GaMG parental cells. This suggested either rapid and effective DSBs repair or a replication process that bypasses the strand breaks caused by TMZ. As mentioned in section 1.3.4, TMZ-induced DSBs were usually repaired by HR (Roos et al., 2009). By pharmacologically inhibiting HR, the role of HR in this process and any additional novel mechanisms could be elucidated. For instance, RAD51 inhibitors had been described to inhibit HR and the inhibitory effect could be determined by assessing RAD51 foci formation (Berte et al., 2016, Lodhia et al., 2015).

It had been shown that RRM2 inhibition led to increased replication stress (Rasmussen et al., 2016), and increased replication

stress had been demonstrated to cause radioresistant phenotype in the GSCs (Carruthers et al., 2018). Herein, *RRM2* had been validated as being downregulated in the TMZ-resistant sublines (Figure 4.22), and in one preliminary experiment (not included in the thesis), *RRM2* depletion appeared to increase TMZ resistance in GaMG parental cells. If time had allowed, this experiment could have been repeated. There might be some sort of aberrant replication which allowed the resistant cells to proliferate without generating toxic DSBs. The Macaulay lab does possess the reagents and assays to study DNA replication, having found that IGFs regulate *RRM2* expression and rate of DNA replication (Rieunier et al., 2020). For instance, a promoter reporter assay could be done to explore mechanism of altered *RRM2* expression. DNA fiber assays could also be done to investigate whether replication dynamics are altered. Furthermore, assessing foci formation at 10 mins, 2 hours and 4 hours could reveal whether SSBs and DSBs are produced and quickly repaired or not generated at all in the T-100 cells. Lastly, alkaline comet assay could be performed to quantify SSBs and DSBs, or DSBs only by neutral comet assay.

TMZ resistance results in the inevitable recurrence of GBM tumours. The role of *RRM2* in the acquisition of TMZ resistance would merit further investigation. Besides, the scRNA-seq analysis had identified many DE genes that could guide future investigations to shed light on the resistance drivers.

Chapter 7: References

Agarwal, S., Manchanda, P., Vogelbaum, M. A., Ohlfest, J. R. & Elmquist, W. F. 2013. Function of the blood-brain barrier and restriction of drug delivery to invasive glioma cells: findings in an orthotopic rat xenograft model of glioma. *Drug metabolism and disposition: the biological fate of chemicals,* 41**,** 33-39.

Agarwala, S. S. & Kirkwood, J. M. 2000. Temozolomide, a Novel Alkylating Agent with Activity in the Central Nervous System, May Improve the Treatment of Advanced Metastatic Melanoma. *The Oncologist,* 5**,** 144-151.

Agnihotri, S., Burrell, K. E., Wolf, A., Jalali, S., Hawkins, C., Rutka, J. T. & Zadeh, G. 2013. Glioblastoma, a Brief Review of History, Molecular Genetics, Animal Models and Novel Therapeutic Strategies. *Archivum Immunologiae et Therapiae Experimentalis,* 61**,** 25-41.

Agnihotri, S., Gajadhar, A. S., Ternamian, C., Gorlia, T., Diefes, K. L., Mischel, P. S., Kelly, J., Mcgown, G., Thorncroft, M., Carlson, B. L., Sarkaria, J. N., Margison, G. P., Aldape, K., Hawkins, C., Hegi, M. & Guha, A. 2012. Alkylpurine-DNA-N-glycosylase confers resistance to temozolomide in xenograft models of glioblastoma multiforme and is associated with poor survival in patients. *The Journal of clinical investigation,* 122**,** 253-266.

Aldape, K., Brindle, K. M., Chesler, L., Chopra, R., Gajjar, A., Gilbert, M. R., Gottardo, N., Gutmann, D. H., Hargrave, D., Holland, E. C., Jones, D. T. W., Joyce, J. A., Kearns, P., Kieran, M. W., Mellinghoff, I. K., Merchant, M., Pfister, S. M., Pollard, S. M., Ramaswamy, V., Rich, J. N., Robinson, G. W., Rowitch, D. H., Sampson, J. H., Taylor, M. D., Workman, P. & Gilbertson, R. J. 2019. Challenges to curing primary brain tumours. *Nat Rev Clin Oncol,* 16**,** 509-520.

Almenawer, S. A., Badhiwala, J. H., Alhazzani, W., Greenspoon, J., Farrokhyar, F., Yarascavitch, B., Algird, A., Kachur, E., Cenic, A., Sharieff, W., Klurfan, P., Gunnarsson, T., Ajani, O., Reddy, K., Singh, S. K. & Murty, N. K. 2015. Biopsy versus partial versus gross total resection in older patients with high-grade glioma: a systematic review and meta-analysis. *Neuro-oncology,* 17**,** 868-881.

Ames, A., 3rd 2000. CNS energy metabolism as related to function. *Brain Res Brain Res Rev,* 34**,** 42-68.

An, Z., Aksoy, O., Zheng, T., Fan, Q.-W. & Weiss, W. A. 2018. Epidermal growth factor receptor and EGFRvIII in glioblastoma: signaling pathways and targeted therapies. *Oncogene,* 37**,** 1561-1575.

Andersen, A. P. 1978. Postoperative Irradiation of Glioblastomas: Results in a Randomized Series. *Acta Radiologica: Oncology, Radiation, Physics, Biology,* 17**,** 475-484.

Attwell, D., Buchan, A. M., Charpak, S., Lauritzen, M., Macvicar, B. A. & Newman, E. A. 2010. Glial and neuronal control of brain blood flow. *Nature,* 468**,** 232-243.

Aye, Y., Li, M., Long, M. J. C. & Weiss, R. S. 2015. Ribonucleotide reductase and cancer: biological mechanisms and targeted therapies. *Oncogene,* 34**,** 2011-2021.

Banelli, B., Carra, E., Barbieri, F., Würth, R., Parodi, F., Pattarozzi, A., Carosio, R., Forlani, A., Allemanni, G., Marubbi, D., Florio, T., Daga, A. & Romani, M. 2015. The histone demethylase KDM5A is a key factor for the resistance to temozolomide in glioblastoma. *Cell Cycle,* 14**,** 3418-3429.

Bao, S., Wu, Q., Mclendon, R. E., Hao, Y., Shi, Q., Hjelmeland, A. B., Dewhirst, M. W., Bigner, D. D. & Rich, J. N. 2006. Glioma stem cells promote radioresistance by preferential activation of the DNA damage response. *Nature,* 444**,** 756-760.

Bax, D. A., Mackay, A., Little, S. E., Carvalho, D., Viana-Pereira, M., Tamber, N., Grigoriadis, A. E., Ashworth, A., Reis, R. M., Ellison, D. W., Al-Sarraj, S., Hargrave, D. & Jones, C. 2010. A distinct spectrum of copy number aberrations in pediatric high-grade gliomas. *Clinical cancer research : an official journal of the American Association for Cancer Research,* 16**,** 3368-3377.

Becht, E., Mcinnes, L., Healy, J., Dutertre, C.-A., Kwok, I. W. H., Ng, L. G., Ginhoux, F. & Newell, E. W. 2019. Dimensionality reduction for visualizing single-cell data using UMAP. *Nature Biotechnology,* 37**,** 38-44.

Behnan, J., Finocchiaro, G. & Hanna, G. 2019. The landscape of the mesenchymal signature in brain tumours. *Brain : a journal of neurology,* 142**,** 847-866.

Beranek, D. T. 1990. Distribution of methyl and ethyl adducts following alkylation with monofunctional alkylating agents. *Mutation Research/Fundamental and Molecular Mechanisms of Mutagenesis,* 231**,** 11-30.

Berte, N., Piée-Staffa, A., Piecha, N., Wang, M., Borgmann, K., Kaina, B. & Nikolova, T. 2016. Targeting Homologous Recombination by Pharmacological Inhibitors Enhances the Killing Response of Glioblastoma Cells Treated with Alkylating Drugs. *Molecular Cancer Therapeutics,* 15**,** 2665.

Bhowmik, A., Khan, R. & Ghosh, M. K. 2015. Blood brain barrier: a challenge for effectual therapy of brain tumors. *BioMed research international,* 2015**,** 320941-320941.

Bondy, M. L., Scheurer, M. E., Malmer, B., Barnholtz-Sloan, J. S., Davis, F. G., Il'yasova, D., Kruchko, C., Mccarthy, B. J., Rajaraman, P., Schwartzbaum, J. A., Sadetzki, S., Schlehofer, B., Tihan, T., Wiemels, J. L., Wrensch, M., Buffler, P. A. & Brain Tumor Epidemiology, C. 2008. Brain tumor epidemiology: consensus from the Brain Tumor Epidemiology Consortium. *Cancer,* 113**,** 1953-1968.

Bradl, M. & Lassmann, H. 2010. Oligodendrocytes: biology and pathology. *Acta neuropathologica,* 119**,** 37-53.
Brandao, M., Simon, T., Critchley, G. & Giamas, G. 2019. Astrocytes, the rising stars of the glioblastoma microenvironment. *Glia,* 67**,** 779-790.
Brennan, C. W., Verhaak, R. G. W., Mckenna, A., Campos, B., Noushmehr, H., Salama, S. R., Zheng, S., Chakravarty, D., Sanborn, J. Z., Berman, S. H., Beroukhim, R., Bernard, B., Wu, C.-J., Genovese, G., Shmulevich, I., Barnholtz-Sloan, J., Zou, L., Vegesna, R., Shukla, S. A., Ciriello, G., Yung, W. K., Zhang, W., Sougnez, C., Mikkelsen, T., Aldape, K., Bigner, D. D., Van Meir, E. G., Prados, M., Sloan, A., Black, K. L., Eschbacher, J., Finocchiaro, G., Friedman, W., Andrews, D. W., Guha, A., Iacocca, M., O'neill, B. P., Foltz, G., Myers, J., Weisenberger, D. J., Penny, R., Kucherlapati, R., Perou, C. M., Hayes, D. N., Gibbs, R., Marra, M., Mills, G. B., Lander, E., Spellman, P., Wilson, R., Sander, C., Weinstein, J., Meyerson, M., Gabriel, S., Laird, P. W., Haussler, D., Getz, G., Chin, L. & Network, T. R. 2013. The somatic genomic landscape of glioblastoma. *Cell,* 155**,** 462-477.
Brodbelt, A., Greenberg, D., Winters, T., Williams, M., Vernon, S., Collins, V. P. & National Cancer Information Network Brain Tumour, G. 2015. Glioblastoma in England: 2007-2011. *Eur J Cancer,* 51**,** 533-42.
Calabrese, C., Poppleton, H., Kocak, M., Hogg, T. L., Fuller, C., Hamner, B., Oh, E. Y., Gaber, M. W., Finklestein, D., Allen, M., Frank, A., Bayazitov, I. T., Zakharenko, S. S., Gajjar, A., Davidoff, A. & Gilbertson, R. J. 2007. A Perivascular Niche for Brain Tumor Stem Cells. *Cancer Cell,* 11**,** 69-82.
Caldecott, K. W. 2008. Single-strand break repair and genetic disease. *Nature Reviews Genetics,* 9**,** 619-631.
Carruthers, R. D., Ahmed, S. U., Ramachandran, S., Strathdee, K., Kurian, K. M., Hedley, A., Gomez-Roman, N., Kalna, G., Neilson, M., Gilmour, L., Stevenson, K. H., Hammond, E. M. & Chalmers, A. J. 2018. Replication Stress Drives Constitutive Activation of the DNA Damage Response and Radioresistance in Glioblastoma Stem-like Cells. *Cancer research,* 78**,** 5060-5071.
Ceccaldi, R., Sarangi, P. & D'andrea, A. D. 2016. The Fanconi anaemia pathway: new players and new functions. *Nature Reviews Molecular Cell Biology,* 17**,** 337-349.
Cenciarini, M., Valentino, M., Belia, S., Sforna, L., Rosa, P., Ronchetti, S., D'adamo, M. C. & Pessia, M. 2019. Dexamethasone in Glioblastoma Multiforme Therapy: Mechanisms and Controversies. *Frontiers in molecular neuroscience,* 12**,** 65-65.
Chaichana, K. L., Zadnik, P., Weingart, J. D., Olivi, A., Gallia, G. L., Blakeley, J., Lim, M., Brem, H. & Quiñones-Hinojosa, A. 2013.

Multiple resections for patients with glioblastoma: prolonging survival. *Journal of neurosurgery,* 118**,** 812-820.
Chen, C. C., Taniguchi, T. & D'andrea, A. 2007. The Fanconi anemia (FA) pathway confers glioma resistance to DNA alkylating agents. *Journal of Molecular Medicine,* 85**,** 497-509.
Chen, J.-R., Yao, Y., Xu, H.-Z. & Qin, Z.-Y. 2016. Isocitrate Dehydrogenase (IDH)1/2 Mutations as Prognostic Markers in Patients With Glioblastomas. *Medicine,* 95**,** e2583-e2583.
Cheng, C. L., Johnson, S. P., Keir, S. T., Quinn, J. A., Ali-Osman, F., Szabo, C., Li, H., Salzman, A. L., Dolan, M. E., Modrich, P., Bigner, D. D. & Friedman, H. S. 2005. Poly(ADP-ribose) polymerase-1 inhibition reverses temozolomide resistance in a DNA mismatch repair-deficient malignant glioma xenograft. *Mol Cancer Ther,* 4**,** 1364-8.
Cho, H. R., Jeon, H., Park, C.-K., Park, S.-H., Kang, K. M. & Choi, S. H. 2017. BCAT1 is a New MR Imaging-related Biomarker for Prognosis Prediction in IDH1-wildtype Glioblastoma Patients. *Scientific Reports,* 7**,** 17740.
Clinicaltrials.Gov. 2020a. *Temozolomide With or Without Veliparib in Treating Patients With Newly Diagnosed Glioblastoma Multiforme (NCT02152982)* [Online]. U.S. National Library of Medicine. Available: **https://ClinicalTrials.gov/show/NCT02152982** [Accessed 13 May 2020].
Clinicaltrials.Gov. 2020b. *A Trial of Enzastaurin Plus Temozolomide During and Following Radiation Therapy in Patients With Newly Diagnosed Glioblastoma With or Without the Novel Genomic Biomarker, DGM1* [Online]. U.S. National Library of Medicine. Available: **https://ClinicalTrials.gov/show/NCT03776071** [Accessed 13 May 2020].
Cohen, M. H., Johnson, J. R. & Pazdur, R. 2005. Food and Drug Administration Drug approval summary: temozolomide plus radiation therapy for the treatment of newly diagnosed glioblastoma multiforme. *Clin Cancer Res,* 11**,** 6767-71.
Comba, A., Dunn, P. J., Argento, A. E., Kadiyala, P., Ventosa, M., Zamler, D. B., Patel, P., Zhao, L., Nunez, F. J., Castro, M. G. & Lowenstein, P. R. 2019. The Proto-Oncogene Fyn Inhibits the Anti-Glioblastoma Immune Response. *bioRxiv***,** 608505.
Cronk, J. C. & Kipnis, J. 2013. Microglia - the brain's busy bees. *F1000prime reports,* 5**,** 53-53.
Cruk, C. R. U. *Brain, other CNS and intracranial tumours statistics* [Online]. Available: **https://www.cancerresearchuk.org/health-professional/cancer-statistics/statistics-by-cancer-type/brain-other-cns-and-intracranial-tumours#heading-Zero** [Accessed 16 Dec 2020].

Curtin, N. J., Wang, L. Z., Yiakouvaki, A., Kyle, S., Arris, C. A., Canan-Koch, S., Webber, S. E., Durkacz, B. W., Calvert, H. A., Hostomsky, Z. & Newell, D. R. 2004. Novel poly(ADP-ribose) polymerase-1 inhibitor, AG14361, restores sensitivity to temozolomide in mismatch repair-deficient cells. *Clin Cancer Res,* 10**,** 881-9.

Dallerac, G. & Rouach, N. 2016. Astrocytes as new targets to improve cognitive functions. *Prog Neurobiol,* 144**,** 48-67.

Dang, L., White, D. W., Gross, S., Bennett, B. D., Bittinger, M. A., Driggers, E. M., Fantin, V. R., Jang, H. G., Jin, S., Keenan, M. C., Marks, K. M., Prins, R. M., Ward, P. S., Yen, K. E., Liau, L. M., Rabinowitz, J. D., Cantley, L. C., Thompson, C. B., Vander Heiden, M. G. & Su, S. M. 2009. Cancer-associated IDH1 mutations produce 2-hydroxyglutarate. *Nature,* 462**,** 739-744.

Davis, B. M., Encell, L. P., Zielske, S. P., Christians, F. C., Liu, L., Friebert, S. E., Loeb, L. A. & Gerson, S. L. 2001. Applied molecular evolution of O6-benzylguanine-resistant DNA alkyltransferases in human hematopoietic cells. *Proceedings of the National Academy of Sciences of the United States of America,* 98**,** 4950-4954.

Degregori, J. & Johnson, D. G. 2006. Distinct and Overlapping Roles for E2F Family Members in Transcription, Proliferation and Apoptosis. *Curr Mol Med,* 6**,** 739-48.

Diksin, M., Smith, S. J. & Rahman, R. 2017. The Molecular and Phenotypic Basis of the Glioma Invasive Perivascular Niche. *Int J Mol Sci,* 18.

Ding, J., Wu, S., Zhang, C., Garyali, A., Martinez-Ledesma, E., Gao, F., Pokkulandra, A., Li, X., Bristow, C., Carugo, A., Koul, D. & Yung, W. A. 2019. BRCA1 identified as a modulator of temozolomide resistance in P53 wild-type GBM using a high-throughput shRNA-based synthetic lethality screening. *American journal of cancer research,* 9**,** 2428-2441.

Dunwoodie, L. J., Poehlman, W. L., Ficklin, S. P. & Feltus, F. A. 2018. Discovery and validation of a glioblastoma co-expressed gene module. *Oncotarget,* 9**,** 10995-11008.

El-Brolosy, M. A. & Stainier, D. Y. R. 2017. Genetic compensation: A phenomenon in search of mechanisms. *PLoS genetics,* 13**,** e1006780-e1006780.

Ellis, H. P., Mcinerney, C. E., Schrimpf, D., Sahm, F., Stupnikov, A., Wadsley, M., Wragg, C., White, P., Prise, K. M., Mcart, D. G. & Kurian, K. M. 2019. Clinically Actionable Insights into Initial and Matched Recurrent Glioblastomas to Inform Novel Treatment Approaches. *Journal of oncology,* 2019**,** 4878547-4878547.

Esteller, M., Garcia-Foncillas, J., Andion, E., Goodman, S. N., Hidalgo, O. F., Vanaclocha, V., Baylin, S. B. & Herman, J. G. 2000. Inactivation of the DNA-repair gene MGMT and the clinical

response of gliomas to alkylating agents. *N Engl J Med,* 343**,** 1350-4.
Fagerberg, L., Hallström, B. M., Oksvold, P., Kampf, C., Djureinovic, D., Odeberg, J., Habuka, M., Tahmasebpoor, S., Danielsson, A., Edlund, K., Asplund, A., Sjöstedt, E., Lundberg, E., Szigyarto, C. a.-K., Skogs, M., Takanen, J. O., Berling, H., Tegel, H., Mulder, J., Nilsson, P., Schwenk, J. M., Lindskog, C., Danielsson, F., Mardinoglu, A., Sivertsson, A., Von Feilitzen, K., Forsberg, M., Zwahlen, M., Olsson, I., Navani, S., Huss, M., Nielsen, J., Ponten, F. & Uhlén, M. 2014. Analysis of the human tissue-specific expression by genome-wide integration of transcriptomics and antibody-based proteomics. *Molecular & cellular proteomics : MCP,* 13**,** 397-406.
Fan, C. H., Liu, W. L., Cao, H., Wen, C., Chen, L. & Jiang, G. 2013. O6-methylguanine DNA methyltransferase as a promising target for the treatment of temozolomide-resistant gliomas. *Cell death & disease,* 4**,** e876-e876.
Felsberg, J., Thon, N., Eigenbrod, S., Hentschel, B., Sabel, M. C., Westphal, M., Schackert, G., Kreth, F. W., Pietsch, T., Loffler, M., Weller, M., Reifenberger, G., Tonn, J. C. & German Glioma, N. 2011. Promoter methylation and expression of MGMT and the DNA mismatch repair genes MLH1, MSH2, MSH6 and PMS2 in paired primary and recurrent glioblastomas. *Int J Cancer,* 129**,** 659-70.
Finneran, M., Marotta, D. A., Altenburger, D. & Nardone, E. 2020. Long-term Survival in a Patient with Butterfly Glioblastoma: A Case Report. *Cureus,* 12**,** e6914.
Forsyth, P. A. & Posner, J. B. 1993. Headaches in patients with brain tumors: a study of 111 patients. *Neurology,* 43**,** 1678-83.
Frackowiak, R. S. J. 2007. *Human brain function,* Amsterdam, Elsevier, Acad. Press.
Friedman, H. S., Keir, S., Pegg, A. E., Houghton, P. J., Colvin, O. M., Moschel, R. C., Bigner, D. D. & Dolan, M. E. 2002. O6-benzylguanine-mediated enhancement of chemotherapy. *Mol Cancer Ther,* 1**,** 943-8.
Friedman, H. S., Kerby, T. & Calvert, H. 2000. Temozolomide and Treatment of Malignant Glioma. *Clinical Cancer Research,* 6**,** 2585.
Fu, D., Calvo, J. A. & Samson, L. D. 2012. Balancing repair and tolerance of DNA damage caused by alkylating agents. *Nature reviews. Cancer,* 12**,** 104-120.
Futawatari, N., Fukuyama, T., Yamamura, R., Shida, A., Takahashi, Y., Nishi, Y., Ichiki, Y., Kobayashi, N., Yamazaki, H. & Watanabe, M. 2017. Early gastric cancer frequently has high expression of KK-LC-1, a cancer-testis antigen. *World journal of gastroenterology,* 23**,** 8200-8206.

Gil Del Alcazar, C. R., Todorova, P. K., Habib, A. A., Mukherjee, B. & Burma, S. 2016. Augmented HR Repair Mediates Acquired Temozolomide Resistance in Glioblastoma. *Mol Cancer Res,* 14**,** 928-940.

Gilbert, M. R., Liu, Y., Neltner, J., Pu, H., Morris, A., Sunkara, M., Pittman, T., Kyprianou, N. & Horbinski, C. 2014. Autophagy and oxidative stress in gliomas with IDH1 mutations. *Acta neuropathologica,* 127**,** 221-233.

Goellner, E. M., Grimme, B., Brown, A. R., Lin, Y.-C., Wang, X.-H., Sugrue, K. F., Mitchell, L., Trivedi, R. N., Tang, J.-B. & Sobol, R. W. 2011. Overcoming temozolomide resistance in glioblastoma via dual inhibition of NAD+ biosynthesis and base excision repair. *Cancer research,* 71**,** 2308-2317.

González-Gómez, P., Sánchez, P. & Mira, H. 2011. MicroRNAs as Regulators of Neural Stem Cell-Related Pathways in Glioblastoma Multiforme. *Molecular Neurobiology,* 44**,** 235-249.

Gorlia, T., Van Den Bent, M. J., Hegi, M. E., Mirimanoff, R. O., Weller, M., Cairncross, J. G., Eisenhauer, E., Belanger, K., Brandes, A. A., Allgeier, A., Lacombe, D. & Stupp, R. 2008. Nomograms for predicting survival of patients with newly diagnosed glioblastoma: prognostic factor analysis of EORTC and NCIC trial 26981-22981/CE.3. *Lancet Oncol,* 9**,** 29-38.

Guan, X., Hasan, M. N., Maniar, S., Jia, W. & Sun, D. 2018. Reactive Astrocytes in Glioblastoma Multiforme. *Molecular Neurobiology,* 55**,** 6927-6938.

Gupta, A. & Dwivedi, T. 2017. A Simplified Overview of World Health Organization Classification Update of Central Nervous System Tumors 2016. *Journal of neurosciences in rural practice,* 8**,** 629-641.

Gygi, S. P., Rochon, Y., Franza, B. R. & Aebersold, R. 1999. Correlation between protein and mRNA abundance in yeast. *Molecular and cellular biology,* 19**,** 1720-1730.

Haj, A., Doenitz, C., Schebesch, K.-M., Ehrensberger, D., Hau, P., Putnik, K., Riemenschneider, M. J., Wendl, C., Gerken, M., Pukrop, T., Brawanski, A. & Proescholdt, M. A. 2017. Extent of Resection in Newly Diagnosed Glioblastoma: Impact of a Specialized Neuro-Oncology Care Center. *Brain sciences,* 8**,** 5.

Han, X., Xue, X., Zhou, H. & Zhang, G. 2017. A molecular view of the radioresistance of gliomas. *Oncotarget,* 8**,** 100931-100941.

Hanif, F., Muzaffar, K., Perveen, K., Malhi, S. M. & Simjee, S. U. 2017. Glioblastoma Multiforme: A Review of its Epidemiology and Pathogenesis through Clinical Presentation and Treatment. *Asian Pacific journal of cancer prevention : APJCP,* 18**,** 3-9.

Haque, A., Engel, J., Teichmann, S. A. & Lönnberg, T. 2017. A practical guide to single-cell RNA-sequencing for biomedical research and clinical applications. *Genome Medicine,* 9**,** 75.

Hatiboglu, M. A., Wildrick, D. M. & Sawaya, R. 2013. The role of surgical resection in patients with brain metastases. *Ecancermedicalscience,* 7**,** 308-308.

Hegi, M. E., Diserens, A. C., Godard, S., Dietrich, P. Y., Regli, L., Ostermann, S., Otten, P., Van Melle, G., De Tribolet, N. & Stupp, R. 2004. Clinical trial substantiates the predictive value of O-6-methylguanine-DNA methyltransferase promoter methylation in glioblastoma patients treated with temozolomide. *Clin Cancer Res,* 10**,** 1871-4.

Hegi, M. E., Diserens, A. C., Gorlia, T., Hamou, M. F., De Tribolet, N., Weller, M., Kros, J. M., Hainfellner, J. A., Mason, W., Mariani, L., Bromberg, J. E., Hau, P., Mirimanoff, R. O., Cairncross, J. G., Janzer, R. C. & Stupp, R. 2005. MGMT gene silencing and benefit from temozolomide in glioblastoma. *N Engl J Med,* 352**,** 997-1003.

Henrik Heiland, D., Ravi, V. M., Behringer, S. P., Frenking, J. H., Wurm, J., Joseph, K., Garrelfs, N. W. C., Strähle, J., Heynckes, S., Grauvogel, J., Franco, P., Mader, I., Schneider, M., Potthoff, A.-L., Delev, D., Hofmann, U. G., Fung, C., Beck, J., Sankowski, R., Prinz, M. & Schnell, O. 2019. Tumor-associated reactive astrocytes aid the evolution of immunosuppressive environment in glioblastoma. *Nature Communications,* 10**,** 2541.

Herculano-Houzel, S. 2014. The glia/neuron ratio: How it varies uniformly across brain structures and species and what that means for brain physiology and evolution. *Glia,* 62**,** 1377-1391.

Hide, T., Shibahara, I. & Kumabe, T. 2019. Novel concept of the border niche: glioblastoma cells use oligodendrocytes progenitor cells (GAOs) and microglia to acquire stem cell-like features. *Brain Tumor Pathology,* 36**,** 63-73.

Ho, I. a. W. & Shim, W. S. N. 2017. Contribution of the Microenvironmental Niche to Glioblastoma Heterogeneity. *BioMed research international,* 2017**,** 9634172-9634172.

Hombach-Klonisch, S., Mehrpour, M., Shojaei, S., Harlos, C., Pitz, M., Hamai, A., Siemianowicz, K., Likus, W., Wiechec, E., Toyota, B. D., Hoshyar, R., Seyfoori, A., Sepehri, Z., Ande, S. R., Khadem, F., Akbari, M., Gorman, A. M., Samali, A., Klonisch, T. & Ghavami, S. 2018. Glioblastoma and chemoresistance to alkylating agents: Involvement of apoptosis, autophagy, and unfolded protein response. *Pharmacology & Therapeutics,* 184**,** 13-41.

Hoover, J. M., Nwojo, M., Puffer, R., Mandrekar, J., Meyer, F. B. & Parney, I. F. 2013. Surgical outcomes in recurrent glioma: clinical article. *J Neurosurg,* 118**,** 1224-31.

Hu, F., Ku, M.-C., Markovic, D., Dzaye, O. D. A., Lehnardt, S., Synowitz, M., Wolf, S. A. & Kettenmann, H. 2014. Glioma-associated microglial MMP9 expression is upregulated by TLR2

signaling and sensitive to minocycline. *International journal of cancer,* 135**,** 2569-2578.
Huang, J., Dewees, T., Campian, J. L., Chheda, M. G., Ansstas, G., Tsien, C., Zipfel, G. J., Dunn, G. P., Ippolito, J. E., Cairncross, J. G., Easaw, J. C., Rubin, J. & Kim, A. H. 2019. A TITE-CRM phase I/II study of disulfiram and copper with concurrent radiation therapy and temozolomide for newly diagnosed glioblastoma. *Journal of Clinical Oncology,* 37**,** 2033-2033.
Huang, P. H., Miraldi, E. R., Xu, A. M., Kundukulam, V. A., Del Rosario, A. M., Flynn, R. A., Cavenee, W. K., Furnari, F. B. & White, F. M. 2010. Phosphotyrosine signaling analysis of site-specific mutations on EGFRvIII identifies determinants governing glioblastoma cell growth. *Molecular bioSystems,* 6**,** 1227-1237.
Inda, M.-D.-M., Bonavia, R. & Seoane, J. 2014. Glioblastoma multiforme: a look inside its heterogeneous nature. *Cancers,* 6**,** 226-239.
Ito, S., Shiraishi, M., Tsuchihashi, K., Takatsuka, R., Yamamoto, J., Kuraoka, I. & Iwai, S. 2018. Fluorescence detection of DNA mismatch repair in human cells. *Scientific Reports,* 8**,** 12181.
Jacobs, A. L. & Schär, P. 2012. DNA glycosylases: in DNA repair and beyond. *Chromosoma,* 121**,** 1-20.
Jiang, G., Jiang, A.-J., Xin, Y., Li, L.-T., Cheng, Q. & Zheng, J.-N. 2014. Progression of O6-methylguanine-DNA methyltransferase and temozolomide resistance in cancer research. *Molecular Biology Reports,* 41**,** 6659-6665.
Jones, C., Perryman, L. & Hargrave, D. 2012. Paediatric and adult malignant glioma: close relatives or distant cousins? *Nature Reviews Clinical Oncology,* 9**,** 400-413.
Jun, H. T., Sun, J., Rex, K., Radinsky, R., Kendall, R., Coxon, A. & Burgess, T. L. 2007. AMG 102, A Fully Human Anti-Hepatocyte Growth Factor/Scatter Factor Neutralizing Antibody, Enhances the Efficacy of Temozolomide or Docetaxel in U-87 MG Cells and Xenografts. *Clinical Cancer Research,* 13**,** 6735.
Kaina, B., Margison, G. P. & Christmann, M. 2010. Targeting O6-methylguanine-DNA methyltransferase with specific inhibitors as a strategy in cancer therapy. *Cellular and Molecular Life Sciences,* 67**,** 3663-3681.
Kanemaru, Y., Natsumeda, M., Okada, M., Saito, R., Kobayashi, D., Eda, T., Watanabe, J., Saito, S., Tsukamoto, Y., Oishi, M., Saito, H., Nagahashi, M., Sasaki, T., Hashizume, R., Aoyama, H., Wakai, T., Kakita, A. & Fujii, Y. 2019. Dramatic response of BRAF V600E-mutant epithelioid glioblastoma to combination therapy with BRAF and MEK inhibitor: establishment and xenograft of a cell line to predict clinical efficacy. *Acta Neuropathologica Communications,* 7**,** 119.

Kitange, G. J., Carlson, B. L., Schroeder, M. A., Grogan, P. T., Lamont, J. D., Decker, P. A., Wu, W., James, C. D. & Sarkaria, J. N. 2009. Induction of MGMT expression is associated with temozolomide resistance in glioblastoma xenografts. *Neuro-oncology,* 11**,** 281-291.

Kobak, D. & Berens, P. 2019. The art of using t-SNE for single-cell transcriptomics. *Nature Communications,* 10**,** 5416.

Kondo, Y., Fukuyama, T., Yamamura, R., Futawatari, N., Ichiki, Y., Tanaka, Y., Nishi, Y., Takahashi, Y., Yamazaki, H., Kobayashi, N. & Watanabe, M. 2018. Detection of KK-LC-1 Protein, a Cancer/Testis Antigen, in Patients with Breast Cancer. *Anticancer Res,* 38**,** 5923-5928.

Kozak, K. R. & Moody, J. S. 2009. Giant cell glioblastoma: a glioblastoma subtype with distinct epidemiology and superior prognosis. *Neuro-oncology,* 11**,** 833-841.

Kristiansen, K., Hagen, S., Kollevold, T., Torvik, A., Holme, I., Nesbakken, R., Hatlevoll, R., Lindgren, M., Brun, A., Lindgren, S., Notter, G., Andersen, A. P. & Elgen, K. 1981. Combined modality therapy of operated astrocytomas grade III and IV. Confirmation of the value of postoperative irradiation and lack of potentiation of bleomycin on survival time: a prospective multicenter trial of the Scandinavian Glioblastoma Study Group. *Cancer,* 47**,** 649-52.

Krokan, H. E. & Bjørås, M. 2013. Base excision repair. *Cold Spring Harbor perspectives in biology,* 5**,** a012583-a012583.

Kuger, S., Graus, D., Brendtke, R., Gunther, N., Katzer, A., Lutyj, P., Polat, B., Chatterjee, M., Sukhorukov, V. L., Flentje, M. & Djuzenova, C. S. 2013. Radiosensitization of Glioblastoma Cell Lines by the Dual PI3K and mTOR Inhibitor NVP-BEZ235 Depends on Drug-Irradiation Schedule. *Transl Oncol,* 6**,** 169-79.

Kumar, D., Bansal, G., Narang, A., Basak, T., Abbas, T. & Dash, D. 2016. Integrating transcriptome and proteome profiling: Strategies and applications. *PROTEOMICS,* 16**,** 2533-2544.

Lee, S. Y. 2016. Temozolomide resistance in glioblastoma multiforme. *Genes & diseases,* 3**,** 198-210.

Lesueur, P., Lequesne, J., Grellard, J.-M., Dugué, A., Coquan, E., Brachet, P.-E., Geffrelot, J., Kao, W., Emery, E., Berro, D. H., Castera, L., Goardon, N., Lacroix, J., Lange, M., Capel, A., Leconte, A., Andre, B., Léger, A., Lelaidier, A., Clarisse, B. & Stefan, D. 2019. Phase I/IIa study of concomitant radiotherapy with olaparib and temozolomide in unresectable or partially resectable glioblastoma: OLA-TMZ-RTE-01 trial protocol. *BMC Cancer,* 19**,** 198.

Li, G.-M. 2008. Mechanisms and functions of DNA mismatch repair. *Cell Research,* 18**,** 85-98.

Li, Y., Liu, Y., Ren, J., Deng, S., Yi, G., Guo, M., Shu, S., Zhao, L., Peng, Y. & Qi, S. 2018. miR-1268a regulates ABCC1 expression to mediate temozolomide resistance in glioblastoma. *Journal of Neuro-Oncology,* 138**,** 499-508.

Li, Z., Pearlman, A. H. & Hsieh, P. 2016. DNA mismatch repair and the DNA damage response. *DNA Repair (Amst),* 38**,** 94-101.

Liang, H., Wang, R., Jin, Y., Li, J. & Zhang, S. 2016. MiR-422a acts as a tumor suppressor in glioblastoma by targeting PIK3CA. *American journal of cancer research,* 6**,** 1695-1707.

Liu, L., Markowitz, S. & Gerson, S. L. 1996. Mismatch repair mutations override alkyltransferase in conferring resistance to temozolomide but not to 1,3-bis(2-chloroethyl)nitrosourea. *Cancer Res,* 56**,** 5375-9.

Liu, X., Chen, X., Shi, L., Shan, Q., Cao, Q., Yue, C., Li, H., Li, S., Wang, J., Gao, S., Niu, M. & Yu, R. 2019. The third-generation EGFR inhibitor AZD9291 overcomes primary resistance by continuously blocking ERK signaling in glioblastoma. *Journal of Experimental & Clinical Cancer Research,* 38**,** 219.

Liu, Y., Beyer, A. & Aebersold, R. 2016. On the Dependency of Cellular Protein Levels on mRNA Abundance. *Cell,* 165**,** 535-50.

Livak, K. J. & Schmittgen, T. D. 2001. Analysis of relative gene expression data using real-time quantitative PCR and the 2(-Delta Delta C(T)) Method. *Methods,* 25**,** 402-8.

Lodhia, K. A., Gao, S., Aleksic, T., Esashi, F. & Macaulay, V. M. 2015. Suppression of homologous recombination sensitizes human tumor cells to IGF-1R inhibition. *International journal of cancer,* 136**,** 2961-2966.

Louis, D. N., Perry, A., Reifenberger, G., Von Deimling, A., Figarella-Branger, D., Cavenee, W. K., Ohgaki, H., Wiestler, O. D., Kleihues, P. & Ellison, D. W. 2016. The 2016 World Health Organization Classification of Tumors of the Central Nervous System: a summary. *Acta Neuropathol,* 131**,** 803-20.

Lutterbach, J., Guttenberger, R. & Pagenstecher, A. 2001. Gliosarcoma: a clinical study. *Radiotherapy and Oncology,* 61**,** 57-64.

Ma, V. 2019. *Investigating Glioblastoma Multiforme Transcriptome Heterogeneity during the Acquisition of Chemotherapy Resistance to Inform Targeted Therapeutic Strategies.* DPhil in Oncology, University of Oxford.

Maher, E. A., Marin-Valencia, I., Bachoo, R. M., Mashimo, T., Raisanen, J., Hatanpaa, K. J., Jindal, A., Jeffrey, F. M., Choi, C., Madden, C., Mathews, D., Pascual, J. M., Mickey, B. E., Malloy, C. R. & Deberardinis, R. J. 2012. Metabolism of [U-13 C]glucose in human brain tumors in vivo. *NMR in biomedicine,* 25**,** 1234-1244.

Maitra, R., Grigoryev, D. N., Bera, T. K., Pastan, I. H. & Lee, B. 2003. Cloning, molecular characterization, and expression analysis of Copine 8. *Biochem Biophys Res Commun,* 303**,** 842-7.

Marin-Valencia, I., Yang, C., Mashimo, T., Cho, S., Baek, H., Yang, X.-L., Rajagopalan, K. N., Maddie, M., Vemireddy, V., Zhao, Z., Cai, L., Good, L., Tu, B. P., Hatanpaa, K. J., Mickey, B. E., Matés, J. M., Pascual, J. M., Maher, E. A., Malloy, C. R., Deberardinis, R. J. & Bachoo, R. M. 2012. Analysis of tumor metabolism reveals mitochondrial glucose oxidation in genetically diverse human glioblastomas in the mouse brain in vivo. *Cell metabolism,* 15**,** 827-837.

Martinez, R., Roggendorf, W., Baretton, G., Klein, R., Toedt, G., Lichter, P., Schackert, G. & Joos, S. 2007. Cytogenetic and molecular genetic analyses of giant cell glioblastoma multiforme reveal distinct profiles in giant cell and non-giant cell subpopulations. *Cancer Genetics and Cytogenetics,* 175**,** 26-34.

Mashimo, T., Pichumani, K., Vemireddy, V., Hatanpaa, K. J., Singh, D. K., Sirasanagandla, S., Nannepaga, S., Piccirillo, S. G., Kovacs, Z., Foong, C., Huang, Z., Barnett, S., Mickey, B. E., Deberardinis, R. J., Tu, B. P., Maher, E. A. & Bachoo, R. M. 2014. Acetate is a bioenergetic substrate for human glioblastoma and brain metastases. *Cell,* 159**,** 1603-1614.

Maxwell, J. A., Johnson, S. P., Mclendon, R. E., Lister, D. W., Horne, K. S., Rasheed, A., Quinn, J. A., Ali-Osman, F., Friedman, A. H., Modrich, P. L., Bigner, D. D. & Friedman, H. S. 2008. Mismatch repair deficiency does not mediate clinical resistance to temozolomide in malignant glioma. *Clinical cancer research : an official journal of the American Association for Cancer Research,* 14**,** 4859-4868.

Mcfaline-Figueroa, J. L., Braun, C. J., Stanciu, M., Nagel, Z. D., Mazzucato, P., Sangaraju, D., Cerniauskas, E., Barford, K., Vargas, A., Chen, Y., Tretyakova, N., Lees, J. A., Hemann, M. T., White, F. M. & Samson, L. D. 2015. Minor Changes in Expression of the Mismatch Repair Protein MSH2 Exert a Major Impact on Glioblastoma Response to Temozolomide. *Cancer research,* 75**,** 3127-3138.

Mclendon, R., Friedman, A., Bigner, D., Van Meir, E. G., Brat, D. J., M. Mastrogianakis, G., Olson, J. J., Mikkelsen, T., Lehman, N., Aldape, K., Alfred Yung, W. K., Bogler, O., Vandenberg, S., Berger, M., Prados, M., Muzny, D., Morgan, M., Scherer, S., Sabo, A., Nazareth, L., Lewis, L., Hall, O., Zhu, Y., Ren, Y., Alvi, O., Yao, J., Hawes, A., Jhangiani, S., Fowler, G., San Lucas, A., Kovar, C., Cree, A., Dinh, H., Santibanez, J., Joshi, V., Gonzalez-Garay, M. L., Miller, C. A., Milosavljevic, A., Donehower, L., Wheeler, D. A., Gibbs, R. A., Cibulskis, K., Sougnez, C., Fennell, T., Mahan, S., Wilkinson, J., Ziaugra, L.,

Onofrio, R., Bloom, T., Nicol, R., Ardlie, K., Baldwin, J., Gabriel, S., Lander, E. S., Ding, L., Fulton, R. S., Mclellan, M. D., Wallis, J., Larson, D. E., Shi, X., Abbott, R., Fulton, L., Chen, K., Koboldt, D. C., Wendl, M. C., Meyer, R., Tang, Y., Lin, L., Osborne, J. R., Dunford-Shore, B. H., Miner, T. L., Delehaunty, K., Markovic, C., Swift, G., Courtney, W., Pohl, C., Abbott, S., Hawkins, A., Leong, S., Haipek, C., Schmidt, H., Wiechert, M., Vickery, T., Scott, S., Dooling, D. J., Chinwalla, A., Weinstock, G. M., Mardis, E. R., Wilson, R. K., Getz, G., Winckler, W., Verhaak, R. G. W., Lawrence, M. S., O'kelly, M., Robinson, J., Alexe, G., Beroukhim, R., Carter, S., Chiang, D., Gould, J., et al. 2008. Comprehensive genomic characterization defines human glioblastoma genes and core pathways. *Nature,* 455**,** 1061-1068.

Meng, X., Zhao, Y., Han, B., Zha, C., Zhang, Y., Li, Z., Wu, P., Qi, T., Jiang, C., Liu, Y. & Cai, J. 2020. Dual functionalized brain-targeting nanoinhibitors restrain temozolomide-resistant glioma via attenuating EGFR and MET signaling pathways. *Nature Communications,* 11**,** 594.

Meyer, M., Reimand, J., Lan, X., Head, R., Zhu, X., Kushida, M., Bayani, J., Pressey, J. C., Lionel, A. C., Clarke, I. D., Cusimano, M., Squire, J. A., Scherer, S. W., Bernstein, M., Woodin, M. A., Bader, G. D. & Dirks, P. B. 2015. Single cell-derived clonal analysis of human glioblastoma links functional and genomic heterogeneity. *Proceedings of the National Academy of Sciences of the United States of America,* 112**,** 851-856.

Michael, D. W., Eben, A., William, E. H., Collin, S. M., Mahaley, M. S., John, M., Horace, A. N., Guy, O., Joseph, R., Charles, B. W., Edmund, A. G. & Thomas, A. S. 1978. Evaluation of BCNU and/or radiotherapy in the treatment of anaplastic gliomas. *Journal of Neurosurgery,* 49**,** 333-343.

Middleton, M. R., Grob, J. J., Aaronson, N., Fierlbeck, G., Tilgen, W., Seiter, S., Gore, M., Aamdal, S., Cebon, J., Coates, A., Dreno, B., Henz, M., Schadendorf, D., Kapp, A., Weiss, J., Fraass, U., Statkevich, P., Muller, M. & Thatcher, N. 2000. Randomized Phase III Study of Temozolomide Versus Dacarbazine in the Treatment of Patients With Advanced Metastatic Malignant Melanoma. *Journal of Clinical Oncology,* 18**,** 158-158.

Molenaar, R. J., Maciejewski, J. P., Wilmink, J. W. & Van Noorden, C. J. F. 2018. Wild-type and mutated IDH1/2 enzymes and therapy responses. *Oncogene,* 37**,** 1949-1960.

Moncayo, G., Grzmil, M., Smirnova, T., Zmarz, P., Huber, R. M., Hynx, D., Kohler, H., Wang, Y., Hotz, H.-R., Hynes, N. E., Keller, G., Frank, S., Merlo, A. & Hemmings, B. A. 2018. SYK inhibition blocks proliferation and migration of glioma cells and modifies the tumor microenvironment. *Neuro-Oncology,* 20**,** 621-631.

Moody, C. L. & Wheelhouse, R. T. 2014. The medicinal chemistry of imidazotetrazine prodrugs. *Pharmaceuticals (Basel),* 7**,** 797-838.

Munoz, J. L., Rodriguez-Cruz, V., Greco, S. J., Nagula, V., Scotto, K. W. & Rameshwar, P. 2014. Temozolomide Induces the Production of Epidermal Growth Factor to Regulate MDR1 Expression in Glioblastoma Cells. *Molecular Cancer Therapeutics,* 13**,** 2399.

Munoz, J. L., Rodriguez-Cruz, V., Ramkissoon, S. H., Ligon, K. L., Greco, S. J. & Rameshwar, P. 2015a. Temozolomide resistance in glioblastoma occurs by miRNA-9-targeted PTCH1, independent of sonic hedgehog level. *Oncotarget,* 6**,** 1190-1201.

Munoz, J. L., Walker, N. D., Scotto, K. W. & Rameshwar, P. 2015b. Temozolomide competes for P-glycoprotein and contributes to chemoresistance in glioblastoma cells. *Cancer Letters,* 367**,** 69-75.

Nagel, Z. D., Beharry, A. A., Mazzucato, P., Kitange, G. J., Sarkaria, J. N., Kool, E. T. & Samson, L. D. 2019. Fluorescent reporter assays provide direct, accurate, quantitative measurements of MGMT status in human cells. *PloS one,* 14**,** e0208341-e0208341.

Nakada, M., Kita, D., Watanabe, T., Hayashi, Y., Teng, L., Pyko, I. V. & Hamada, J.-I. 2011. Aberrant signaling pathways in glioma. *Cancers,* 3**,** 3242-3278.

Nci. 2019. *Drugs Approved for Brain Tumors* [Online]. National Cancer Institute. Available: **https://www.cancer.gov/about-cancer/treatment/drugs/brain** [Accessed 13 May 2020].

Nechanitzky, R., Akbas, D., Scherer, S., György, I., Hoyler, T., Ramamoorthy, S., Diefenbach, A. & Grosschedl, R. 2013. Transcription factor EBF1 is essential for the maintenance of B cell identity and prevention of alternative fates in committed cells. *Nature Immunology,* 14**,** 867-875.

Nice. 2018. *Brain tumours (primary) and brain metastases in adults (NICE Guideline 99)* [Online]. National Institute for Health and Care Excellence. Available: **https://www.nice.org.uk/guidance/ng99/chapter/Recommendations** [Accessed 12 May 2020].

Nuryadi, E., Mayang Permata, T. B., Komatsu, S., Oike, T. & Nakano, T. 2018. Inter-assay precision of clonogenic assays for radiosensitivity in cancer cell line A549. *Oncotarget,* 9**,** 13706-13712.

Oh, J. E., Ohta, T., Nonoguchi, N., Satomi, K., Capper, D., Pierscianek, D., Sure, U., Vital, A., Paulus, W., Mittelbronn, M., Antonelli, M., Kleihues, P., Giangaspero, F. & Ohgaki, H. 2016.

Genetic Alterations in Gliosarcoma and Giant Cell Glioblastoma. *Brain Pathology,* 26**,** 517-522.
Ohgaki, H. 2009. Epidemiology of Brain Tumors. *In:* VERMA, M. (ed.) *Cancer Epidemiology: Modifiable Factors.* Totowa, NJ: Humana Press.
Ohgaki, H. & Kleihues, P. 2013. The Definition of Primary and Secondary Glioblastoma. *Clinical Cancer Research,* 19**,** 764.
Omuro, A. & Deangelis, L. M. 2013. Glioblastoma and Other Malignant Gliomas: A Clinical Review. *JAMA,* 310**,** 1842-1850.
Ostrom, Q. T., Gittleman, H., Farah, P., Ondracek, A., Chen, Y., Wolinsky, Y., Stroup, N. E., Kruchko, C. & Barnholtz-Sloan, J. S. 2013. CBTRUS statistical report: Primary brain and central nervous system tumors diagnosed in the United States in 2006-2010. *Neuro-oncology,* 15 Suppl 2**,** ii1-ii56.
Paret, C., Simon, P., Vormbrock, K., Bender, C., Kölsch, A., Breitkreuz, A., Yildiz, Ö., Omokoko, T., Hubich-Rau, S., Hartmann, C., Häcker, S., Wagner, M., Roldan, D. B., Selmi, A., Türeci, Ö. & Sahin, U. 2015. CXorf61 is a target for T cell based immunotherapy of triple-negative breast cancer. *Oncotarget,* 6**,** 25356-25367.
Parsons, D. W., Jones, S., Zhang, X., Lin, J. C.-H., Leary, R. J., Angenendt, P., Mankoo, P., Carter, H., Siu, I. M., Gallia, G. L., Olivi, A., Mclendon, R., Rasheed, B. A., Keir, S., Nikolskaya, T., Nikolsky, Y., Busam, D. A., Tekleab, H., Diaz, L. A., Hartigan, J., Smith, D. R., Strausberg, R. L., Marie, S. K. N., Shinjo, S. M. O., Yan, H., Riggins, G. J., Bigner, D. D., Karchin, R., Papadopoulos, N., Parmigiani, G., Vogelstein, B., Velculescu, V. E. & Kinzler, K. W. 2008. An Integrated Genomic Analysis of Human Glioblastoma Multiforme. *Science,* 321**,** 1807.
Paugh, B. S., Qu, C., Jones, C., Liu, Z., Adamowicz-Brice, M., Zhang, J., Bax, D. A., Coyle, B., Barrow, J., Hargrave, D., Lowe, J., Gajjar, A., Zhao, W., Broniscer, A., Ellison, D. W., Grundy, R. G. & Baker, S. J. 2010. Integrated molecular genetic profiling of pediatric high-grade gliomas reveals key differences with the adult disease. *Journal of clinical oncology : official journal of the American Society of Clinical Oncology,* 28**,** 3061-3068.
Pegg, A. E. 2000. Repair of O6-alkylguanine by alkyltransferases. *Mutation Research/Reviews in Mutation Research,* 462**,** 83-100.
Peng, W.-X., Han, X., Zhang, C.-L., Ge, L., Du, F.-Y., Jin, J. & Gong, A.-H. 2017. FoxM1-mediated RFC5 expression promotes temozolomide resistance. *Cell Biology and Toxicology,* 33**,** 527-537.
Petővári, G., Dankó, T., Krencz, I., Hujber, Z., Rajnai, H., Vetlényi, E., Raffay, R., Pápay, J., Jeney, A. & Sebestyén, A. 2020. Inhibition of Metabolic Shift can Decrease Therapy Resistance in Human High-Grade Glioma Cells. *Pathology & Oncology Research,* 26**,** 23-33.

Phillips, H. S., Kharbanda, S., Chen, R., Forrest, W. F., Soriano, R. H., Wu, T. D., Misra, A., Nigro, J. M., Colman, H., Soroceanu, L., Williams, P. M., Modrusan, Z., Feuerstein, B. G. & Aldape, K. 2006. Molecular subclasses of high-grade glioma predict prognosis, delineate a pattern of disease progression, and resemble stages in neurogenesis. *Cancer Cell,* 9**,** 157-173.

Qu, M., Yu, J., Liu, H., Ren, Y., Ma, C., Bu, X. & Lan, Q. 2017. The Candidate Tumor Suppressor Gene SLC8A2 Inhibits Invasion, Angiogenesis and Growth of Glioblastoma. *Molecules and cells,* 40**,** 761-772.

Quinn, J. A., Jiang, S. X., Reardon, D. A., Desjardins, A., Vredenburgh, J. J., Rich, J. N., Gururangan, S., Friedman, A. H., Bigner, D. D., Sampson, J. H., Mclendon, R. E., Herndon, J. E., 2nd, Walker, A. & Friedman, H. S. 2009. Phase II trial of temozolomide plus o6-benzylguanine in adults with recurrent, temozolomide-resistant malignant glioma. *Journal of clinical oncology : official journal of the American Society of Clinical Oncology,* 27**,** 1262-1267.

Quiros, S., Roos, W. P. & Kaina, B. 2010. Processing of O6-methylguanine into DNA double-strand breaks requires two rounds of replication whereas apoptosis is also induced in subsequent cell cycles. *Cell Cycle,* 9**,** 168-178.

Rabé, M., Dumont, S., Álvarez-Arenas, A., Janati, H., Belmonte-Beitia, J., Calvo, G. F., Thibault-Carpentier, C., Séry, Q., Chauvin, C., Joalland, N., Briand, F., Blandin, S., Scotet, E., Pecqueur, C., Clairambault, J., Oliver, L., Perez-Garcia, V., Nadaradjane, A., Cartron, P.-F., Gratas, C. & Vallette, F. M. 2020. Identification of a transient state during the acquisition of temozolomide resistance in glioblastoma. *Cell Death & Disease,* 11**,** 19.

Rai, Y., Pathak, R., Kumari, N., Sah, D. K., Pandey, S., Kalra, N., Soni, R., Dwarakanath, B. S. & Bhatt, A. N. 2018. Mitochondrial biogenesis and metabolic hyperactivation limits the application of MTT assay in the estimation of radiation induced growth inhibition. *Scientific reports,* 8**,** 1531-1531.

Rama, A. R., Alvarez, P. J., Madeddu, R. & Aranega, A. 2014. ABC transporters as differentiation markers in glioblastoma cells. *Molecular Biology Reports,* 41**,** 4847-4851.

Ramcharan, R., Aleksic, T., Kamdoum, W. P., Gao, S., Pfister, S. X., Tanner, J., Bridges, E., Asher, R., Watson, A. J., Margison, G. P., Woodcock, M., Repapi, E., Li, J.-L., Middleton, M. R. & Macaulay, V. M. 2015. IGF-1R inhibition induces schedule-dependent sensitization of human melanoma to temozolomide. *Oncotarget,* 6**,** 39877-39890.

Ranson, M., Hersey, P., Thompson, D., Beith, J., Mcarthur, G. A., Haydon, A., Davis, I. D., Kefford, R. F., Mortimer, P., Harris, P. A., Baka, S., Seebaran, A., Sabharwal, A., Watson, A. J.,

Margison, G. P. & Middleton, M. R. 2007. Randomized Trial of the Combination of Lomeguatrib and Temozolomide Compared With Temozolomide Alone in Chemotherapy Naive Patients With Metastatic Cutaneous Melanoma. *Journal of Clinical Oncology,* 25**,** 2540-2545.

Rasmussen, R. D., Gajjar, M. K., Tuckova, L., Jensen, K. E., Maya-Mendoza, A., Holst, C. B., Møllgaard, K., Rasmussen, J. S., Brennum, J., Bartek, J., Jr., Syrucek, M., Sedlakova, E., Andersen, K. K., Frederiksen, M. H., Bartek, J. & Hamerlik, P. 2016. BRCA1-regulated RRM2 expression protects glioblastoma cells from endogenous replication stress and promotes tumorigenicity. *Nature communications,* 7**,** 13398-13398.

Reid, J. M., Stevens, D. C., Rubin, J. & Ames, M. M. 1997. Pharmacokinetics of 3-methyl-(triazen-1-yl)imidazole-4-carboximide following administration of temozolomide to patients with advanced cancer. *Clinical Cancer Research,* 3**,** 2393-2398.

Rieunier, G., Wu, X., Harris, L., Mills, J., Nandakumar, A., Colling, L., Seraia, E., Hatch, S. B., Ebner, D., Folkes, L. K., Weyer-Czernilofsky, U., Bogenrieder, T., Ryan, A. J. & Macaulay, V. M. 2020. IGF targeting perturbs global replication through ribonucleotide reductase dysfunction. *bioRxiv***,** 2020.08.11.245886.

Ringel, F., Pape, H., Sabel, M., Krex, D., Bock, H. C., Misch, M., Weyerbrock, A., Westermaier, T., Senft, C., Schucht, P., Meyer, B., Simon, M. & Group, S. N. S. 2016. Clinical benefit from resection of recurrent glioblastomas: results of a multicenter study including 503 patients with recurrent glioblastomas undergoing surgical resection. *Neuro-oncology,* 18**,** 96-104.

Robey, R. W., Pluchino, K. M., Hall, M. D., Fojo, A. T., Bates, S. E. & Gottesman, M. M. 2018. Revisiting the role of ABC transporters in multidrug-resistant cancer. *Nature reviews. Cancer,* 18**,** 452-464.

Roos, W. P., Frohnapfel, L., Quiros, S., Ringel, F. & Kaina, B. 2018. XRCC3 contributes to temozolomide resistance of glioblastoma cells by promoting DNA double-strand break repair. *Cancer Letters,* 424**,** 119-126.

Roos, W. P., Nikolova, T., Quiros, S., Naumann, S. C., Kiedron, O., Zdzienicka, M. Z. & Kaina, B. 2009. Brca2/Xrcc2 dependent HR, but not NHEJ, is required for protection against O6-methylguanine triggered apoptosis, DSBs and chromosomal aberrations by a process leading to SCEs. *DNA Repair,* 8**,** 72-86.

Rosati, A., Poliani, P. L., Todeschini, A., Cominelli, M., Medicina, D., Cenzato, M., Simoncini, E. L., Magrini, S. M., Buglione, M., Grisanti, S. & Padovani, A. 2013. Glutamine synthetase expression as a valuable marker of epilepsy and longer survival

in newly diagnosed glioblastoma multiforme. *Neuro-oncology,* 15**,** 618-625.
Sagawa, M., Ohguchi, H., Harada, T., Samur, M. K., Tai, Y.-T., Munshi, N. C., Kizaki, M., Hideshima, T. & Anderson, K. C. 2017. Ribonucleotide Reductase Catalytic Subunit M1 (RRM1) as a Novel Therapeutic Target in Multiple Myeloma. *Clinical cancer research : an official journal of the American Association for Cancer Research,* 23**,** 5225-5237.
Sandberg-Wollheim, M., Malmstrom, P., Stromblad, L. G., Anderson, H., Borgstrom, S., Brun, A., Cronqvist, S., Hougaard, K. & Salford, L. G. 1991. A randomized study of chemotherapy with procarbazine, vincristine, and lomustine with and without radiation therapy for astrocytoma grades 3 and/or 4. *Cancer,* 68**,** 22-9.
Sarkaria, J. N., Kitange, G. J., James, C. D., Plummer, R., Calvert, H., Weller, M. & Wick, W. 2008. Mechanisms of chemoresistance to alkylating agents in malignant glioma. *Clinical cancer research : an official journal of the American Association for Cancer Research,* 14**,** 2900-2908.
Schäfer, A., Teufel, J., Ringel, F., Bettstetter, M., Hoepner, I., Rasper, M., Gempt, J., Koeritzer, J., Schmidt-Graf, F., Meyer, B., Beier, C. P. & Schlegel, J. 2012. Aldehyde dehydrogenase 1A1--a new mediator of resistance to temozolomide in glioblastoma. *Neuro-oncology,* 14**,** 1452-1464.
Schiffer, D., Annovazzi, L., Casalone, C., Corona, C. & Mellai, M. 2018a. Glioblastoma: Microenvironment and Niche Concept. *Cancers (Basel),* 11.
Schiffer, D., Mellai, M., Bovio, E., Bisogno, I., Casalone, C. & Annovazzi, L. 2018b. Glioblastoma niches: from the concept to the phenotypical reality. *Neurological Sciences,* 39**,** 1161-1168.
Schwartzentruber, J., Korshunov, A., Liu, X.-Y., Jones, D. T. W., Pfaff, E., Jacob, K., Sturm, D., Fontebasso, A. M., Quang, D.-a. K., Tönjes, M., Hovestadt, V., Albrecht, S., Kool, M., Nantel, A., Konermann, C., Lindroth, A., Jäger, N., Rausch, T., Ryzhova, M., Korbel, J. O., Hielscher, T., Hauser, P., Garami, M., Klekner, A., Bognar, L., Ebinger, M., Schuhmann, M. U., Scheurlen, W., Pekrun, A., Frühwald, M. C., Roggendorf, W., Kramm, C., Dürken, M., Atkinson, J., Lepage, P., Montpetit, A., Zakrzewska, M., Zakrzewski, K., Liberski, P. P., Dong, Z., Siegel, P., Kulozik, A. E., Zapatka, M., Guha, A., Malkin, D., Felsberg, J., Reifenberger, G., Von Deimling, A., Ichimura, K., Collins, V. P., Witt, H., Milde, T., Witt, O., Zhang, C., Castelo-Branco, P., Lichter, P., Faury, D., Tabori, U., Plass, C., Majewski, J., Pfister, S. M. & Jabado, N. 2012. Driver mutations in histone H3.3 and chromatin remodelling genes in paediatric glioblastoma. *Nature,* 482**,** 226-231.

Seystahl, K., Wick, W. & Weller, M. 2016. Therapeutic options in recurrent glioblastoma—An update. *Critical Reviews in Oncology/Hematology,* 99**,** 389-408.
Shapiro, W. R. & Young, D. F. 1976. Treatment of Malignant Glioma: A Controlled Study of Chemotherapy and Irradiation. *Archives of Neurology,* 33**,** 494-500.
Shervington, A. & Lu, C. 2008. Expression of Multidrug Resistance Genes in Normal and Cancer Stem Cells. *Cancer Investigation,* 26**,** 535-542.
Simpson, A. 2016. *Investigating Resistance of Glioblastoma Multiforme to Radiotherapy and Chemotherapy.* MSc by Research in Oncology, University of Oxford.
Simpson, A. D., Soo, Y. W. J., Rieunier, G., Aleksic, T., Ansorge, O., Jones, C. & Macaulay, V. M. 2020. Type 1 IGF receptor associates with adverse outcome and cellular radioresistance in paediatric high-grade glioma. *British Journal of Cancer,* 122**,** 624-629.
Smith, C. & Ironside, J. W. 2007. Diagnosis and pathogenesis of gliomas. *Current Diagnostic Pathology,* 13**,** 180-192.
Stojic, L., Brun, R. & Jiricny, J. 2004. Mismatch repair and DNA damage signalling. *DNA Repair,* 3**,** 1091-1101.
Street, K., Risso, D., Fletcher, R. B., Das, D., Ngai, J., Yosef, N., Purdom, E. & Dudoit, S. 2018. Slingshot: cell lineage and pseudotime inference for single-cell transcriptomics. *BMC genomics,* 19**,** 477-477.
Stritzelberger, J., Distel, L., Buslei, R., Fietkau, R. & Putz, F. 2018. Acquired temozolomide resistance in human glioblastoma cell line U251 is caused by mismatch repair deficiency and can be overcome by lomustine. *Clinical and Translational Oncology,* 20**,** 508-516.
Strobel, H., Baisch, T., Fitzel, R., Schilberg, K., Siegelin, M. D., Karpel-Massler, G., Debatin, K.-M. & Westhoff, M.-A. 2019. Temozolomide and Other Alkylating Agents in Glioblastoma Therapy. *Biomedicines,* 7**,** 69.
Struve, N., Binder, Z. A., Stead, L. F., Brend, T., Bagley, S. J., Faulkner, C., Ott, L., Müller-Goebel, J., Weik, A.-S., Hoffer, K., Krug, L., Rieckmann, T., Bußmann, L., Henze, M., Morrissette, J. J. D., Kurian, K. M., Schüller, U., Petersen, C., Rothkamm, K., O Rourke, D. M., Short, S. C. & Kriegs, M. 2020. EGFRvIII upregulates DNA mismatch repair resulting in increased temozolomide sensitivity of MGMT promoter methylated glioblastoma. *Oncogene,* 39**,** 3041-3055.
Stupp, R., Van Den Bent, M. J. & Hegi, M. E. 2005. Optimal role of temozolomide in the treatment of malignant gliomas. *Curr Neurol Neurosci Rep,* 5**,** 198-206.
Szuchet, S., Nielsen, J. A., Lovas, G., Domowicz, M. S., De Velasco, J. M., Maric, D. & Hudson, L. D. 2011. The genetic signature of

perineuronal oligodendrocytes reveals their unique phenotype. *European Journal of Neuroscience,* 34**,** 1906-1922.
Takasaki, C., Yamasaki, M., Uchigashima, M., Konno, K., Yanagawa, Y. & Watanabe, M. 2010. Cytochemical and cytological properties of perineuronal oligodendrocytes in the mouse cortex. *European Journal of Neuroscience,* 32**,** 1326-1336.
Tang, J.-B., Goellner, E. M., Wang, X.-H., Trivedi, R. N., St Croix, C. M., Jelezcova, E., Svilar, D., Brown, A. R. & Sobol, R. W. 2010. Bioenergetic metabolites regulate base excision repair-dependent cell death in response to DNA damage. *Molecular cancer research : MCR,* 8**,** 67-79.
Tang, J.-B., Svilar, D., Trivedi, R. N., Wang, X.-H., Goellner, E. M., Moore, B., Hamilton, R. L., Banze, L. A., Brown, A. R. & Sobol, R. W. 2011. N-methylpurine DNA glycosylase and DNA polymerase beta modulate BER inhibitor potentiation of glioma cells to temozolomide. *Neuro-oncology,* 13**,** 471-486.
Taniike, M., Mohri, I., Eguchi, N., Beuckmann, C. T., Suzuki, K. & Urade, Y. 2002. Perineuronal Oligodendrocytes Protect against Neuronal Apoptosis through the Production of Lipocalin-Type Prostaglandin D Synthase in a Genetic Demyelinating Model. *The Journal of Neuroscience,* 22**,** 4885.
Tentori, L. & Graziani, G. 2009. Recent approaches to improve the antitumor efficacy of temozolomide. *Curr Med Chem,* 16**,** 245-57.
Tiek, D. M., Rone, J. D., Graham, G. T., Pannkuk, E. L., Haddad, B. R. & Riggins, R. B. 2018. Alterations in Cell Motility, Proliferation, and Metabolism in Novel Models of Acquired Temozolomide Resistant Glioblastoma. *Scientific Reports,* 8**,** 7222.
Tolcher, A. W., Gerson, S. L., Denis, L., Geyer, C., Hammond, L. A., Patnaik, A., Goetz, A. D., Schwartz, G., Edwards, T., Reyderman, L., Statkevich, P., Cutler, D. L. & Rowinsky, E. K. 2003. Marked inactivation of O6-alkylguanine-DNA alkyltransferase activity with protracted temozolomide schedules. *British journal of cancer,* 88**,** 1004-1011.
Tomita, H., Tanaka, K., Tanaka, T. & Hara, A. 2016. Aldehyde dehydrogenase 1A1 in stem cells and cancer. *Oncotarget,* 7**,** 11018-11032.
Tönjes, M., Barbus, S., Park, Y. J., Wang, W., Schlotter, M., Lindroth, A. M., Pleier, S. V., Bai, A. H. C., Karra, D., Piro, R. M., Felsberg, J., Addington, A., Lemke, D., Weibrecht, I., Hovestadt, V., Rolli, C. G., Campos, B., Turcan, S., Sturm, D., Witt, H., Chan, T. A., Herold-Mende, C., Kemkemer, R., König, R., Schmidt, K., Hull, W.-E., Pfister, S. M., Jugold, M., Hutson, S. M., Plass, C., Okun, J. G., Reifenberger, G., Lichter, P. & Radlwimmer, B. 2013. BCAT1 promotes cell proliferation

through amino acid catabolism in gliomas carrying wild-type IDH1. *Nature medicine,* 19**,** 901-908.
Toulany, M. 2019. Targeting DNA Double-Strand Break Repair Pathways to Improve Radiotherapy Response. *Genes,* 10**,** 25.
Vasile, F., Dossi, E. & Rouach, N. 2017. Human astrocytes: structure and functions in the healthy brain. *Brain Structure and Function,* 222**,** 2017-2029.
Vecht, C. J., Kerkhof, M. & Duran-Pena, A. 2014. Seizure prognosis in brain tumors: new insights and evidence-based management. *The oncologist,* 19**,** 751-759.
Venkatesh, H. S., Morishita, W., Geraghty, A. C., Silverbush, D., Gillespie, S. M., Arzt, M., Tam, L. T., Espenel, C., Ponnuswami, A., Ni, L., Woo, P. J., Taylor, K. R., Agarwal, A., Regev, A., Brang, D., Vogel, H., Hervey-Jumper, S., Bergles, D. E., Suvà, M. L., Malenka, R. C. & Monje, M. 2019. Electrical and synaptic integration of glioma into neural circuits. *Nature,* 573**,** 539-545.
Verhaak, R. G. W., Hoadley, K. A., Purdom, E., Wang, V., Qi, Y., Wilkerson, M. D., Miller, C. R., Ding, L., Golub, T., Mesirov, J. P., Alexe, G., Lawrence, M., O'kelly, M., Tamayo, P., Weir, B. A., Gabriel, S., Winckler, W., Gupta, S., Jakkula, L., Feiler, H. S., Hodgson, J. G., James, C. D., Sarkaria, J. N., Brennan, C., Kahn, A., Spellman, P. T., Wilson, R. K., Speed, T. P., Gray, J. W., Meyerson, M., Getz, G., Perou, C. M., Hayes, D. N. & Cancer Genome Atlas Research, N. 2010. Integrated genomic analysis identifies clinically relevant subtypes of glioblastoma characterized by abnormalities in PDGFRA, IDH1, EGFR, and NF1. *Cancer cell,* 17**,** 98-110.
Vigneswaran, K., Neill, S. & Hadjipanayis, C. G. 2015. Beyond the World Health Organization grading of infiltrating gliomas: advances in the molecular genetics of glioma classification. *Annals of translational medicine,* 3**,** 95-95.
Walker, L., Thompson, D., Easton, D., Ponder, B., Ponder, M., Frayling, I. & Baralle, D. 2006. A prospective study of neurofibromatosis type 1 cancer incidence in the UK. *British journal of cancer,* 95**,** 233-238.
Walker, M. D., Green, S. B., Byar, D. P., Alexander, E., Batzdorf, U., Brooks, W. H., Hunt, W. E., Maccarty, C. S., Mahaley, M. S., Mealey, J., Owens, G., Ransohoff, J., Robertson, J. T., Shapiro, W. R., Smith, K. R., Wilson, C. B. & Strike, T. A. 1980. Randomized Comparisons of Radiotherapy and Nitrosoureas for the Treatment of Malignant Glioma after Surgery. *New England Journal of Medicine,* 303**,** 1323-1329.
Wang, Q., Hu, B., Hu, X., Kim, H., Squatrito, M., Scarpace, L., Decarvalho, A. C., Lyu, S., Li, P., Li, Y., Barthel, F., Cho, H. J., Lin, Y.-H., Satani, N., Martinez-Ledesma, E., Zheng, S., Chang, E., Sauvé, C.-E. G., Olar, A., Lan, Z. D., Finocchiaro, G., Phillips, J. J., Berger, M. S., Gabrusiewicz, K. R., Wang, G.,

Eskilsson, E., Hu, J., Mikkelsen, T., Depinho, R. A., Muller, F., Heimberger, A. B., Sulman, E. P., Nam, D.-H. & Verhaak, R. G. W. 2017. Tumor Evolution of Glioma-Intrinsic Gene Expression Subtypes Associates with Immunological Changes in the Microenvironment. *Cancer Cell,* 32**,** 42-56.e6.

Warren, J. J., Forsberg, L. J. & Beese, L. S. 2006. The structural basis for the mutagenicity of O⁶-methyl-guanine lesions. *Proceedings of the National Academy of Sciences,* 103**,** 19701.

Wellenstein, M. D. & De Visser, K. E. 2018. Cancer-Cell-Intrinsic Mechanisms Shaping the Tumor Immune Landscape. *Immunity,* 48**,** 399-416.

Weller, M., Felsberg, J., Hartmann, C., Berger, H., Steinbach, J. P., Schramm, J., Westphal, M., Schackert, G., Simon, M., Tonn, J. C., Heese, O., Krex, D., Nikkhah, G., Pietsch, T., Wiestler, O., Reifenberger, G., Von Deimling, A. & Loeffler, M. 2009. Molecular predictors of progression-free and overall survival in patients with newly diagnosed glioblastoma: a prospective translational study of the German Glioma Network. *J Clin Oncol,* 27**,** 5743-50.

Weller, M., Van Den Bent, M., Hopkins, K., Tonn, J. C., Stupp, R., Falini, A., Cohen-Jonathan-Moyal, E., Frappaz, D., Henriksson, R., Balana, C., Chinot, O., Ram, Z., Reifenberger, G., Soffietti, R. & Wick, W. 2014. EANO guideline for the diagnosis and treatment of anaplastic gliomas and glioblastoma. *The Lancet Oncology,* 15**,** e395-e403.

Wijaya, J., Fukuda, Y. & Schuetz, J. D. 2017. Obstacles to Brain Tumor Therapy: Key ABC Transporters. *International journal of molecular sciences,* 18**,** 2544.

Wippold, F. J., Lämmle, M., Anatelli, F., Lennerz, J. & Perry, A. 2006. Neuropathology for the Neuroradiologist: Palisades and Pseudopalisades. *American Journal of Neuroradiology,* 27**,** 2037.

Wolf, A., Agnihotri, S., Micallef, J., Mukherjee, J., Sabha, N., Cairns, R., Hawkins, C. & Guha, A. 2011. Hexokinase 2 is a key mediator of aerobic glycolysis and promotes tumor growth in human glioblastoma multiforme. *The Journal of experimental medicine,* 208**,** 313-326.

Woo, P., Li, Y., Chan, A., Ng, S., Loong, H., Chan, D., Wong, G. & Poon, W.-S. 2019. A multifaceted review of temozolomide resistance mechanisms in glioblastoma beyond O-6-methylguanine-DNA methyltransferase. *Glioma,* 2**,** 68-82.

Wurdeman, R. L., Douskey, M. C. & Gold, B. 1993. DNA methylation by N-methyl-N-nitrosourea: methylation pattern changes in single- and double-stranded DNA, and in DNA with mismatched or bulged guanines. *Nucleic acids research,* 21**,** 4975-4980.

Yeom, S.-Y., Nam, D.-H. & Park, C. 2014. RRAD Promotes EGFR-Mediated STAT3 Activation and Induces Temozolomide Resistance of Malignant Glioblastoma. *Molecular Cancer Therapeutics,* 13**,** 3049.

Yi, G.-Z., Huang, G., Guo, M., Zhang, X. A., Wang, H., Deng, S., Li, Y., Xiang, W., Chen, Z., Pan, J., Li, Z., Yu, L., Lei, B., Liu, Y. & Qi, S. 2019. Acquired temozolomide resistance in MGMT-deficient glioblastoma cells is associated with regulation of DNA repair by DHC2. *Brain,* 142**,** 2352-2366.

Young, K. M., Psachoulia, K., Tripathi, R. B., Dunn, S. J., Cossell, L., Attwell, D., Tohyama, K. & Richardson, W. D. 2013. Oligodendrocyte dynamics in the healthy adult CNS: evidence for myelin remodeling. *Neuron,* 77**,** 873-85.

Yu, W., Zhang, L., Wei, Q. & Shao, A. 2020. O(6)-Methylguanine-DNA Methyltransferase (MGMT): Challenges and New Opportunities in Glioma Chemotherapy. *Frontiers in oncology,* 9**,** 1547-1547.

Yu, X., Wang, M., Zuo, J., Wahafu, A., Mao, P., Li, R., Wu, W., Xie, W. & Wang, J. 2019. Nuclear factor I A promotes temozolomide resistance in glioblastoma via activation of nuclear factor kappaB pathway. *Life Sci,* 236**,** 116917.

Yuen, T. I., Morokoff, A. P., Bjorksten, A., D'abaco, G., Paradiso, L., Finch, S., Wong, D., Reid, C. A., Powell, K. L., Drummond, K. J., Rosenthal, M. A., Kaye, A. H. & O'brien, T. J. 2012. Glutamate is associated with a higher risk of seizures in patients with gliomas. *Neurology,* 79**,** 883-9.

Zhang, C., Zhu, Q., He, H., Jiang, L., Qiang, Q., Hu, L., Hu, G., Jiang, Y., Ding, X. & Lu, Y. 2015. RIZ1: a potential tumor suppressor in glioma. *BMC Cancer,* 15**,** 990.

Zhang, G., Huang, S., Zhang, J., Wu, Z., Lin, S. & Wang, Y. 2016. Clinical outcome of gliosarcoma compared with glioblastoma multiforme: a clinical study in Chinese patients. *Journal of Neuro-Oncology,* 127**,** 355-362.

Zhang, T., Chai, J. & Chi, L. 2019a. Induction Of XLF And 53BP1 Expression Is Associated With Temozolomide Resistance In Glioblastoma Cells. *OncoTargets and therapy,* 12**,** 10139-10151.

Zhang, Y., Xia, Q. & Lin, J. 2018. Identification of the potential oncogenes in glioblastoma based on bioinformatic analysis and elucidation of the underlying mechanisms. *Oncology reports,* 40**,** 715-725.

Zhang, Z., Wang, Z., Huang, K., Liu, Y., Wei, C., Zhou, J., Zhang, W., Wang, Q., Liang, H., Zhang, A., Wang, G., Zhen, Y. & Han, L. 2019b. PLK4 is a determinant of temozolomide sensitivity through phosphorylation of IKBKE in glioblastoma. *Cancer Letters,* 443**,** 91-107.

Zhou, W. & Wahl, D. R. 2019. Metabolic Abnormalities in Glioblastoma and Metabolic Strategies to Overcome Treatment Resistance. *Cancers,* 11**,** 1231.
Zhu, Y., Guignard, F., Zhao, D., Liu, L., Burns, D. K., Mason, R. P., Messing, A. & Parada, L. F. 2005. Early inactivation of p53 tumor suppressor gene cooperating with NF1 loss induces malignant astrocytoma. *Cancer cell,* 8**,** 119-130.
Zong, H., Verhaak, R. G. W. & Canoll, P. 2012. The cellular origin for malignant glioma and prospects for clinical advancements. *Expert review of molecular diagnostics,* 12**,** 383-394.
Zou, F., Pusch, S., Eisel, J., Ma, T., Zhu, Q., Deng, D., Gu, Y., Xu, Y., Von Deimling, A. & Zha, X. 2016. Identification of a novel selective inhibitor of mutant isocitrate dehydrogenase 1 at allosteric site by docking-based virtual screening. *RSC Advances,* 6**,** 96735-96742.